SOME PHYSICAL PROCESSES INVOLVED IN DEFORMATION AND FRACTURE

by Walter James Cousins

Submitted for the degree of

DOCTOR OF PHILOSOPHY

In PHYSICS at the

Victoria University of Wellington

(February, 1972).

ACKNOWLEDGEMENTS

I wish to express my gratitude to Professors D. Walker and N.F. Barber, and Dr. M.C. Probine and the staff of the Physics and Engineering Laboratory for much help and encouragement during my work; to the University Grants Committee for financial support, and lastly to my wife Margaret for constant encouragement and for the many difficult hours spent typing.

W.J. Cousins

SUMMARY

The effects of strain rate, of moisture content, and of tracheid structure on the transverse fracture properties of Pinus Radiata have been studied. Small rectangular blocks were loaded to failure in transverse tension, with the conditions of fracture being varied as follows:

(i) strain rate - at 2×10^{-6} sec^{-1}, and from 10^{-5} to 10^{2} sec^{-1} in decade steps,

(ii) moisture content - airdry (12.7%) and saturated, and

(iii) structure - springwood and summerwood.

Microscopical examination (both scanning electron and optical) of the surfaces produced by the fracture showed that at the cellular level, either of two types of failure could occur. These are called transwall and intrawall; transwall is the longitudinal splitting of a tracheid wall, and intrawall is a splitting between adjacent tracheids.

The proportion of the fracture surface tracheids broken in the transwall mode was not constant, but depended on all three fracture conditions. When the fracture was located in summerwood there was always little transwall failure under all experimental conditions. In airdry springwood, 20% of the surface tracheids were broken, at all strain rates; but in saturated springwood the percentage varied with strain rate, ranging from nearly zero at 10^{-5} sec^{-1}, to 55%

at 10^2 sec^{-1}.

The transverse strength of Pinus Radiata also was dependent on strain rate and moisture content. At the lowest rate (2×10^{-6} sec^{-1}) the strength of dry wood was 0.9 Kg/mm^2, and that of wet wood 0.2 Kg/mm^2. The transverse strengths of both wet and dry wood increased as strain rate was increased, until at 10^2 sec^{-1} they were equal at 1.1 Kg/mm^2.

A theoretical analysis of the tensile stresses in the region of middle lamella lying at right angles to the applied forces suggests that the lack of transwall failure in summerwood is due, at least in part, to the thickness of the tracheid wall. Since the summerwood tracheids are very well aligned in both radial and tangential directions, it is possible to make the assumption of perfect alignment, which considerably simplifies the analysis.

In springwood, the situation is more complex, for although tracheids show good radial alignment, there is considerable overlap in the tangential direction. For this case the stress analysis necessitates the use of a finite element technique.

The major result of this analysis of springwood failure is that the degree of overlap is the factor exerting most influence on the type of failure. Such factors as tracheid diameter, small changes (up to 25% say) in wall thickness, and variations in the S_2 layer microfibril angle seem to be of little importance. In dry wood only, however, the thickness of the S_1 layer is a factor of considerable significance.

Tracheid walls with thinner than average S_1 layers are more likely to fail in the transwall mode.

In an attempt to gain an estimate of its transverse strength, the tracheid wall is treated as a parallel-fibre-reinforced composite. (Crystalline cellulose microfibrils comprise the reinforcing fibres, and they are embedded in an amorphous matrix of hemicellulose and lignin.)Application of a semi-empirical strength criterion shows that under transverse loading, the amorphous matrix is likely to be the first component to fail, with splits forming in a direction parallel to the microfibrils. However, the theory gives no indication as to whether complete wall failure will follow matrix splitting without further increases in load. Therefore, the stresses at which matrix splitting occurs can be assumed to be lower limits to the walls transverse strengths. These are 1.1 and 3.3 Kg/mm^2 for wet and airdry woods respectively.

The effects of strain rate and moisture content on the transverse strength of wood are shown to arise from the properties of the amorphous matrix. The following relationships are derived:

wet matrix strength = 1.8 x wet summerwood strength,

and dry matrix strength = 2.0 x dry summerwood strength.

They are valid at all strain rates. Therefore, the strength of the matrix exhibits a strain rate dependence very similar to that of bulk wood.

The effect of strain rate on the strength of matrix is investigated theoretically. Hemicellulose and lignin (which comprise the matrix) are polymers, and although both have much branched molecules it is believed that the only important intermolecular linkages are due to hydrogen bonding. Because hydrogen bonds are much weaker than covalent bonds, they have a much higher probability of rupture. As an approximation they are assumed to be the only matrix bonds that fail during deformation of the matrix. They also have low dissociation energies, and, therefore, many break each second as a result of thermal excitation. However, since in an unstressed solid there can be no net breakage of bonds, the rate of thermal dissociation must be countered by an equal rate of recombination. When a tensile load is applied to the material, the rate of breaking increases and the rate of recombination decreases, so that there is a net breakage of bonds. The assumption that bond strain energies are equal to changes in the free energies of activation leads to an expression relating applied tensile stresses to the rate of breaking of bonds. This in turn gives a failure stress - failure time relationship that is in good agreement with experimental data.

The theory also suggests that the rupture of matrix hydrogen bonds must be a co-operative process. In dry matrix, bonds must break in groups of eight or nine, or not at all, and in wet matrix in groups of five.

The concentrations of intermolecular linkages are estimated to be 2.1×10^{-2} moles/litre in dry matrix, and 2.4×10^{-2} moles/litre in

wet matrix. However, at any instant of time many of these are dissociated, and the concentrations actually bearing loads are 7.0×10^{-4} moles/litre in dry matrix, and 1.1×10^{-3} moles/litre in wet matrix. (Note that although there are more load carrying linkages in wet matrix the nature of the co-operative process means that they are much easier to deform.)

Finally, application of the above theory to the rupture of covalent bonds in crystalline cellulose leads to the possibility that the strength of the tracheid wall itself is largely independent of strain rate. Variations in measured wood strengths, and in the proportions of springwood tracheids broken in transwall failure, are likely to be due to the properties of the matrix material that binds adjacent tracheids together.

CONTENTS

LIST OF PLATES

INTRODUCTION

Aims

Many of the manufacturing processes utilising wood as a raw material, require it to be split along the grain, into products which range from sheets of wood (as in plywood manufacture) to mangled individual cells (as in papermaking). All such "splitting" processes absorb large amounts of energy, and are, therefore, costly. In fact, a major portion of the costs of many finished products arises from the initial breakdown of wood.

An example is the mechanical pulping process, in which logs are ground to pulp on a massive grindstone. It takes 70 horsepower-days of work to produce one ton of pulp (1 horsepower-day = 7.6×10^7 joules).

The nature of the surfaces produced during the fracture process are also often of importance. In plywood manufacture, sheets of wood have to be glued together. The microscopic morphology of the sheet surfaces is likely to influence the strength of the glued joint. In papermaking, wet fibres are spread out in a flat sheet. As they dry, they are pulled together by surface tension forces, and eventually become hydrogen-bonded together over regions of contact. The

strength of such fibre-to-fibre bonds will be greatly dependent on the shape and stiffness of the individual fibres.

Almost all of the important mechanical reduction processes (sawing, slicing, grinding) result in the high rate fracture of wood. For example, the velocity of the surface of a grindstone used for mechanical production of pulp is nearly 90 miles an hour (40 m/sec.). If a tracheid has to be moved through a distance equal to one tenth of its diameter (3 micrometres) to become separated from its neighbours, the time taken for the fracture process will be of the order of 10^{-7} seconds.

Unfortunately, it has not proved possible to measure strengths and energies at such high fracture rates, but measurements have been made over as wide a range of rates as possible in order to determine trends which may, with some confidence, be extrapolated back to industrial rates.

The aim of the work described in this thesis is to determine and explain the effects of rate of breaking, moisture content, and tracheid structure, on the strength, energy absorbed in fracture, and fracture surface morphology of small samples of Pinus Radiata, broken by

radial tensile forces.

Chapter 1 PHYSICAL AND CHEMICAL STRUCTURE OF SOFT WOOD

1:1 Bulk Structure of Softwood

Softwood consists mainly of an aglomeration of long, hollow, cylindrical cells, which are called tracheids. The cut edge of a block of wood is shown in Fig. 1. The upper half shows tracheids in cross section, the lower half in radial-longitudinal section.

There is considerable variation in tracheid size. Those with large diameters on the right hand side of the photograph were formed while the tree was growing rapidly in spring and early summer (hence are called springwood), whilst the much narrower cells near the centre were formed as the tree was growing slowly in late summer and autumn (and are called summerwood).

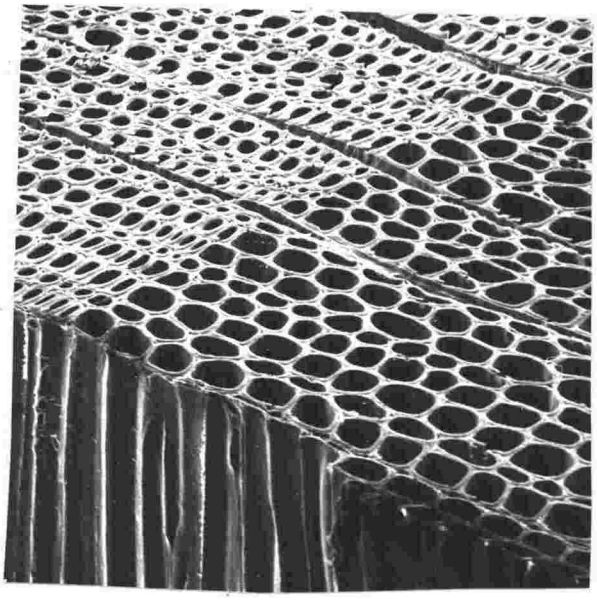

Fig. 1. Scanning electron micrograph of the cut edge of a block of Pinus Radiata. (x 120)

(By courtesy of Mr B. A. Meylan)

When springwood is viewed along the radial direction "R" (from the centre of the tree to the outside) tracheids are well aligned in straight rows, but when viewed along the tangential direction "T" there is no such alignment. In summerwood, tracheids tend to be aligned in both directions. (Note that summerwood and springwood tracheids have similar tangential diameters but greatly different radial diameters.)

Typical tracheid dimensions are -

	Springwood	Summerwood
Tangential diameter (μm)	30	30
Radial diameter (μm)	40	10
Length (μm)	1000 (1mm)	1000

1:2 Layered Structure of the Wood Tracheid Wall

(Reference - Panshin & De Zeeuw (1))

The tracheid wall consists of five distinct layers as shown schematically in Fig. 2.

---

(1) Panshin, A.J., and C. De Zeeuw (1964) (1970) "Textbook of Wood Technology. Vol.1" (McGraw-Hill, N.Y.).

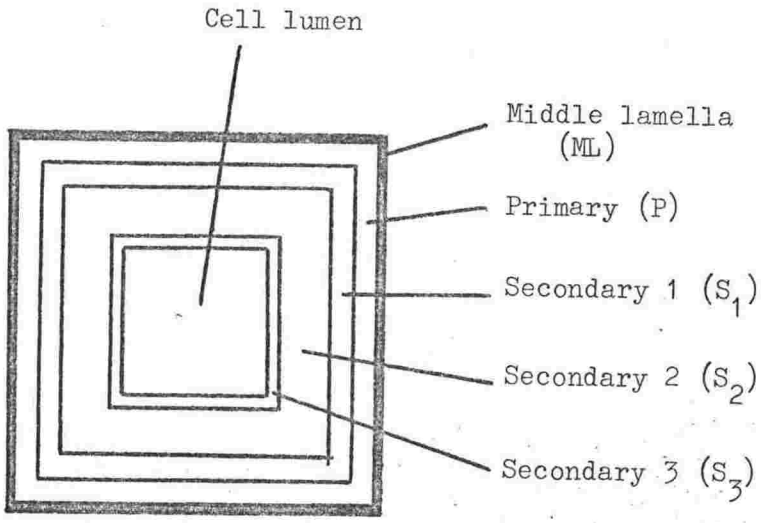

Fig. 2 Cross Section of a Conifer Tracheid.

The outmost layer is called the middle lamella and comprises 75% lignin, 25% hemicellulose. It is completely amorphous and serves to bind adjacent cells together. The remaining four layers all have a fibre reinforced structure. Besides lignin and hemicellulose they contain cellulose in the form of microfibrils. Their properties are summarised in Table 1.

Layer	Percentage Composition			Microfibrillar Orientation
	Cellulose	Hemicellulose	Lignin	
P	10	20	70	Widely dispersed about the mean direction, which is transverse to the tracheid axis.
S_1	25	30	45	Microfibrills are parallel and inclined at angles of ± 80° to the tracheid axis. A crossed structure results.
S_2	50	30	20	Parallel microfibrils at an angle which varies from cell to cell but which is generally in the range 5→40° to the tracheid axis.
S_3	50	30	20	Parallel microfibrils at an angle of 80° to the tracheid axis.

Table 1 : Composition of tracheid wall layers

Fengel, (2) measured the thicknesses of each layer in the tracheid wall for both springwood and summerwood of spruce (Picea Abies). His results showed that the ML, P, S_1 and S_3 thicknesses changed only slightly from springwood to summerwood, but the S_2 showed a threefold increase in thickness. His figures are duplicated in Table 2.

---

(2) Fengel, D. (1969) Wood Sci. and Technol. 3 p.203
"The Ultrastructure of Cellulose from Wood"

	Springwood		Summerwood	
	Thickness (μm)	Linear Distribution (%)	Thickness (μm)	Linear Distribution (%)
P	0.06-<u>0.12</u>-0.20	<u>6.7</u>	0.06-<u>0.11</u>-0.20	<u>2.5</u>
S_1	0.16-<u>0.23</u>-0.29	<u>12.8</u>	0.14-<u>0.30</u>-0.39	<u>6.8</u>
S_2	1.16-<u>1.42</u>-1.73	<u>78.9</u>	2.30-<u>3.99</u>-5.80	<u>89.9</u>
S_3	0.02-<u>0.03</u>-0.04	<u>1.7</u>	0.02-<u>0.04</u>-0.06	<u>0.9</u>
Total	1.52-<u>1.80</u>-2.10		2.72-<u>4.44</u>-6.23	
Tracheid Tangential Diameter	26.4-<u>32.7</u>-38.7		26.4-<u>32.1</u>-38.7	
(Underlined values are means. Others are maxima and minima.)				

<u>Table 2</u> : Thickness of cell wall layers in spruce.

For the Pinus Radiata samples used in the work for this thesis the following measurements were made.

	<u>Springwood</u>	<u>Summerwood</u>
Tracheid Tangential Diameter (μm)	29 ± 7	31 ± 7
Wall Thickness (μm)	1.9 ± 0.45	7.2 ± 1.9

Because the springwood Pinus Radiata wall thickness and cell diameter lie within the ranges given by Fengel for springwood spruce, it has been assumed that -

(a) the mean linear distribution of wall layers will be the same for both species, and

(b) the P, S_1, and S_3 layer thicknesses are the same in springwood and summerwood.

The only layer that varies in thickness is the S_2. In this way the following values were obtained for the thicknesses of wall layers in Pinus Radiata (table 3).

	Springwood		Summerwood	
	Thickness (μm)	Linear Distribution (%)	Thickness (μm)	Linear Distribution (%)
P	0.13)	6.7	0.13)	1.8
S_1	0.24)	12.8	0.24)	3.3
S_2	1.50) each ± 20%	78.9	6.80) each ± 20%	94.5
S_3	0.03)	1.7	0.03)	0.4
Total	1.9 ± 0.45		7.2 ± 1.9	
Tracheid Tangential Diameter	29 ± 7		31 ± 7	

Table 3 : Thickness of tracheid wall layers in Pinus Radiata.

1:3 Ray Cells

Ninety-five per cent of a softwood consists of tracheids. The remaining 5% is made up of thinwalled cells which extend from the centre of the tree to the outside, i.e. in a radial direction. They are called ray cells. Three are shown in Fig.1.

Their major function is horizontal transport of fluids rather than mechanical support, so that they are weak, thinwalled cells. This,

coupled with the fact that they generally occur in vertically aligned groups of five to ten cells, means that they are a source of weakness in wood.

1:4 Intertracheid Pitting

Since one of the functions of tracheids is the conduction of water from the roots to the leaves there must be some means of communication between adjacent tracheids so that water can pass from one to another.

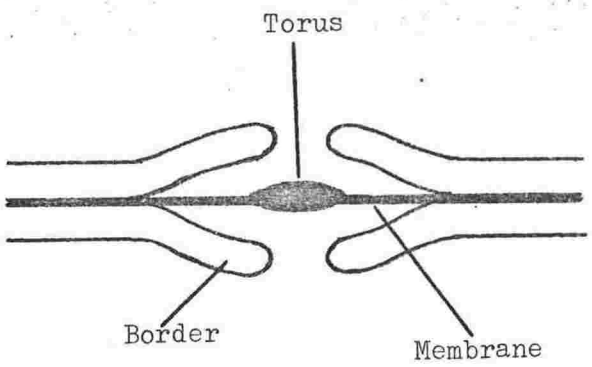

Fig. 3 Cross Section of a bordered pit.

This is provided by means of structures called pits, which are simply holes through the tracheid walls. They are covered by a thin membrane and in conifers are bordered by dish like extensions of the S_2 and S_3 wall layers. Each border has a hole in its centre. The centre of the covering membrane is thickened and impervious to moisture (a region called the torus), so that in conditions of drying on one side, the torus can press against the border to prevent the flow of water.

Pits occur mainly on the tangential faces of tracheids, and if this surface is exposed their distinctive structure leads to an easy identification of the location of the failure plane. When the interior

of a pit can be seen, splitting within the cell wall has occurred, but when the convex pit border is in place, fracture must have crossed the cell walls exposing the cell lumen.

A cross section of a pit is shown in Fig. 3 and many pits are shown in Figs. 16 to 22.

1: 5 Molecular Structure

About 70% of the dry weight of wood consists of a material called holocellulose (cellulose and substances related to it), and most of the remaining 30% of lignin.

Nearly two thirds of the holocellulose is made up of α -cellulose. This is a very high molecular weight substance which is formed by the condensation of β -glucose molecules. The degree of polymerisation is between 5000 and 10,000. Since a glucose unit is 5 Å in length, a cellulose molecule is about 50,000 Å, or 5 μm, in length.

The basic repeating unit is formed from two glucose units, one rotated through 180° with respect to the other. This unit is termed a cellobiose unit and is shown in Fig. 4.

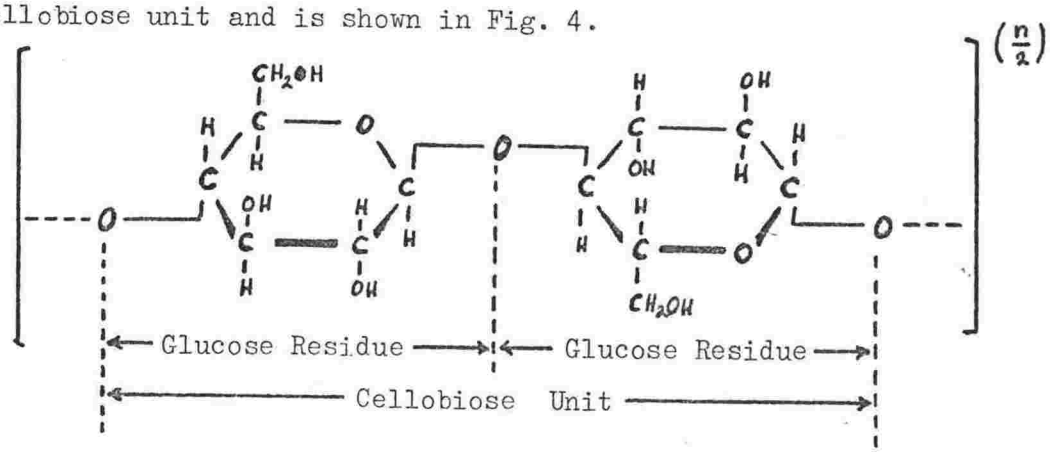

Fig. 4 Structure of α-cellulose.

The remaining third of holocellulose is known as hemicellulose. It is alkali soluble and yields on hydrolysis the C_6 sugars galactose and mannose, the C_5 sugar xylose, and some uronic acid. It has, therefore, been inferred that polymers of these substances must exist in wood and are referred to as galactan, mannan, xylan and polyuronide respectively. (The basic repeating units of polyuronide and xylan are shown in Fig.5.) These polymers are not long chain molecules like cellulose but are smaller, branched molecules. The degree of polymerisation of the backbones is only about 200. (Jane (3)).

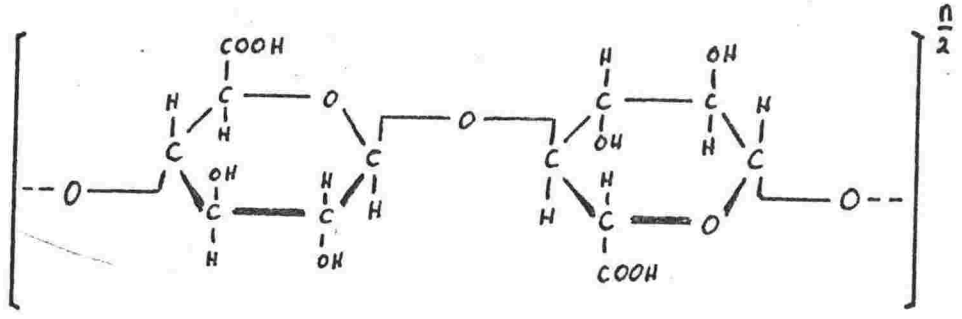

(a) Polyuronide

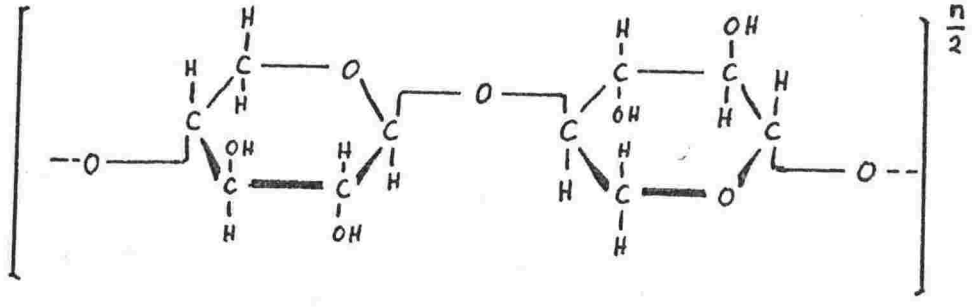

(b) Xylan

Fig. 5 Structures of polyuronide and xylan.

(3) Jane, F.W. (1970) "The Structure of Wood" (Adam & Charles Black, London) p.162

The remaining 30% of wood is made up of lignin. Its structure is not well known but is thought to consist of a complex arrangement of coniferyl units similar to those shown in Fig. 6. Freudenberg (4) postulates a much branched structure formed from 15 such units.

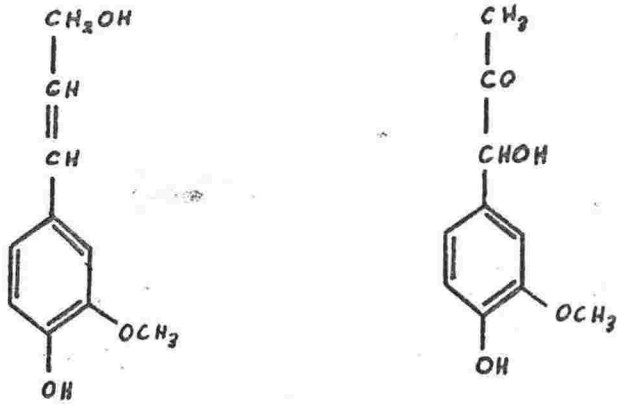

Fig. 6 Coniferyl units : Basic Repeating units of Lignin.

1:6 Crystalline Structure of α- Cellulose

(Reference : Roelofesen (5), Stamm (6), Mühlethaler(7))

The long flat, ribbon-like α-cellulose molecules readily bond together to form a regular crystalline array. The molecules lie parallel to one another and are transversely linked by hydrogen-bonds.

---

(4) Freudenberg, K. (1962) "Biogenesis and Constitution of Lignin" ~~in "Proc. of the Wood Chemistry Symposium, London." (Butterworth)~~. Pure and Applied Chemistry 5 pp 9-20

(5) Roelofsen, P.A. (1959) "The Plant Cell Wall" (Gebruder Borntrager, Berlin).

(6) Stamm, A.J. (1964) "Wood and Cellulose Science" (Ronald Press Co., N.Y.).

(7) Mühlethaler, K. (1964) in W.A. Côté Jr. (Ed). "Cellular Ultrastructure of Wood Plants" (Syracuse Univ. Press, Syracuse).

These may form between two "OH" groups, or between an "OH" group and the "O" atom in the glucose ring structure.

The generally accepted "unit cell" of crystalline cellulose is that proposed by Meyer and Misch in 1937, on the basis of x-ray diffraction data. Their unit cell, together with dimensions, is shown in Fig. 7.

However, unlike inorganic crystalline materials, cellulose is not completely crystalline. The evidence for the existence of non-crystalline cellulose is as follows :

(i) the specific weight of cellulose, even when determined with helium, or fluids which can penetrate the finest pores, is lower than that calculated from the contents and dimensions of the unit cell, and

(ii) cellulose is hygroscopic, but x-ray measurements show that the dimensions of the unit cell do not change when cellulose takes up moisture. Therefore, water molecules cannot be penetrating the crystalline cellulose.

X-ray analysis also shows that on the average, a crystalline region (or crystallite) is only 50 → 100 Å wide, and 600 Å long. Compared with the 50,000 Å length of a cellulose molecule, the length of a crystallite is very small. Therefore, each cellulose molecule must pass through, and link, many crystallites.

The resulting structure is shown in Fig. 8. Cellulose consists of

many such small crystallites, with their longitudinal axes roughly parallel, and separated from one another by regions of amorphous structure.

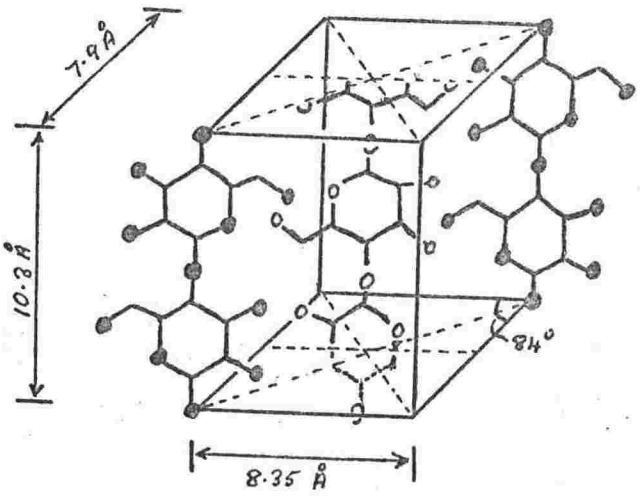

Fig. 7 Unit cell of crystalline cellulose.

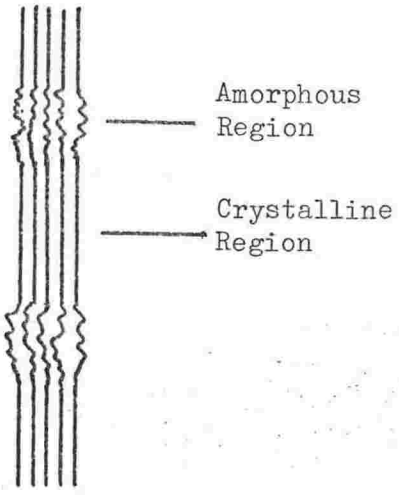

Fig. 8 Crystallites and amorphous cellulose.

In the plant cell wall, crystallites such as those shown in Fig. 8 are grouped together to form long, flat, ribbon-like structures called microfibrils. These are between 100 Å and 250 Å wide, 30 Å deep, and up to 10 μm long. They are one of the basic structural units of the cell wall, and act as reinforcing fibres. Whether or not they are actually discrete fibres is uncertain. Roelofsen (5) lists evidence both for and against this possibility, with the majority of writers favouring the view that microfibrils anastomose. Therefore, it seems that it is a good approximation for the purposes of theoretical calculations to assume that microfibrils are discrete, but infinitely long, reinforcing fibres.

1:7 Physical Structure of Hemicellulose and Lignin

In hemicellulose and lignin, hydrogen bonding is again the major type

of intermolecular bonding. Covalent crosslinks between molecules are thought to be rare. (Hirst (8), Freudenberg (4)).

However, regions of ordered structure, like those of crystalline cellulose, are not found. The molecules form a random network, and any two molecules will be bonded together only over the relatively small areas of close contact. This means that both the density of the material and the density of hydrogen bonding within the material will be lower than in crystalline cellulose.

Hemicellulose and lignin are amorphous and together with α-cellulose microfibrils, make up the fibre reinforced structure of the wood cell wall.

1:8 Sorption of Moisture by Wood

Adsorption is the intimate uptake of a gas, liquid from vapour phase, or solute from solution, by a fine powder, a porous material or a swelling gell substance. In many cases it is a mono-molecular, and in polymolecular cases rarely exceeds 10 molecules thick. Considerable adsorption can occur at low vapour measures (which is not true for absorption, which is the mechanical uptake of a liquid by a porous solid within its gross capillary structure as a result of surface tension forces).

The attractive force of the adsorbate for the adsorbent may be considerably greater than the attractive forces of the adsorbate for itself. In all cases adsorption is accompanied by the evolution of heat.

---

(8) Hirst, E.L. (1962) "Chemical Structure of the Hemicelluloses" ~~in "Proceedings of the Wood Chemistry Symposium, London" (Butterworths)~~. Pure and Applied Chemistry 5 pp 53-66

In wood, water may be held in one of four ways -

1. Water of constitution which can be released only by thermal degradation of wood. (The chemical formula for cellulose is $(C_6H_{10}O_5)^n$ which contains hydrogen and oxygen in the ratio 2 : 1, as in water.)
2. Mono-molecularly held water, which is believed to be held on exposed surfaces by hydrogen bonding.
3. Water held in solid solution in the wood substance. Solid-solid interfaces are replaced by solid-liquid-solid interfaces. (Wood can hold up to 30% of its own weight of water by means of methods 2 and 3.)
4. Capillary condensation in the tracheid lumen. Wood can absorb a further 150% of its weight of water by this means.

Uptake by methods 2 and 3 is true adsorption, and arises because of the large numbers of hydroxyl groups present in wood material. Hydrogen bonding between an "OH" group of a holocellulose or lignin molecule and a water molecule is possible provided the water molecule is able to approach close to the "OH" group. The open structures of hemicellulose and lignin are easily penetrated by water molecules, so that these materials will adsorb much water. Because intermolecular bonds occur in small groups, it is possible for water molecules to break these and enter into the structure. Molecule ... molecule H-bonds are replaced by molecule ... water ... molecule bonds, as illustrated in Fig. 9.

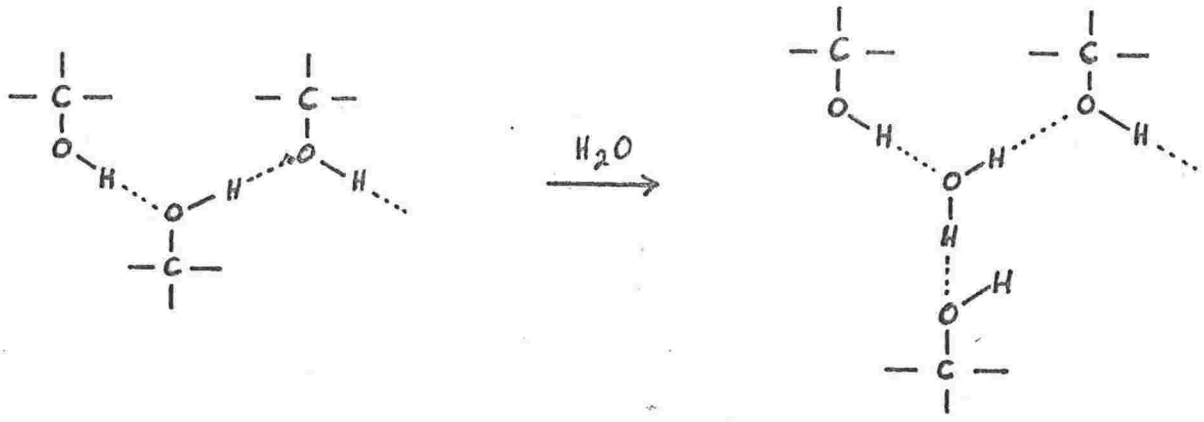

Fig. 9 : Adsorption of water by holocellulose and lignin.

Kauman (9) estimated that 6% of the hydroxyl groups that are available for the adsorption of water take part in intermolecular bonding. Therefore, approximately 3% of the adsorbed water may form linkages between molecules as shown in Fig. 9.

On the other hand, crystalline cellulose is too strongly bonded to be penetrated by water molecules. The only ways in which cellulose can take up moisture are by adsorption on the surfaces of crystallines, and in the amorphous regions between crystallites.

---

(9) Kauman, W.G. (1966) Holz als Roh - und Werkstoff 24(11) p.551 "On the Deformation and Setting of the Plant Cell Wall".

Chapter 2 PREVIOUS WORK

2:1 Effects of Strain-rate on Strength, Maximum Strain and Energy Absorbed during Fracture

It has long been known that the strength of wood, or wood-based materials, increases as the rate of loading is increased. Some of the earliest measurements on wood were tabulated by Garrett (10) after a series of tensile tests parallel to the grain. His figures are plotted in Fig. 10, in which relative strength is plotted against log (time). More recently, Rance (11) recorded the times to failure for similar strips of paper under static loads. He observed a nearly linear relationship between applied load and the logarithm of time to failure, over most of his range of loads. (See also Fig.10.) At the same time the breaking strain of the paper appeared to remain constant.

Steenberg (12) carried out some impact tests in which the time to failure was about one millisecond. He states that increasing the rate of loading by one million times results in a tenfold increase in the breaking load of newsprint. Once again maximum strain did not vary significantly.

---

(10) Garrett, G.A. (1931) "The Mechanical Properties of Wood" (Chapman & Hall, London) p.159.

(11) Rance, H.F. (1948) Proc. Papermakers' Assn. G.B.I. 29 p.449 "Some New Studies on the Strength Properties of Paper".

(12) Steenberg, P. (1949) Pulp. Pap. Mag. Canada 50(3) p.207 "Behaviour of Paper Under Stress and Strain".

Liska (13) carried out a series of tests in flexure and compression parallel to the grain on Sitka Spruce, Douglas Fir, Maple and Birch specimens at approximately 12% moisture content. The modulus of rupture and ultimate compressive strength increased as the time to failure decreased. For failure times in the range 0.3 sec to 750 secs, the increase was approximately 8% for a tenfold increase in loading rate. The effects of the loading rate on the modulus of elasticity, and deformations to maximum load, were insignificant. Work to maximum load showed a slight increase as loading rate was increased.

Liska's work was extended a few years later by James (14) who carried out bending tests on red oak, yellow birch and sweetgum in both green and airdry conditions. His results were very similar to Liska's; but there were some important additional observations. For example, the increases in strength and work to maximum load, as strain rate was increased, were greater for green wood than for airdry wood. The two bending rates he used differed by a factor of 10^4, giving failure times of 0.1 secs and 1200 secs. The increases in strength and in work to maximum load he observed (on increasing the bending rate by 10^4) are given below -

---

(13) Liska, J.A. (1955) For. Prod. Lab. Report No. 1767 "Effect of Rapid Loading on the Compressive and Flexural Strength of Wood".

(14) James, W.L. (1962) For. Prod. J. p.253. Vol. 12(6) "Dynamic Strength and Elastic Properties of Wood".

	Increase in Strength	Increase in Work to Maximum Load
Green Wood	45%	30%
Airdry Wood	30%	20%

In both cases green wood shows a 50% greater increase than does dry wood. This suggests that perhaps the water absorbing components of the wood cell wall, are also the strain-rate sensitive components.

Panshin & De Zeeuw (1) quote figures covering a very wide range of rates for tensile strengths parallel to the grain.

Strength Ratio	1.40	1.14	1.00	0.85	0.65	0.35	0.25	0.20
Time to Failure (secs)	1	60	240	3.6×10^3	8.6×10^4	3.15×10^7	3.15×10^8	1.58×10^9
	1 sec	1 min	4 min	1 hour	1 day	1 year	10 years	50years

To explain these results they assumed that failure occurs when a certain critical strain is reached. At long times, viscous flow (creep) is able to occur, and, therefore, failure occurs at lower loads.

Ylinen (15) also attempted to explain this type of phenomenon in wood by assuming that failure occurs at the same strain regardless of rate of breaking. Combining this with Maxwell's relaxation theory he obtained

---

(15) Ylinen, A. (1959) Holz als Roh - und Werkstoff 17(6) p.231 "On the Influence of the Rate of Deformation Upon the Ultimate Strength of Wood". (In German).

the following expression for breaking stress -

$$\sigma_B = Y_\infty \varepsilon_B + \dot{\varepsilon} t \left(Y - Y_\infty\right)\left(1 - e^{-\varepsilon_B/\dot{\varepsilon} t}\right)$$

σ_B = breaking stress

ε_B = breaking strain

$\dot{\varepsilon}$ = strain rate

Y = Young's modulus (Y_∞ is the long term Young's modulus).

t = time.

He was able to fit a curve to his results, but unfortunately the data he quotes covers only a very limited range of strain rates, and does not confirm the changes in gradient of his theoretical curve. Furthermore, the model is phenomenological and takes no account of the physical and chemical structure of wood.

The next major step was to treat the rheological properties of wood as though they were rate processes. Kingston & Clarke (16) treated creep in wood as though it was a chemical reaction, and were able to calculate an activation energy for the process. This work and that of others was reviewed by Kauman (9) who also pointed out that the "activation energies" and "heats of reaction" of many of the rheological properties of wood are similar in magnitude to activation energies and heats of reaction of chemical reactions involving the rupture of hydrogen bonds. This suggests

---

(16) Kingston, R.S.T., and L.N. Clarke (1961) Aust. J. Appl. Sci. 12(2) p.211 "Some aspects of the Rheological Behaviour of Wood".

that the rheological properties of wood may be governed by hydrogen-bonding.

Indeed, this idea was used by Nissan (17, 18) to explain the stress-relaxation behaviour of paper. He assumed that all deformation is due to the extension of hydrogen-bonds. Further, stress-relaxation occurs because thermally dissociated bonds are able to reform in a non-stressed conformation. The decrease in the number of load carrying bonds results in a decrease in Young's modulus, and hence a decrease in stress.

The breaking of H -bonds is a rate process, and is, therefore, governed by the following equation -

$$-\frac{d(N/N_o)}{dt} = k_2 (N/N_o)^n$$

N_o = density of bonds at t = o

N = density of bonds at time t

k_2 = reaction-rate constant.

Exponent "n" (the order of the reaction) represents the number of bonds that must break simultaneously in order for a relaxation unit to pass from a stress-supporting state to an unstressed state. For paper, "n" was found to be 6.0. In other words, bonds must break in groups of 6 or not at all.

(17, Nissan, A.H. (1957) Trans. Farady Soc. 53 p.700 "The Rheological Behaviour of Hydrogen-bonded Solids".

(18) _____ and S.S. Sternstein (1962) ~~Proc. Wood. Chem. Symp., Montreal p.131~~ Pure and Applied Chemistry 5 p 181 "Cellulose as a Viscoelastic Material"

Similar work on cellophane yielded a value for "n" of 3.0. Nissan attributed this lower value to the presence of a small amount of plasticiser in the cellophane.

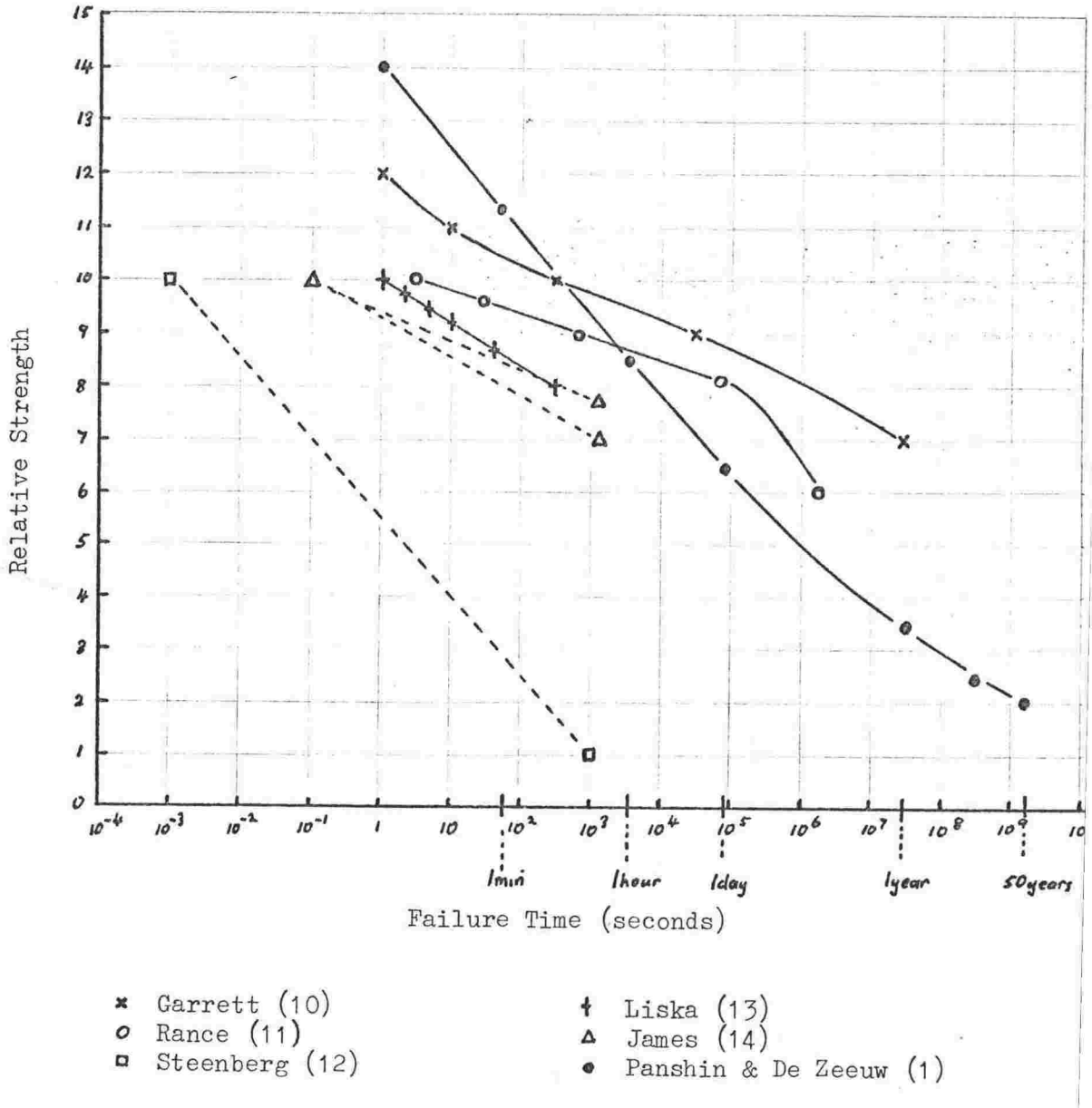

Fig. 10 Summary of Previous Work on the Effects of Strain Rate on the Strengths of Wood and Paper.

2:2 Effects of Moisture Content on Strength

The moisture content of wood is expressed as a percentage of the oven-dry weight of wood (i.e. the weight of wood at zero moisture content). If the weight of a sample containing no moisture is m_o and the weight of the same sample containing water is m_w, the moisture content of the wood is given by the formula -

$$M.C. = \frac{m_w - m_o}{m_o} \times \frac{100}{1} \%$$

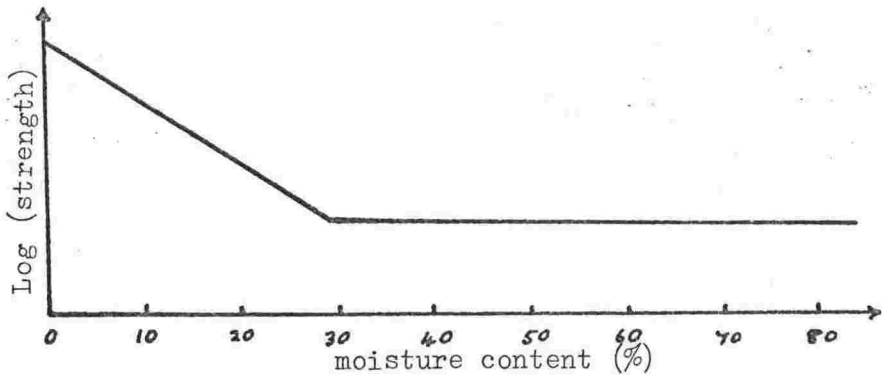

Fig. 11 Variation of strength with Moisture Content

The relationship between moisture content and strength is illustrated in Fig. 11. Wood strength decreases as moisture content is increased until a moisture content known as the fibre-saturation-point (f.s.p.) is reached. In this range, the relationship between logarithm strength and moisture content is nearly linear. F.s.p. varies from species to species, but is generally near a moisture content of 30%.

For increases in moisture content beyond f.s.p., no further change in strength occurs. On referring back to section 1:8 the reasons for this behaviour become clear. While water is being taken up by adsorption

within the tracheid wall material, the properties of the wall and hence of bulk wood will change, since adsorbed moisture takes part in intermolecular bonding in amorphous wall components. Because the adsorption reaction is exothermic (i.e. heat is evolved as water is adsorbed) adsorption will occur even when the relative humidity (Rh) of the surrounding air is very low (only a few percent). However, the tracheid wall can take up no more than 30% of its own weight of water. Any further uptake must be by capillary condensation within the tracheid lumen. Water taken up in this way can have no effect on wall material, and so has no effect on wood strength. Capillaries of the size of a tracheid lumen (about 30 μm diameter) will not full with water until very high Rh's are reached. Stamm (6) states that a capillary with 21 μm diameter will not fill with water until the Rh of the surrounding air is 99.99%. At such Rh's adsorption will be complete, so no further changes in cell wall properties can occur. Therefore, wall properties will not vary as the tracheid lumen is being filled.

2:3 Effect of Moisture Content on Energy Absorbed during Fracture

When a solid is fractured, large numbers of bonds are broken, and energy must, therefore, be supplied in order to produce the new surfaces. Griffith (19) postulated that this energy (called the surface energy) is supplied by the release of elastic strain energy stored in the body. A second postulate was that all bodies contain microscopic cracks or

---

(19) Griffith, A.A. (1921) Phil. Trans. Roy. Soc. A 221 p.180 "The Phenomena of Rupture and Flow in Solids".

flaws and it is the propagation of one or more of these cracks that leads to failure. Such a crack will propagate only if the strain energy released by its propagation is greater than the energy required for the formation of the new surfaces. Using this energy balance criterion of fracture, Griffith derived an expression for the tensile strength of a solid containing a single elliptically shaped crack passing right through the solid, when a tensile force is applied in a direction perpendicular to the crack.

The expression is:

$$\sigma = \left(\frac{4 Y \gamma}{\pi d}\right)^{1/2}$$

σ = tensile stress
Y = Young's modulus
γ = surface energy
d = crack length

Griffith verified this expression for the brittle fracture of glass, and the surface energies he obtained agreed well with those obtained by other methods. $(0.1 \rightarrow 1.0$ joules/$m^2)$.

The above equation may also be applied to ductile fracture, provided the plastic deformation is confined to a thin layer near the crack surfaces, and the bulk of the specimen remains in a state of elastic strain. The only change necessary is that the surface energy γ be replaced by an effective surface energy γ', where γ' is the sum of the surface energy and the plastic work dissipated in the formation of unit surface area.

Atack, May, Morris & Sproule (20) applied Griffith's theory to the fracture of green spruce under tensile loading perpendicular to the grain. They obtained a relationship between crack length and tensile strength of the form $\sigma = k d^{-0.6}$ which is close to the Griffith formula of $\sigma = k d^{-0.5}$. The effective surface energy, γ', was 10^2 Joules/m^2 showing that much plastic deformation must have occurred. Scanning electron micrographs showed that extremely complex surfaces were produced.

A series of low rate cleavage tests were carried out by Porter (21) on White Pine to determine the effects of moisture content and temperature on the effective surface energy. At -195°C and at moisture contents from 0 to 30%, γ' had a value of 1.4×10^2 Joules/m^2. At higher termperatures (20 → 80°C), the value of γ' increased with increasing moisutre content, as shown in Fig. 12. This increased energy was attributed to the viscous flow of molecules, which would be reduced at low temperatures and moisture contents.

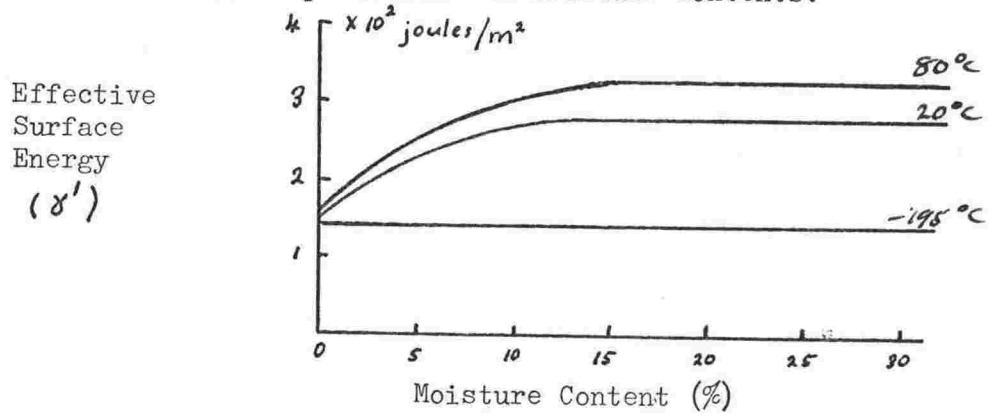

Fig. 12 Variation of Fracture Surface energy in wood with moisture content and temperature.

---

(20) Atack, D., W.D. May, E.L. Morris & R.N. Sproule. (1961) Tappi 44(8) p.555 "The energy of Tensile and Cleavage Fracture of Black Spruce."

(21) Porter, A.W. (1964) For. Prod. J. 14(8) p.325 "On the Mechanics of Fracture in Wood".

Debaise, Porter & Pentoney (22) attempted to verify this by detecting and counting the acoustic emissions that occur during crack growth. They observed that at low temperatures and moisture contents the crack propagated in a few large unstable movements, whereas at high temperatures and moisture contents, crack growth was slower and more stable. They stated that slow stable crack growth would take place within the cell wall (intrawall failure), and that rapid crack growth resulted in complete fracture across the tracheid wall (transwall failure). The decrease in transwall failure at high temperatures as observed by Koran (23, 24) tends to verify this.

2:4 Surfaces Produced by Fracture

When wood is split by radial or tangential tensile loads there are two quite distinct locations for the fracture plane.

The first, shown by a ... a in Fig. 13 results in a splitting across the tracheid wall and is called transwall failure. The tracheid is split into two portions, exposing its lumen.

The second type of failure, b ... b is a splitting within the tracheid wall, and is called intrawall failure. It results in the separation of

---

(22) Debaise, G.R., A.W. Porter & R.E. Pentoney (1966) Materials Res. & Std 6(10) p.493 "Morphology and Mechanics of Wood Fracture".

(23) Koran, Z. (1966) P.P.R.I.C. Technical Report No. 472. "Electron Microscopy of Black Spruce Fibre Surfaces Separated by Tensile Failure at Various Temperatures".

(24) _____ (1967) P.P.R.I.C. Technical Report No. 514 "Electron Microscopy of Tangential Tracheid Surfaces of Black Spruce Produced by Tensile Failure at Various Temperatures".

Also:

(23) Koran, Z. (1967) Tappi 50(2) p 60

(24) —— (1968) Svensk Papperstidning 17(15) p 567

two adjacent tracheids without the splitting of either.

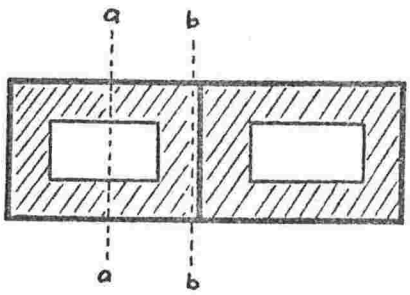

Fig. 13 Trans and Intrawall Failure

Koran (23,24) measured the relative amounts of the two types of failure that occurred when samples of Black Spruce were split in tension by radial and tangential forces. By means of transmission and scanning electron microscopy he was able to show that intrawall failure always occurred within the P or S_1 layers of the tracheid wall; but never in the M.L., S_2, or at the S_1, S_2 interface. At a strain rate of 0.1 sec^{-1} and at $0^{\circ}C$, fifty per cent of the tracheids in the fracture surface were broken in transwall failure. As the temperature was raised to $150^{\circ}C$, the amount of transwall failure decreased by 77%, and the strength of the samples decreased by 82%. The decrease was almost linear in each case over this range. Koran attributed these decreases to thermal softening of lignin and hemicelluloses. (Transwall failure requires the splitting of many cellulose microfibrils, whereas intrawall failure, which is a splitting between layers of microfibrils, results in the breaking of very few.)

As an extension to Koran's work the effects of moisture content, strain rate, and wood density on transwall failure will be examined in Pinus Radiata.

Chapter 3 EXPERIMENTAL RESULTS

3:1 Introduction

Small rectangular specimens of Pinus Radiata were broken by radial and tangential tensile loads, at strain rates ranging from 2×10^{-6} sec^{-1} to 10^{2} sec^{-1}. Load and extension were recorded continuously, so that the stress at failure, strain at failure, and the energy absorbed in the fracture, could be determined. After failure, the fraction of cells broken in the transwall mode was determined by microscopical examination of the fracture surfaces.

Specimen details are given in Fig. 14. Faces of the specimens were cut parallel to the major axes of the tree as shown. (Note that failure in a "tangential" plane ("tangential" failure) results from radial loading, and vice versa.) Symmetrical notches were cut at the centres of the specimens so that the fracture plane could be located in the desired regions of the growth ring.

Attachment to the specimens was via small aluminium blocks which were glued to each end with "Araldite" epoxy resin. Provided the specimen was kept dry until the adhesive had hardened, it could later be soaked without serious weakening of the joints. Only a few specimens failed at the glued surfaces during the tests.

The remaining conditions of fracture to be varied were moisture content and "structure". Specimens were broken in both saturated and airdry states, and in the springwood and summerwood regions of

the growth ring.

Further details of the fracture conditions, and the design and limitations of loading and recording equipment are given in appendix 1.

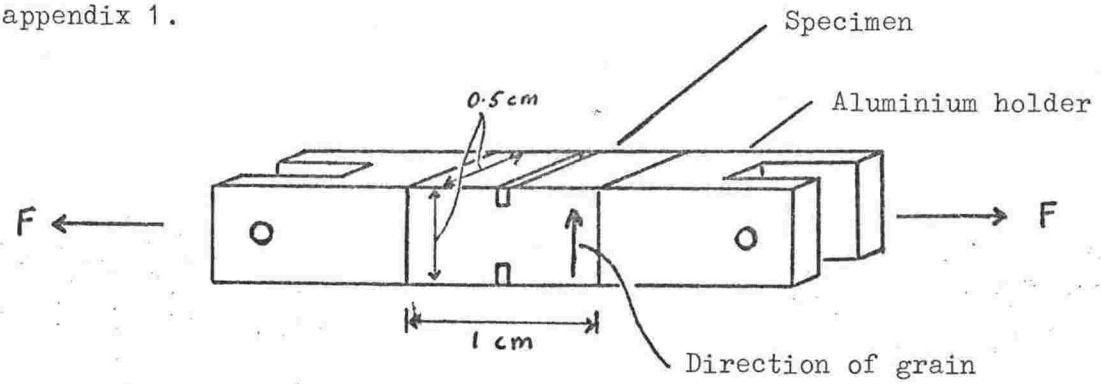

(a) Specimen shape and dimensions.

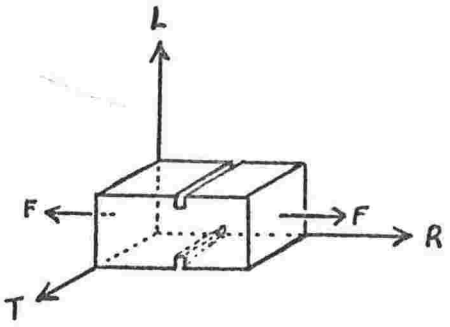

"Tangential" Fracture

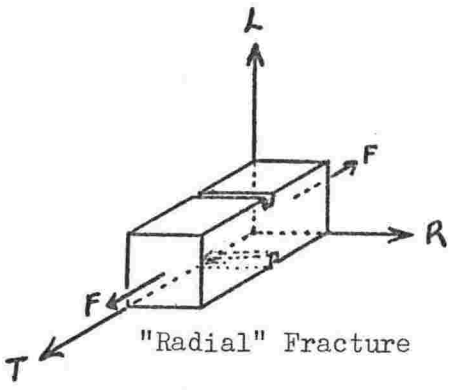

"Radial" Fracture

(b) Specimen Orientation

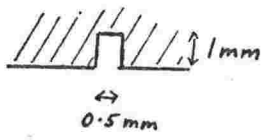

Summerwood

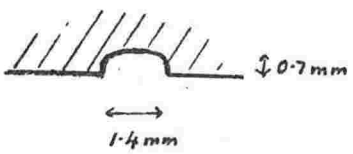

Springwood

(c) Notch Dimensions

Fig. 14 Specimen Details

3:2 Fracture Surface Morphology

Both scanning electron microscopy and optical microscopy were used to examine the surfaces produced during fracture. As in Koran's fracture experiments, both trans and intrawall types of failure were observed, but the form of the transwall failure differed from radial fracture to tangential fracture. The amount was greatly dependent on all three variables, rate of breaking, moisture content, and bulk density.

Radial Transwall Failure

Fig. 16 shows an example of the type of transwall failure that occurs during radial fracture. In the upper and lower portions of the photograph, failure is intrawall, but in the centre it is transwall. (The vertical cells are tracheids, the horizontal ones are ray cells.) The fracture plane seems to have sliced diagonally across a layer of tracheids, as shown schematically in Fig. 15(a). Only a small portion of the lumen of each tracheid is exposed. It seems that the fracture plane has shifted from one intrawall position to another intrawall position, one tracheid lower.

Fig. 15(a) Radial Transwall Failure

Fig. 15(b) Tangential Transwall Failure

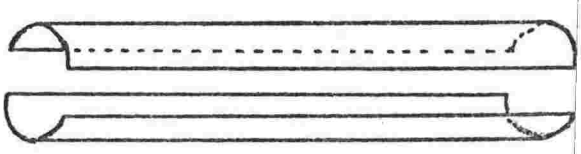

A likely reason for this behaviour is that splitting has been

initiated and has spread in two different planes, which were displaced in a radial direction by one or more tracheid thicknesses. The two fractures can join only by passing around the ends of the interleaving tracheids, or by splitting through them. The latter results in transwall failure.

Fig. 17 is a higher magnification view of radial transwall failure. The central broken tracheid wall is flanked by bordered pits. As the pit borders are complete, intrawall failure has not occurred. (The two horizontal grooves are artifacts produced by the electron beam.)

Tangential Transwall Failure

The type of transwall failure that occurs during tangential fracture is illustrated in Figs. 15(b) and 25. Fig. 25 shows a mixture of trans and intrawall failure. The tracheids indicated by arrows have been split along their length in transwall failure and show relatively smooth lumen interiors. The others show the rougher surfaces produced by intrawall failure. (Note the absence of pits.)

Fig. 18 shows where transwall failure has crossed a pit, splitting it in two. Figs. 19 and 20 were obtained by cutting away part of the fracture surface to expose the ends of the broken tracheids. They show both trans and intrawall failure.

Intrawall Failure

Examples of intrawall failure are given in Figs. 21 to 23 and 25 to 29. The features of this type of failure seem to be very similar to those described by Koran (23,24). Failure occurs in a layer that is reinforced by fibres lying almost perpendicularly to the tracheid longitudinal axis (as evidenced by the lines of tearing in Fig. 21). The only such layer is the S_1. In some cases a crossed pattern is observed on the exposed surface, which is further evidence that the exposed layer is the S_1. The lower right corner of Fig. 21 shows signs of such a crossed pattern.

Failure does not seem to occur in the middle lamella, and only rarely is any S_2 surface exposed.

Fig. 22 shows the effect of radial intrawall failure through pits. All of the upper borders have been removed, and in the L.H. row the membranes and torus' have also been torn away, exposing the lower border. Fig. 23 shows a common type of serrated tearing.

3:3 Measurement of Transwall Failure

To obtain estimates of the proportion of surface area exposed by transwall failure, 40 micron thick cross sections of the fracture surface were examined at a magnification of 250x in a light microscope. Tracheids along the section edge that were broken away by transwall failure were counted, and the number expressed as a percentage of the total number of tracheids along the edge. (See Fig. 24.) Two sections were examined for each specimen. The figure obtained was

called the "percentage transwall failure" of the specimen, and was equated with the percentage of surface exposed by transwall failure. This is a reliable procedure for tangential failure, as tracheids broken in transwall failure are evenly distributed over the fracture surface. However, in the case of radial fracture, "patches" of transwall failure occur, so this method gives questionable results. For this reason, and for others listed below, it was decided to carry out detailed tests in tangential failure only.

Reasons for neglect of radial fracture -

(a) Transwall failure in radial fracture does not seem to be dependent on tracheid wall properties. Rather it seems to be dependent on the simultaneous occurrence of two or more areas of splitting, on different levels. This in turn will depend on the distribution of "defects" within the sample. (Ray cells may in fact constitute such defects.)

(b) The properties of springwood and summerwood cannot be examined separately unless very small specimens are used.

Effects of Strain Rate, Moisture Content, and Density on the Tangential Splitting of Wood

3:4 Transwall Failure

Fig. 30 shows the effects of rate of breaking, moisture content, and bulk density on percent transwall failure. (For later convenience the independent variable plotted is time to failure, but corresponding strain rates are indicated.) It can be seen that all three variables

are important. They are briefly examined below -

Bulk Density

Percent transwall failure decreases as bulk density increases. In fact, for summerwood, the amount of transwall failure is almost negligible. The reasons for the lower percent transwall failure in summerwood are -

(a) the summerwood tracheid walls are much thicker (about four times as thick as springwood ones), and

(b) there is very little tangential overlap between tracheids in the fracture plane. In fact, in summerwood, the fracture surface is often almost flat. (See Fig. 24(b)).

Moisture Content) Because of the large interaction, it is
Strain Rate) easier to consider these together.

In airdry wood, percent transwall failure does not vary with strain rate. It is constant at 20%. In saturated wood, percent transwall failure increases dramatically as strain rate increases.

Photographs showing the surfaces produced are given in Figs. 25 to 29. Fig. 25 shows wet springwood broken at a strain rate of 10^{2} sec^{-1}. Fifty percent of the tracheids are split lengthways. Fig. 26 shows wet springwood broken at a strain rate of 10^{-4} sec^{-1}. Only a few tracheids are broken and most of these show the fibre-shortening type of failure discussed by Koran. It seems that the longitudinal splitting of tracheids occurs only at the higher rates of breaking. Fig. 27, which is very similar to Fig. 26, shows wet summerwood

broken at the high strain rate. Transwall failure is rarely seen.

Fig. 28 shows wet summerwood broken at a low strain rate. Again transwall failure is rare, and many tracheids appear to have been partially pulled away from the surface.

The surfaces produced during the fracture of dry wood do not vary greatly in appearance from springwood to summerwood, and from high to low strain rates. A typical example is shown in Fig. 29. The surfaces are always very much rougher than the corresponding wet wood ones.

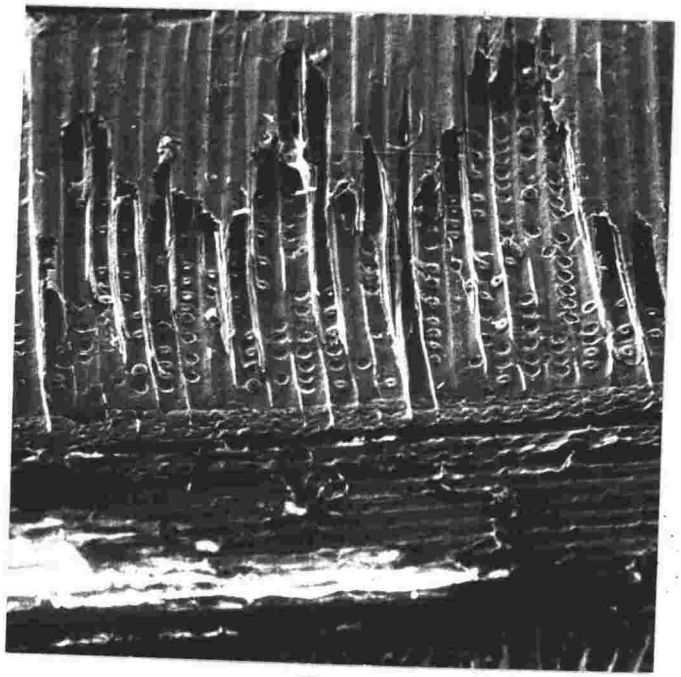

Fig. 16 : Radial Transwall Failure (x 110).

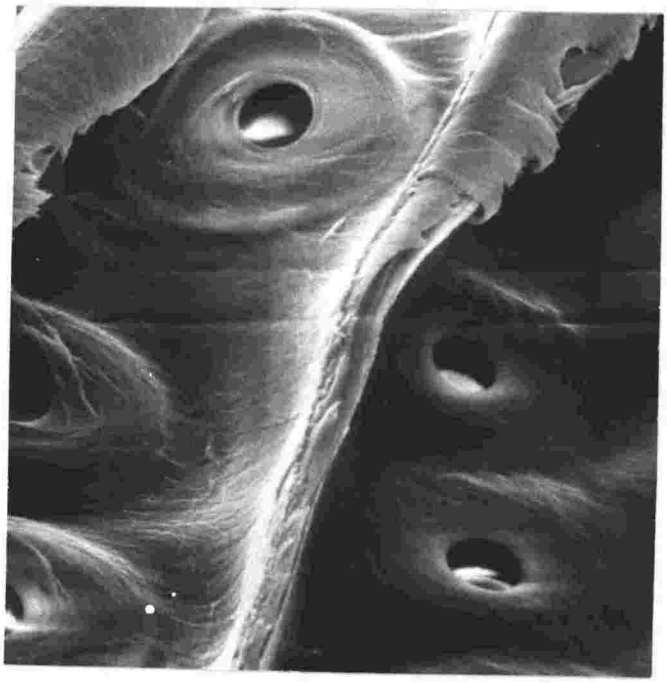

Fig. 17 : Radial Transwall Failure (x 1900).

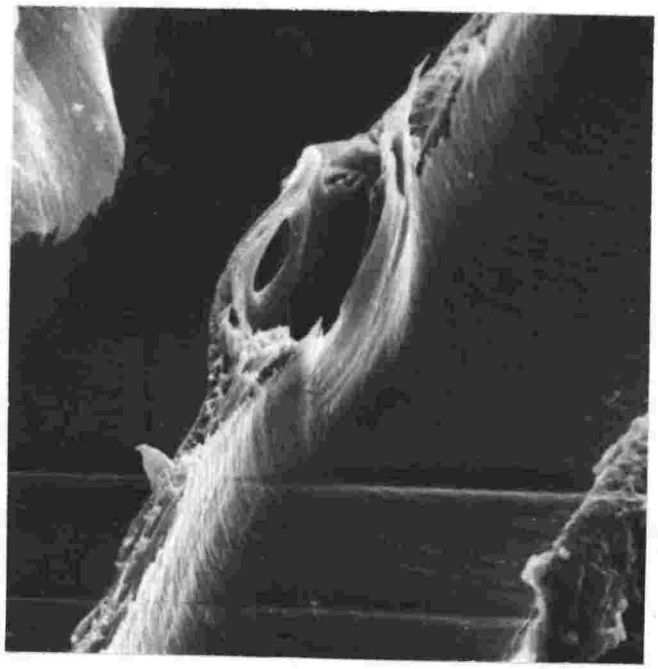

Fig. 18 : Transwall Failure showing a broken Pit, (x 2000).

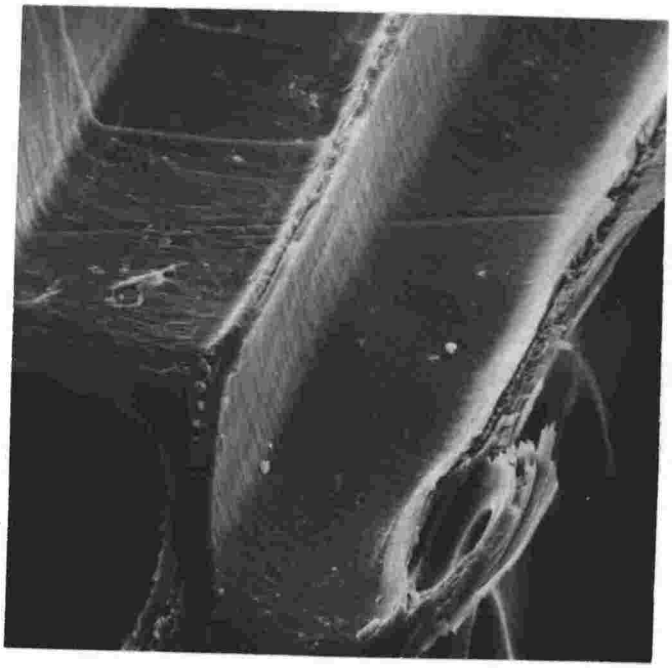

Fig. 19 : Intrawall and Transwall Failure, (x 1400).
Upper left - intrawall
Lower right - transwall.

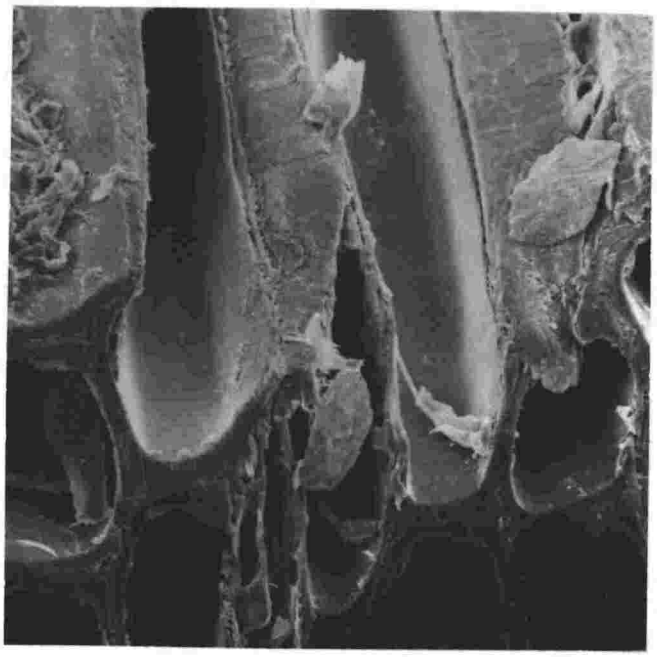

Fig. 20 : Transwall and Intrawall Failure, (x 700).

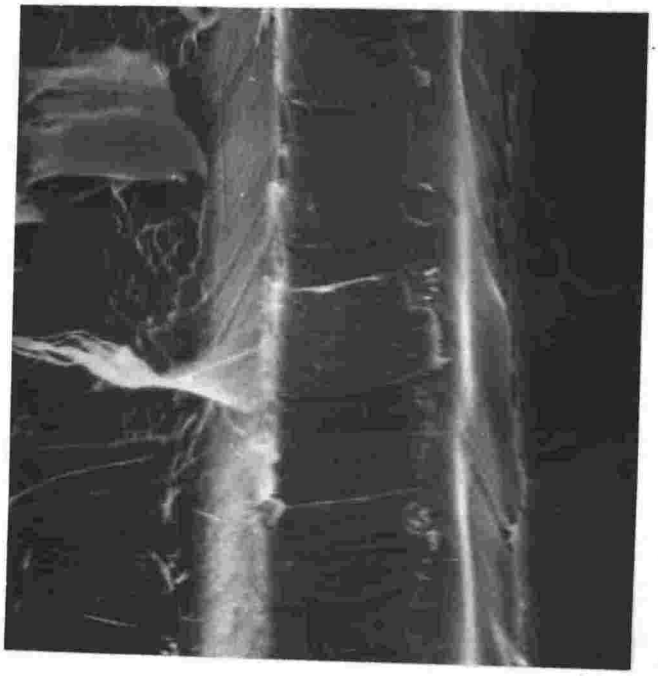

Fig. 21 : Intrawall Failure showing cross-strip tearing, and some evidence of a "crossed" microfibrillar structure in the lower right corner, (x1100).

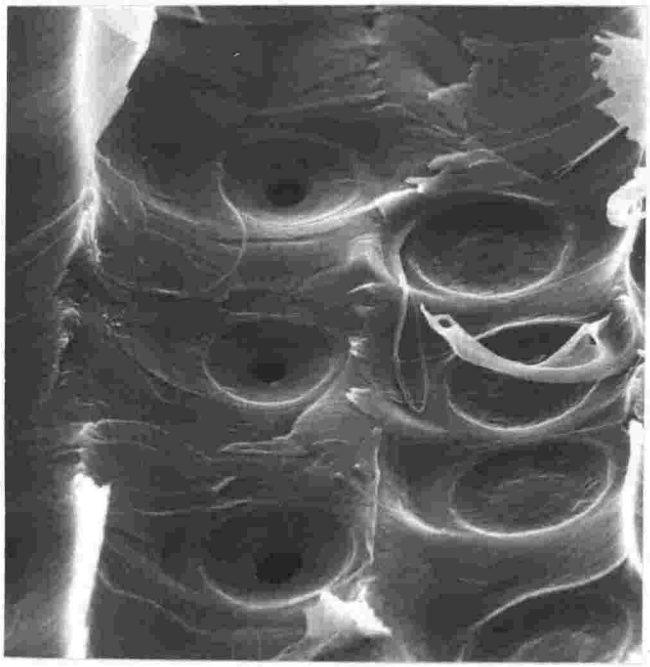

Fig. 22 : Radial Intrawall Failure showing exposed pit interiors, (x 1100).

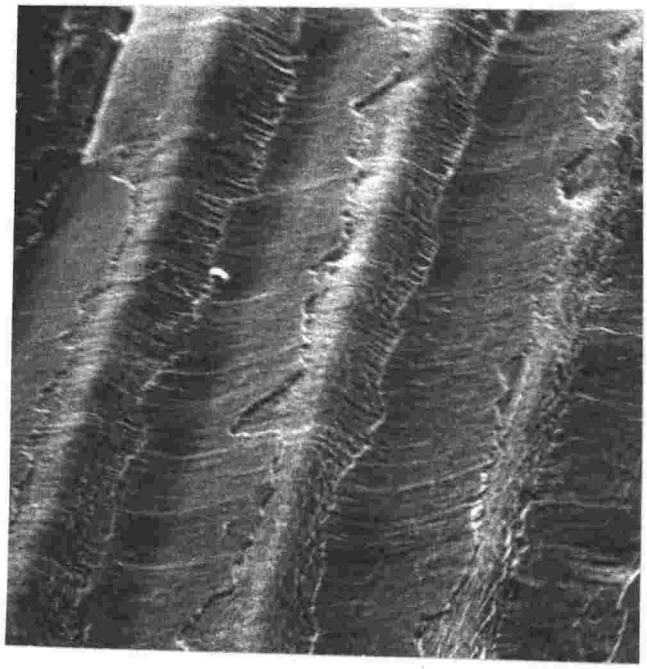

Fig. 23 : Serrated intrawall Failure, (x 900).

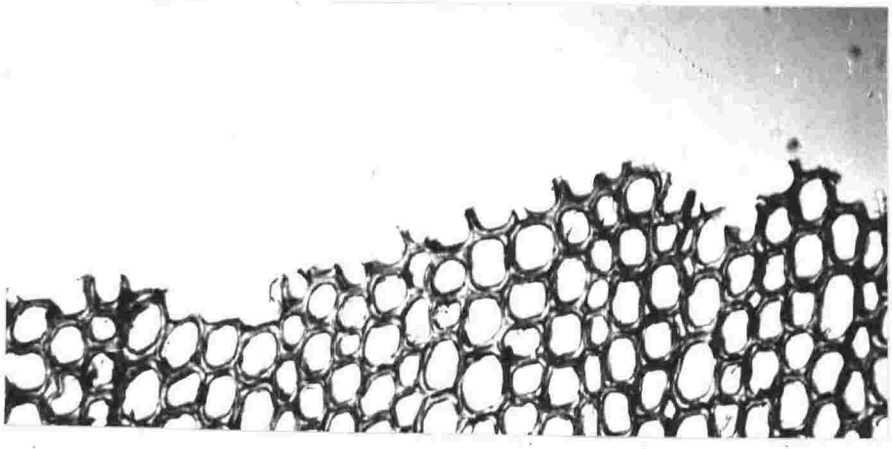

Fig. 24(a) : Cross-section of a springwood fracture surface showing trans and intra wall failure, (x 100).

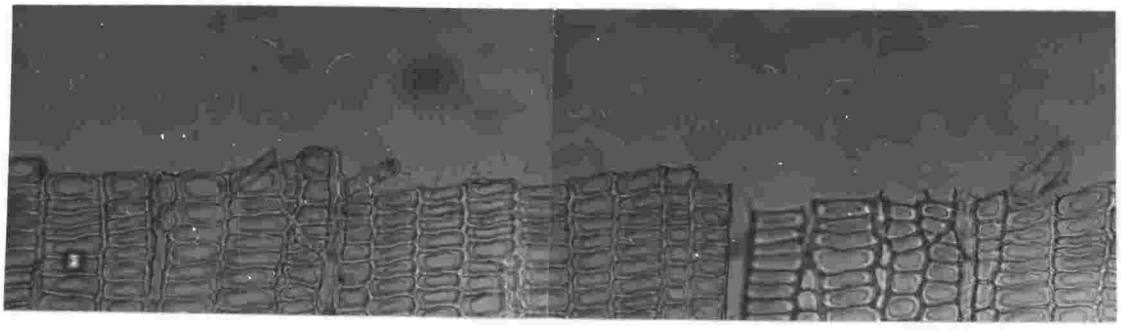

Fig. 24(b) : Cross-section of a summerwood fracture surface. Failure is all intrawall. Note the lack of overlap between cells. (x 150)

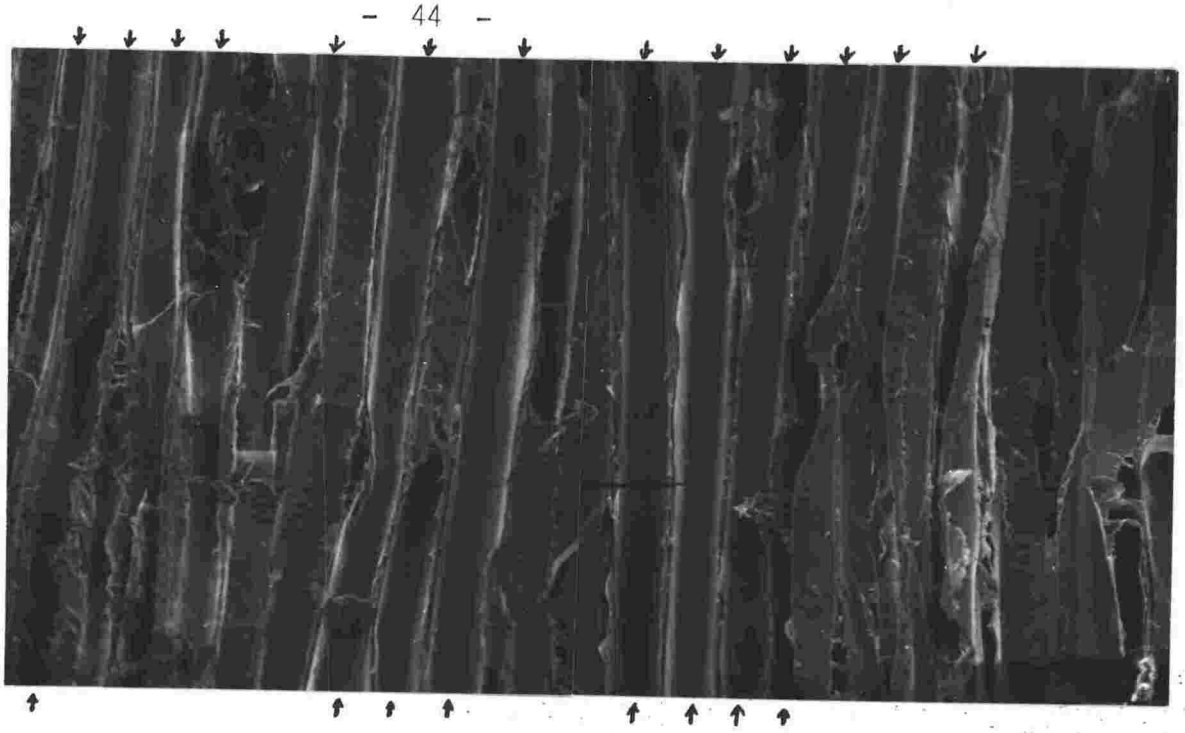

Fig. 25 : Wet springwood broken at a high strain rate. (50% transwall failure.) Arrowed cells are broken in transwall failure. (x 230)

Fig. 26 : Wet springwood broken at a low strain rate. (Mainly intra-wall failure.) (x 230)

Fig. 27 : Wet summerwood broken at a high strain rate. (Mainly intra-wall failure.) (x 230)

Fig. 28 : Wet summerwood broken at a low strain rate. Some tracheids are partially pulled away from the surface. (x 230)

Fig. 29 : Typical dry wood failure surface. Note the very rough appearance. (x 230)

3:5 Transverse Strength

(Figs. 31 and 34)

Both springwood and summerwood strengths increase as the rate of breaking is increased. The magnitude of the change is greatest for wet wood in each case, in agreement with previously reported trends. Strengths of wet springwood and summerwood are similar, but strengths of dry springwood are approximately 20% lower than the corresponding strengths of dry summerwood.

3:6 Failure Strain

(Figs. 32 and 35)

Springwood and summerwood results are almost indistinguishable. This is to be expected, since each specimen, being 1 cm long, encompasses portions of three growth rings and, therefore, contains both springwood and summerwood cells. There is considerable scatter in the results, but distinct overall trends are evident. For both wet and dry woods, failure strain decreases as the strain rate is increased. The decrease, in going from a strain rate of 2×10^{-6} sec^{-1} to one of 10^{2} sec^{-1}, is approximately 20% for wet wood and 40% for dry. Also, at most strain rates, the failure strain of dry wood is less than that of wet wood.

3:7 Energy Absorbed during Fracture

(Figs. 33 and 36)

Once again, springwood and summerwood results are similar. However, there is a marked change in the effect of moisture content. As strain

rate is increased the energy absorbed by dry wood decreases, but the energy absorbed by wet wood increases. (This probably reflects the considerable decrease in wet wood strengths at low strain rates.)

At low strain rates, the energies absorbed are approximately 1.0×10^{-2} and 0.5×10^{-2} joules in dry and saturated specimens respectively. At high strain rates, the figures are interchanged.

When the energy absorbed is divided by the area of surface produced in the fracture, figures very close to those given by Porter are obtained. (See Fig. 12.) However, exact comparison is difficult, since rates of straining in cleavage tests are difficult to define, and crack velocities are not known.

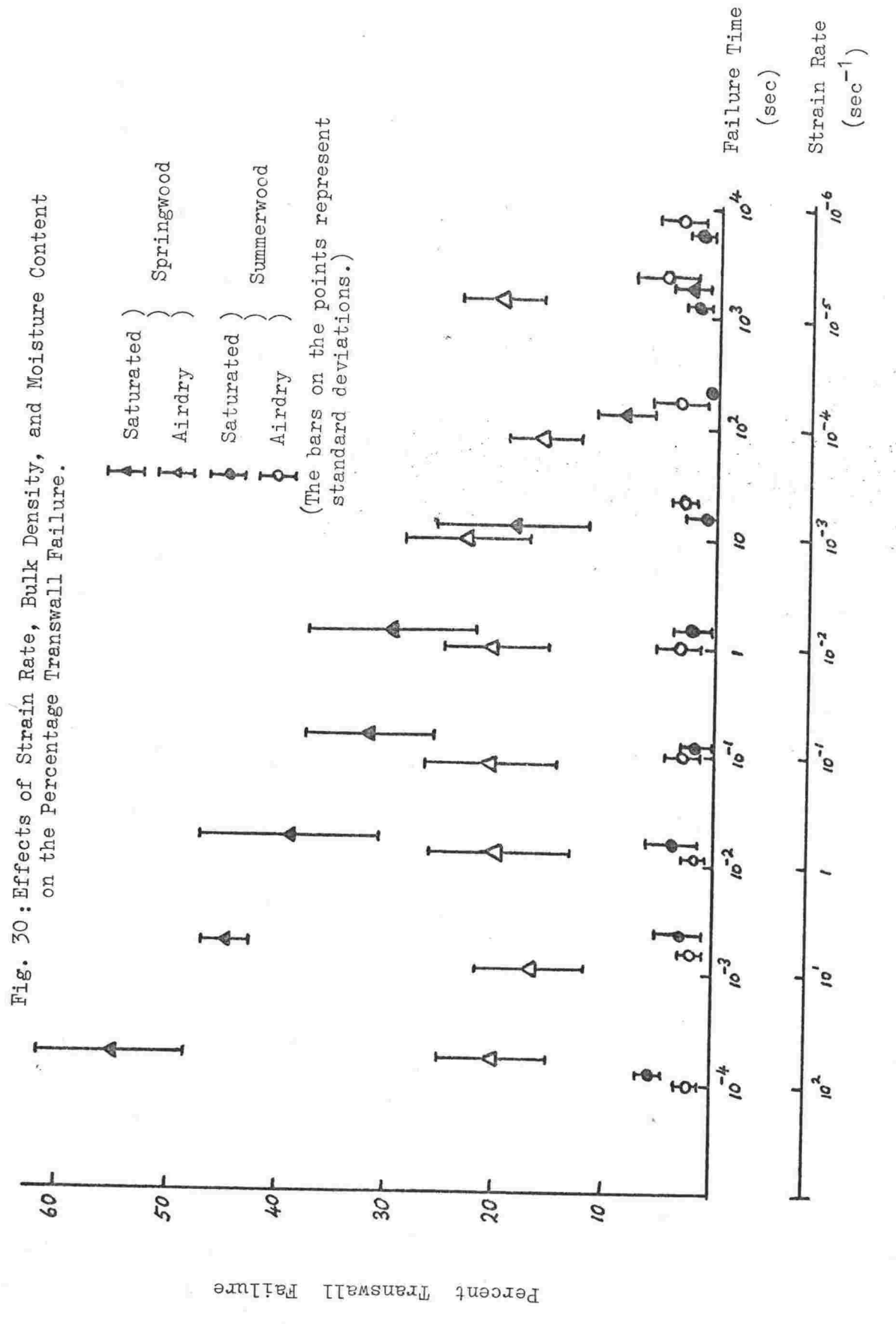

Fig. 30 : Effects of Strain Rate, Bulk Density, and Moisture Content on the Percentage Transwall Failure.

Fig. 31 : Effects of Strain Rate and Moisture Content on the Strength of Springwood.

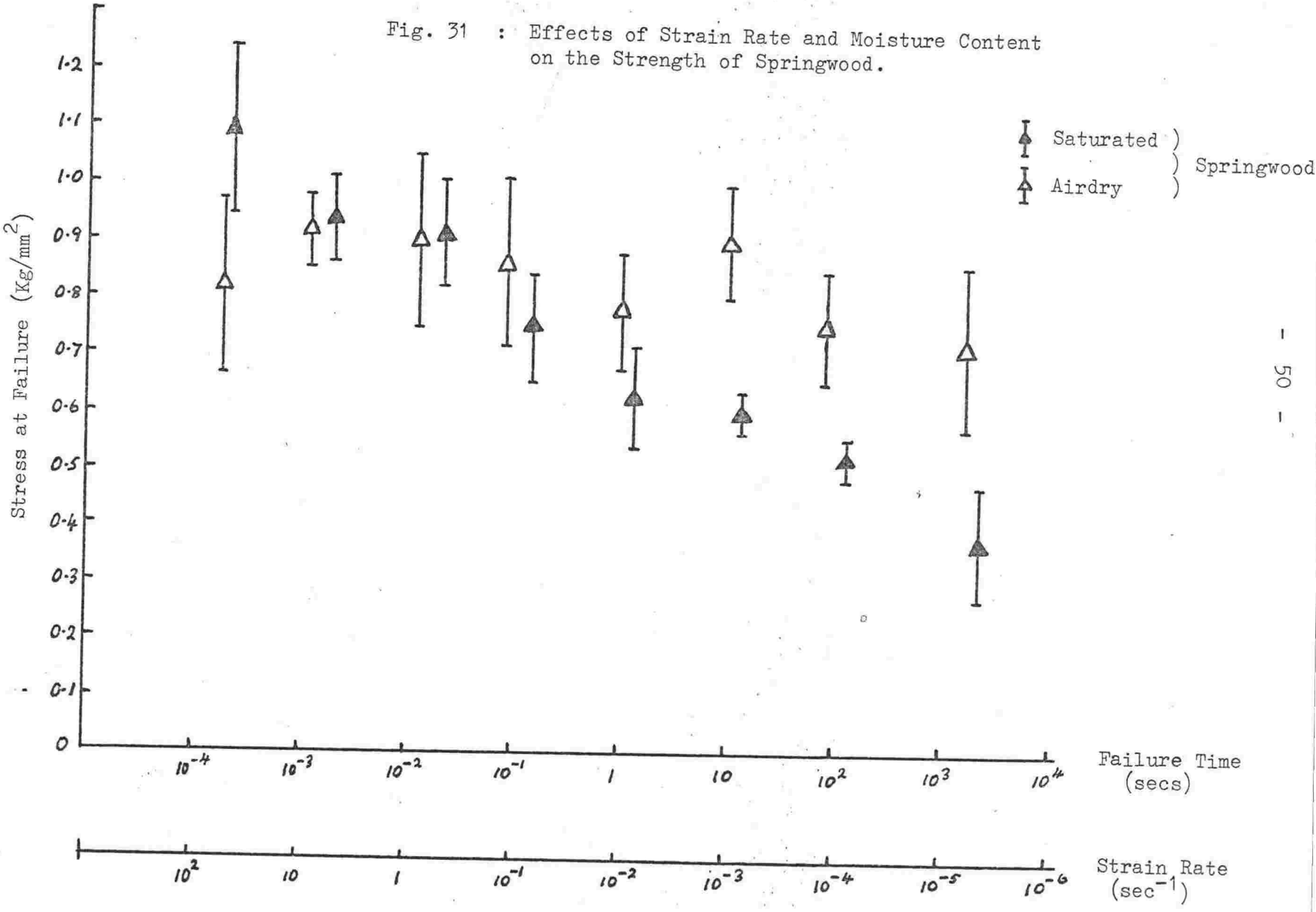

Fig. 32 : Effects of Strain Rate and Moisture Content on Springwood Failure Strain

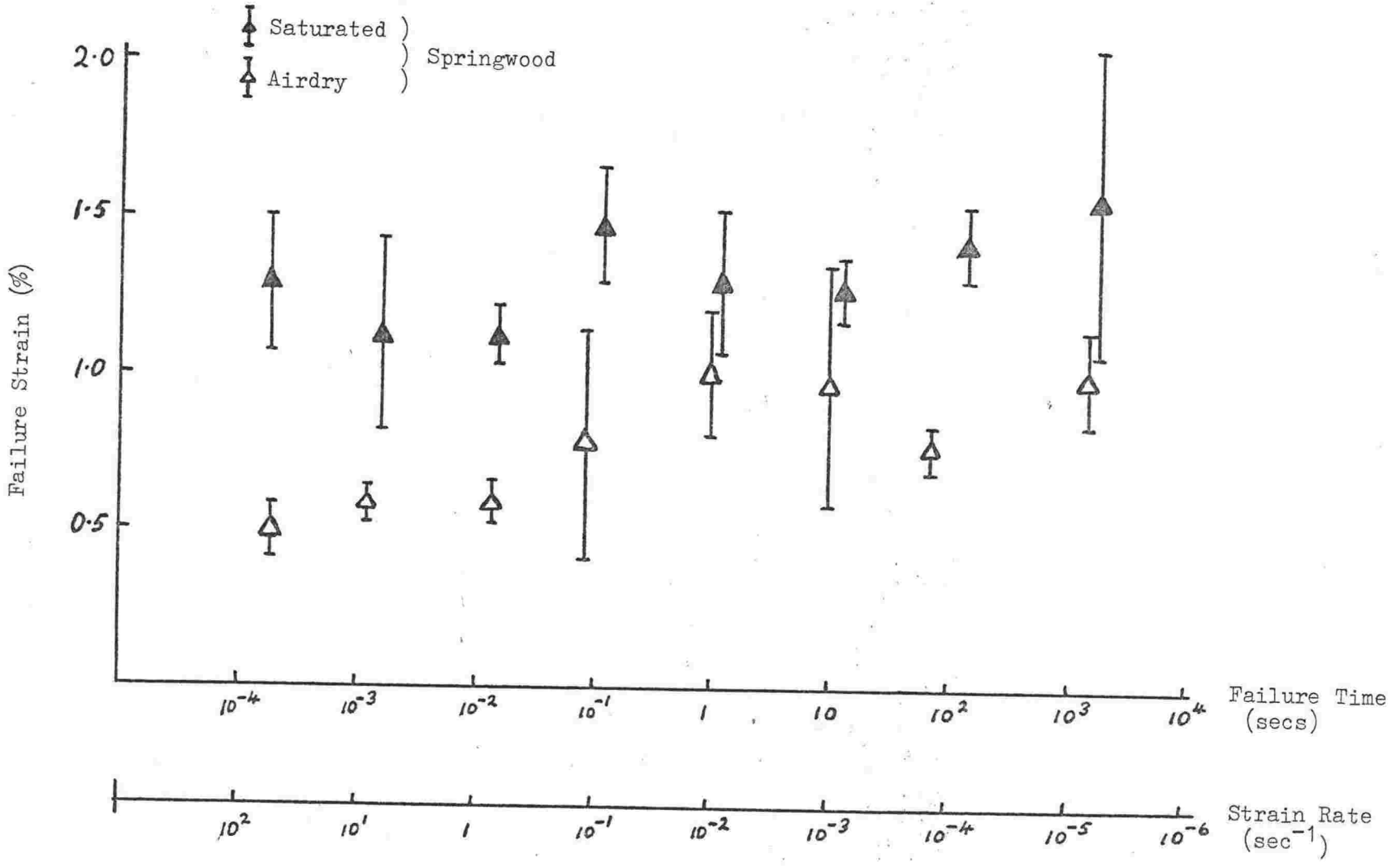

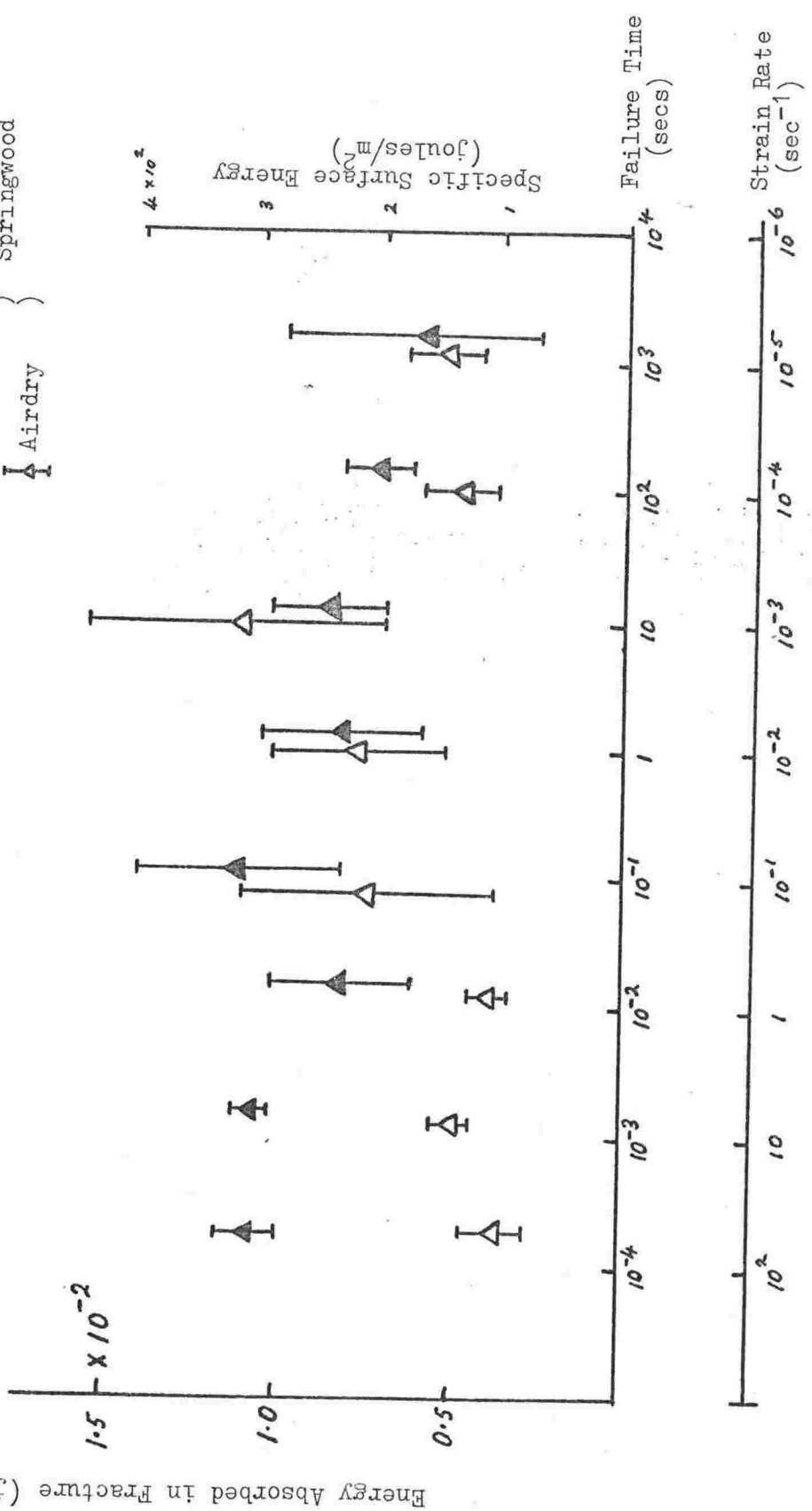

Fig. 33 : Effects of Strain Rate and Moisture Content on the energy absorbed during the fracture of Springwood.

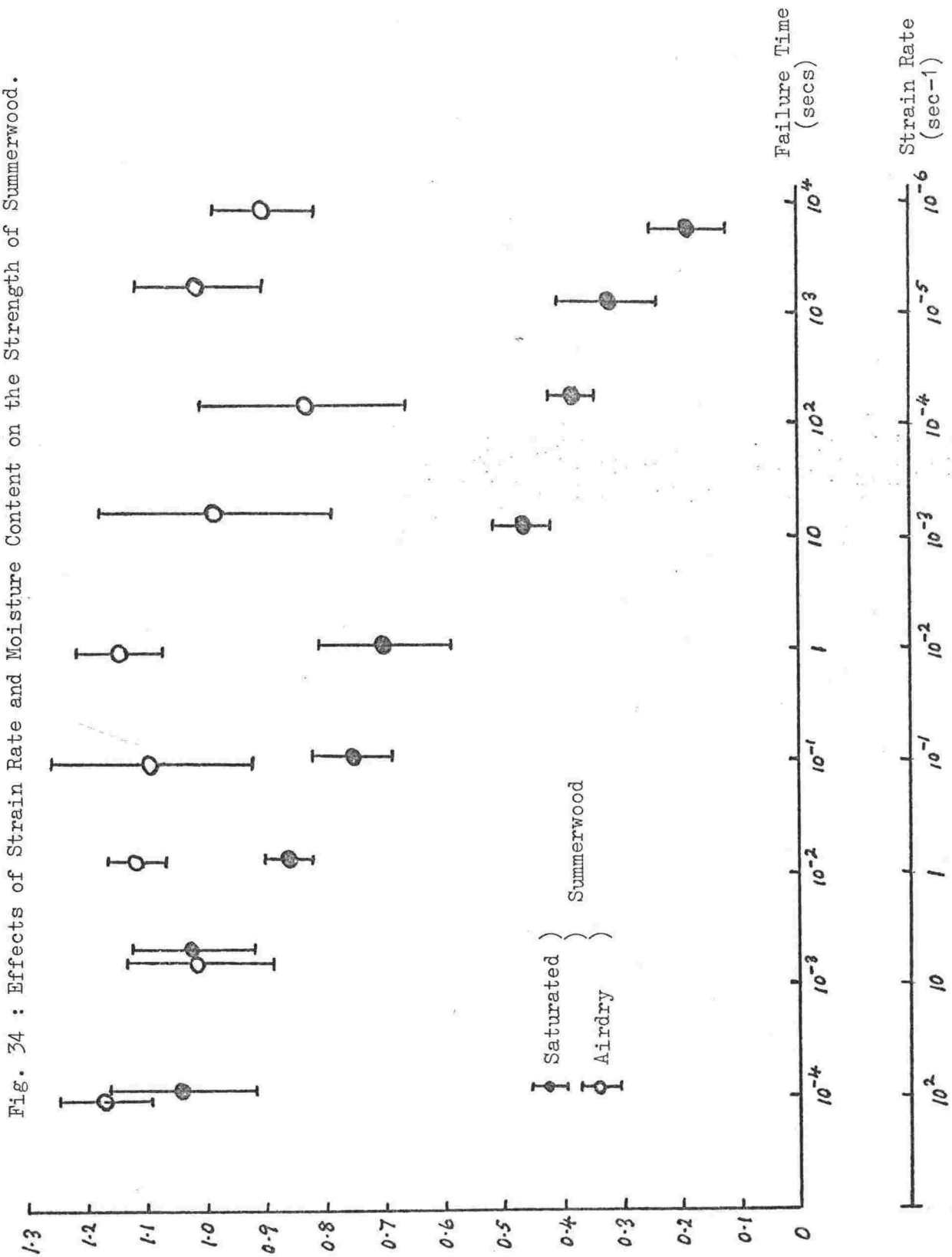

Fig. 34 : Effects of Strain Rate and Moisture Content on the Strength of Summerwood.

Fig. 35 Effects of Strain Rate and Moisture Content on Summerwood Failure Strain

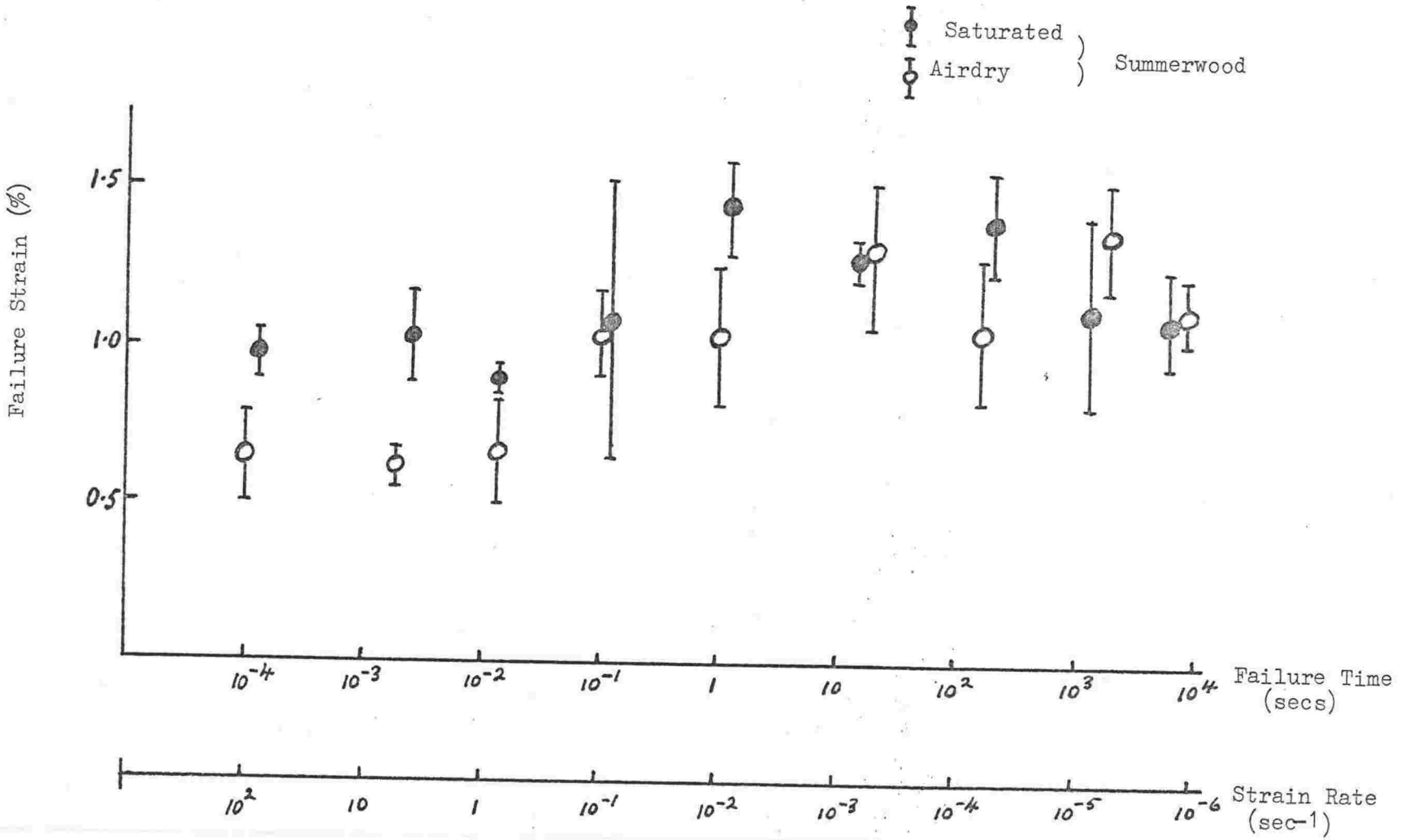

Fig. 36 Effect of Strain Rate and Moisture Content on the Energy Absorbed During the Fracture of Summerwood

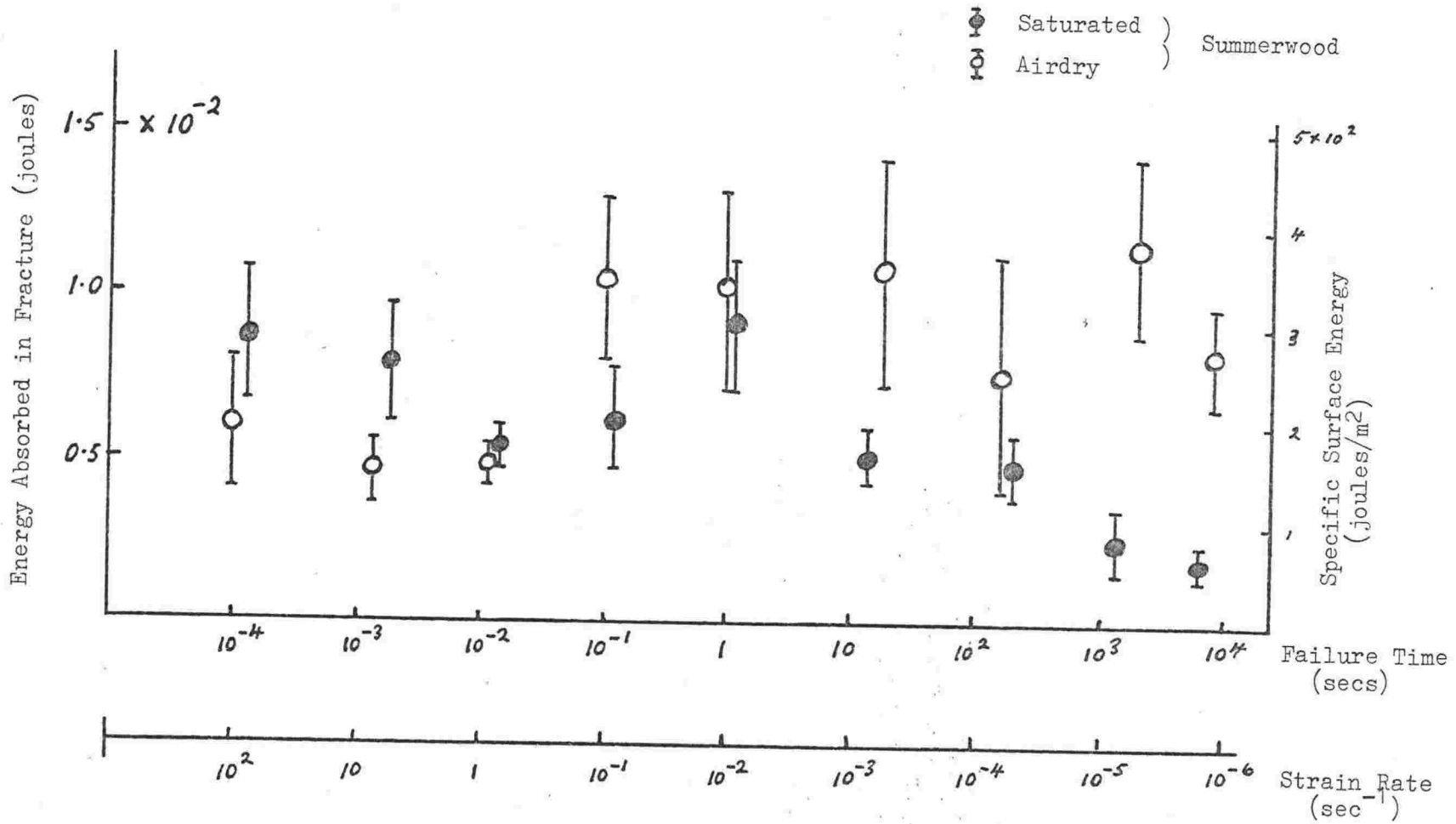

PRELUDE TO THEORETICAL CHAPTERS

The remainder of this thesis is devoted to the development of explanations of the above observed phenomena. These involve mainly -

(i) cellular geometry,

(ii) the elasticity of the tracheid wall, and

(iii) the rate sensitivity of hemicellulose and lignin.

The first necessity is a model of the tracheid wall that can be described mathematically. A suitable one is outlined in appendix 2. Briefly, the wall is assumed to consist of two unequal layers of a parallel-fibre-reinforced material. The reinforcing fibres of the larger of the two layers (the S_2) are aligned at an angle of 15° to the tracheid longitudinal axis, and those of the other layer (the S_1), are equally divided between the two possible orientations of $+80^\circ$ and -80°. Crystalline cellulose microfibrils are the reinforcing fibres, and they are embedded in an amorphous, isotropic matrix of hemicellulose and lignin. This same matrix also serves to bind adjacent tracheids together.

The major part of the explanations can be reduced to two problems -

(i) the reasons why only some tracheids are split longitudinally, and

(ii) the effects of moisture content and strain rate on the strengths of hemicellulose and lignin.

When wood is split along the grain, whether or not transwall failure

will occur depends on the relative magnitudes of the two ratios wall stress/wall strength and middle lamella stress/middle lamella strength. If the former is the greater, failure is transwall. Otherwise, failure is intrawall. Although intrawall splitting is located in either the P or the S_1 layer, the direction of splitting is such that very little crystalline cellulose is broken. Therefore, it is assumed that intrawall failure will occur when the stresses in the middle lamella, which consists of matrix, reach the strength of matrix.

In Chapter 4 from analyses of the stresses about the tracheid wall,

(i) a relationship between matrix strength and summerwood strength,

(ii) the reasons for the lack of transwall failure in summerwood, and

(iii) the reasons why some, but not all, springwood tracheids fail, are found. Furthermore, limits are set on the tracheid wall transverse strengths.

In Chapter 5, fibre-reinforced composite strength theory is applied to the tracheid wall to obtain a second estimate of its strengths, and in Chapter 6, the dependence of matrix strength on the rate of breaking is explained in terms of the behaviour of its component hydrogen bonds. Also, in Chapter 6, an estimate is made of the effect of rate on the strength of crystalline cellulose, and hence the dependence of percent transwall failure on strain rate is explained.

Much of the work that follows is based on the elastic properties of the tracheid wall, which requires a knowledge of its elastic constants. Therefore, these are derived and tabulated in appendix 2.

(Note: Throughout this work, the tensor stresses, strains, and elastic constants are expressed in their reduced matrix forms. For a complete explanation of this method of notation, the reader is referred to Nye (25).)

---

(25) Nye, J.F. (1967) "Physical Properties of Crystals" "Their Representation by Tensors and Matrices" (Oxford, Clarendon Press).

Chapter 4 TRACHEID WALL STRESSES

Middle Lamella Tensile Stresses

4:1 "Bent-Plate" Problem

In summerwood, tracheids are generally well aligned in both tangential and radial directions. They are approximately rectangular in cross-section. Therefore, the point where four corners meet resembles a cross-roads, as shown in Fig. 37.

When summerwood is stressed in a radial direction, the loads are transmitted along the radial tracheid walls as shown. Because of the symmetry of the situation, a plane (A...A) drawn through the centre of the tangential regions of the middle lamella represents a "neutral surface", or "surface of zero displacement". If only the half of the diagram above the neutral surface is considered (Fig. 38) it can be seen that the tangential tracheid walls approximate to a plate, which is attached to an elastic foundation of middle lamella. The plate is loaded at its centre by stresses transmitted along the radial tracheid walls. Because of the stiffness of the plate, middle lamella stresses are spread over a wider area than applied stresses, and are, therefore, smaller than applied stresses.

The equivalent "beam" problem has been treated by Timoshenko (26) and his method is easily extended to a "plate" situation.

With reference to Fig. 39, let σ be the applied stress, and let y

---

(26) Timoshenko, S. (1945) "Strength of Materials part 2. Advanced Theory and Problems" (Van Nostrand & Co., N.Y.).

be the plate deflection at any point B. It can be shown that -

(a) when B lies outside of the stressed region of the plate -

$$y = \frac{\sigma}{2K}\left[e^{-\beta a}\cos\beta a - e^{-\beta b}\cos\beta b\right], \quad \ldots\ldots(1)$$

and

(b) when B lies inside the stressed region -

$$y = \frac{\sigma}{2K}\left[2 - e^{-\beta a}\cos\beta a - e^{-\beta b}\cos\beta b\right]. \quad \ldots\ldots(2)$$

Also, $\beta = \sqrt[4]{\frac{K}{4D}}$, where $D = \frac{Y_2 h^3}{12(1-\nu_{23}\nu_{32})}$.

Y_2 is the plate Young's modulus,

ν_{23}, ν_{32} are plate poissons ratios, and

h is the plate thickness (= 7.2 μm in summerwood, and 1.9 μm in springwood).

K is the foundation "spring" constant, and is given by "foundation Young's modulus" divided by "foundation thickness".

Note that y, the plate deflection, is also the extension of the elastic foundation, and in the above example, half of the total middle lamella extension.

The way in which y varies along the tracheid wall "bent-plate" is

illustrated in Figs. 40 to 43. In each figure, the positions of the radial walls and middle lamellae are indicated. Figs. 40 and 41 are for summerwood walls, and 42 and 43 for springwood. (Note that a value for G, the matrix shear modulus is given with each diagram. In the derivation of elastic constants (appendix 2) it was necessary to assume a range of values of G for both wet and airdry matrix. The abovementioned curves are drawn for representative values of G.)

"y" is at a maximum at the centre of each stressed region of the wall, and falls to zero a short distance outside of this region. In some tracheids the "plate" deflection curves arising from adjacent radial walls overlap (Figs. 40, 41), but only in very narrow tracheids is the peak value of y changed. In fact, in springwood, the peak value of y depends on diameter only in tracheids with diameters of less than 12 μm.

The plate deflections of Figs. 40 to 43 are those arising from a tracheid wall stress of 1.0 Kg/mm^2. Therefore, the relationships between "maximum middle lamella stress" and "radial wall stress" are easily found. Also, since the summerwood tracheid diameter is 2.2 times its wall thickness, the relationships between "maximum middle lamella stress" and "bulk applied stress" can be found. ("Bulk applied stress" is the stress actually applied to the sample of wood.)

The ratios maximum middle lamella stress/radial wall stress $\left(\sigma_{ML(max)}/\sigma_{wall}\right)$

and maximum middle lamella stress/bulk applied stress $\left(\sigma_{ML(max)}/\sigma_{app}\right)$ are tabulated in Table 4 for various values of the matrix shear modulus G. The ranges corresponding to wet and airdry matrix are indicated.

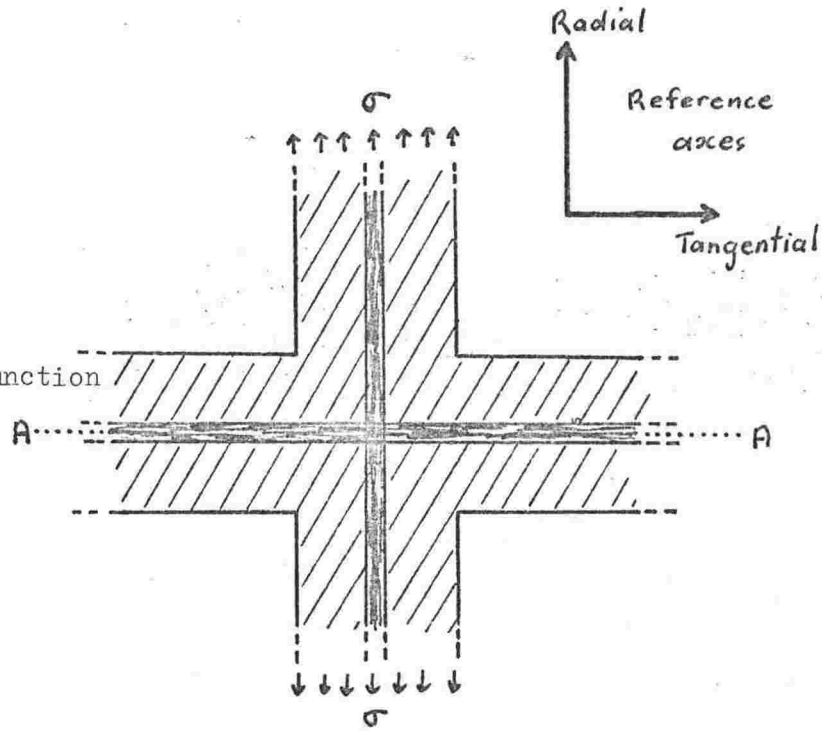

Fig. 37 : Summerwood Tracheid Junction

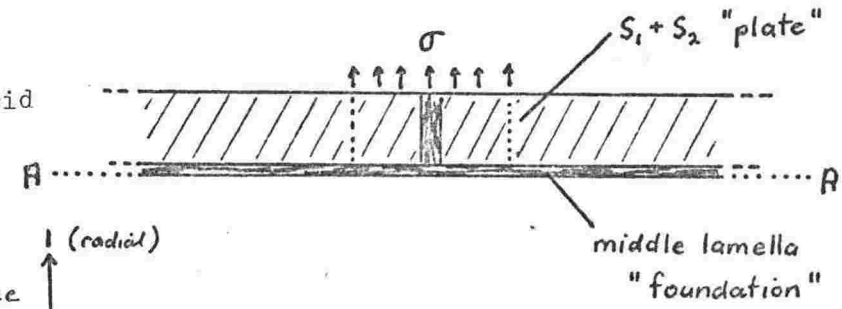

Fig. 38 : Tracheid walls above the neutral surface.

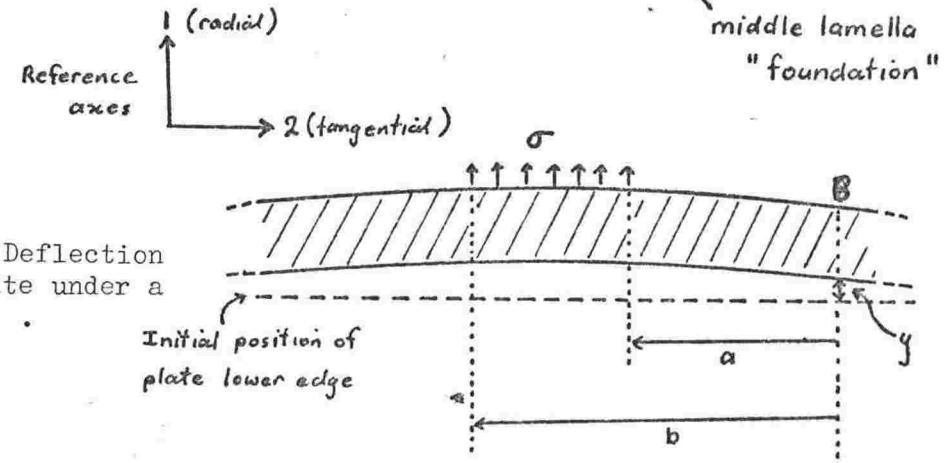

Fig. 39 : Deflection of the plate under a stress σ .

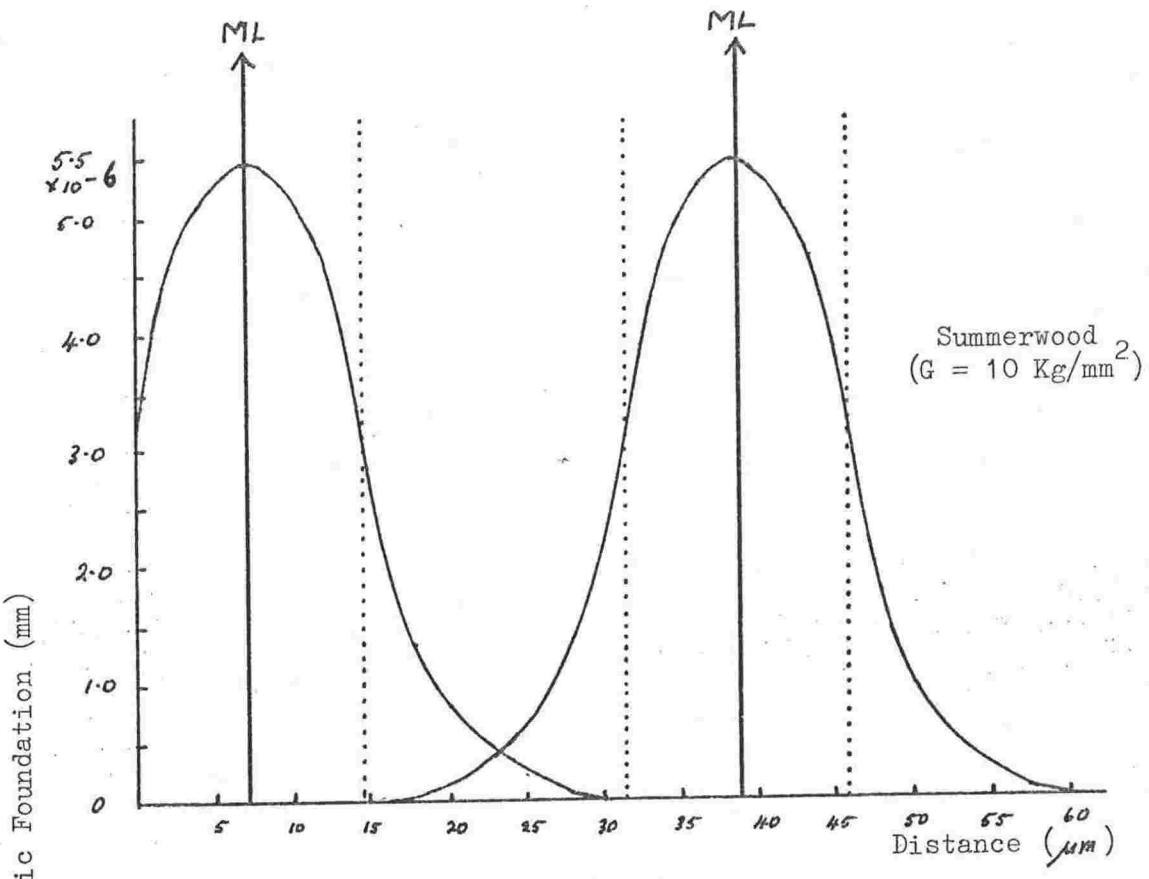

Extension of Elastic Foundation (mm)

Fig. 40 : Extension of Elastic Foundation.

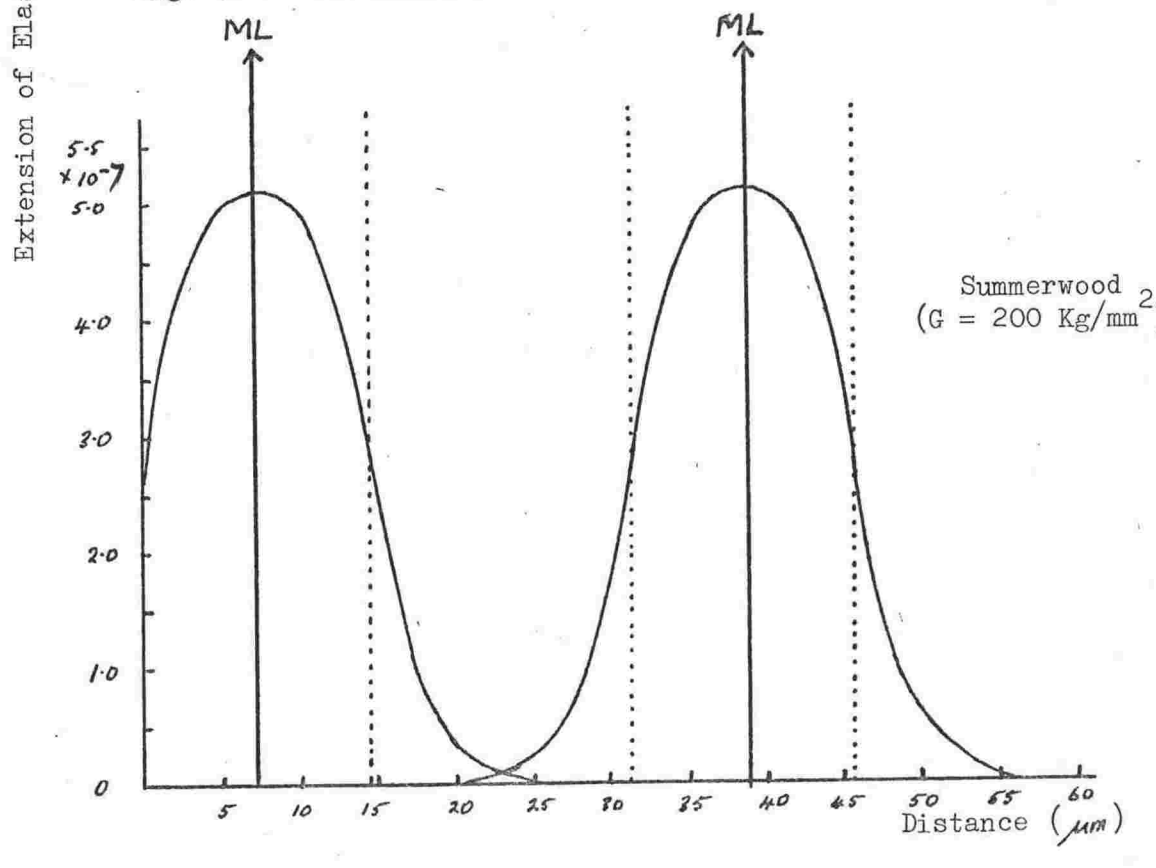

Fig. 41 : Extension of Elastic Foundation

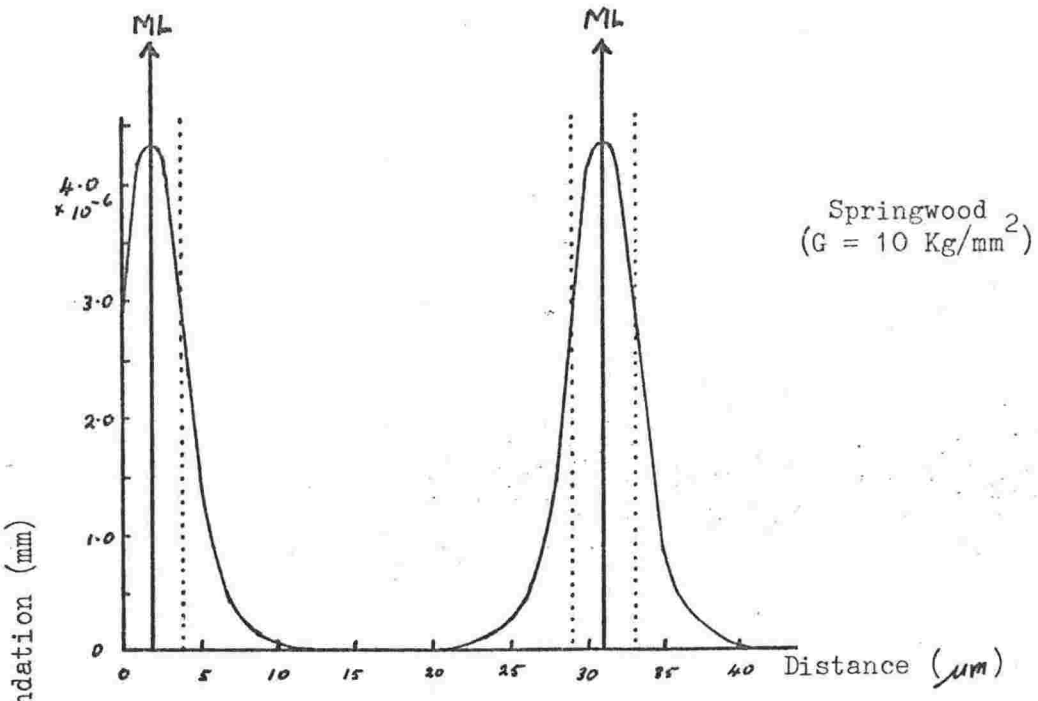

Fig. 42 : Extension of Elastic Foundation

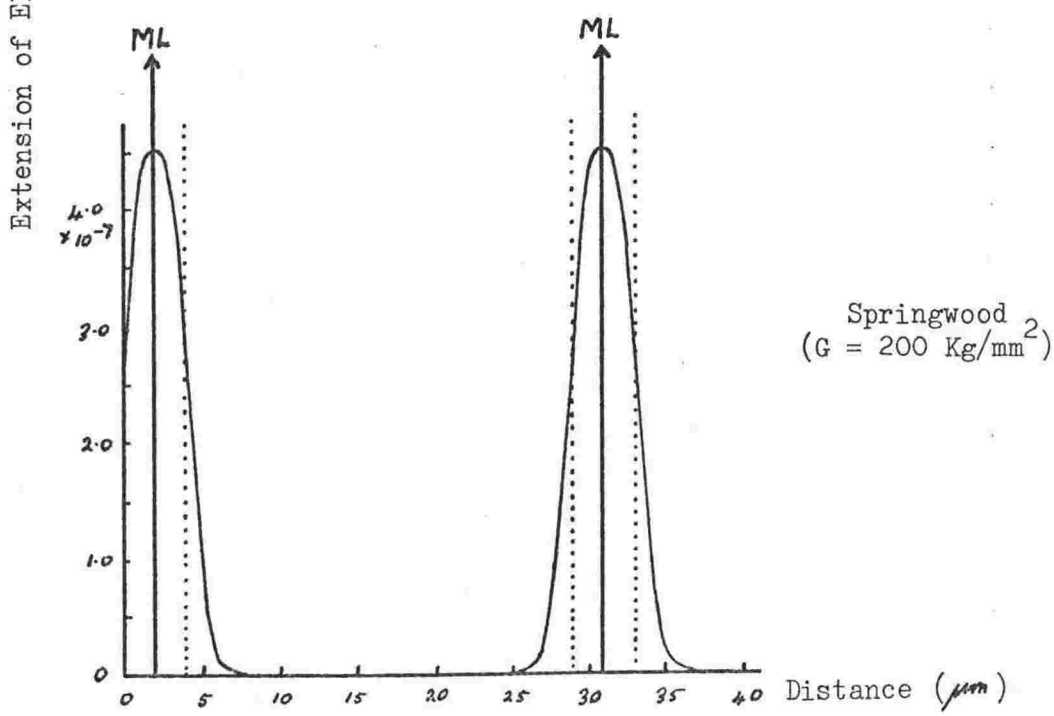

Fig. 43 : Extension of Elastic Foundation

		Wet Matrix				Airdry Matrix	
	G(Kg/mm^2)	2	10	50	100	200	500
Summerwood (	$\sigma_{ML}(max)/\sigma_{wall}$	.71	.83	.89	.91	.92	.93
(	$\sigma_{ML}(max)/\sigma_{app.}$	1.55	1.82	1.95	1.99	2.03	2.06
Springwood	$\sigma_{ML}(max)/\sigma_{wall}$	.51	.66	.75	.78	.82	.84

Table 4 : Middle Lamella Stresses.

In the case of wet summerwood, the possible values of $\sigma_{ML}(max)/\sigma_{app.}$ vary by not more than 25% so it seems reasonable to assume that the average of the values given (1.8) is the true value. The same may be done for airdry summerwood. Then, including the fact that the middle lamella is composed of matrix, and assuming that matrix obeys Hooke's Law until failure, leads to the following very useful equations -

wet matrix strength = 1.8 x wet summerwood strength

dry matrix strength = 2.0 x dry summerwood strength

.....(3)

Note also that the ratio $\sigma_{ML}(max)/\sigma_{wall}$ is greater in summerwood than in springwood, for any value of G. This implies that when intrawall failure occurs, the springwood tracheid wall is more highly stressed than the summerwood tracheid wall. (Intrawall failure is a splitting in matrix material near the edge of the middle lamella and will occur when $\sigma_{ML}(max)$ reaches the strength of matrix.) Therefore, transwall failure is more likely to occur in springwood than in summerwood.

The changes in stress which occur on going from springwood to summerwood are approximately 24% in wet wood, and 12% in dry, which may be sufficiently large to account for the lack of transwall failure in summerwood. However, the changes require a four-fold increase in wall thickness, so this mechanism is of little help in explaining why some springwood tracheids do not split. Variations in springwood wall thicknesses are rarely greater than 25% of the mean wall thickness.

Also, variations in springwood tracheid diameter must have little effect on the occurrence of transwall failure. The ratio $\sigma_{ML}(max)/\sigma_{wall}$ is independent of tracheid diameter, so long as "plate" deflections arising from adjacent radial walls do not overlap. Such overlapping can occur only in tracheids of less than 12 μm diameter and these are extremely rare in Pinus Radiata.

4:2 Variation of Elastic Moduli with Strain Rate

So far, no mention has been made of the strain rate at which the elastic constants used in the above calculations were measured. Since the elastic properties of some materials vary with the rate of loading, it is necessary to examine the effects of rate on wood. Very little of this type of work seems to have been done on wood, but available reports are summarised below.

Hearmon (27) showed that transverse Young's modulus and rigidity

---

(27) Hearmon, R.F.S. (1948) D.S.I.R. Forest Products Research Special Report No. 7. (H.M.S.O.).

modulus are independent of frequency in the range 26 → 1370 H_z at 12% moisture content.

Dunell & Price (28) Dynamic Young's modulus of viscose rayon (a cellulosic material) is independent of frequency in the range 8→80 H_z, at all temperatures between 0 and -80°C.

Suzuki, Nakato, and Aikawa (29) measured Young's modulus of wood in the frequency range 100 → 1000H_z. At 12% moisture content there seemed to be a 5% increase over this range, but at 24.5%, there was no increase. (Scatter in figures was about 10%.)

Goldsmith and Grossman (30) showed that although the Young's modulus of airdry wood (12% moisture content) did vary in the frequency range 8 → 400 H_z there was no overall increase or decrease.

Becker and Noack (31) obtained similar results for the torsion modulus of wet wood at lower frequencies (0.5 → 4 H_z) for temperatures in the range 20°C → 95°C.

---

(28) Dunell, B.A., and S.J.W. Price (1955) J. Polymer Sci. 18 p.305 "Dispersion of Mechanical Properties of Viscose Rayon at Low Temperatures".

(29) Suzuki, M., K. Nakato, and K. Aikawa (1965) J. Japan Wood Res. Soc. 11(3) p. 76 "Frequency Dependence of Dynamic Young's Modulus of Wood and its Relation to Creep".

(30) Goldsmith, V., and P.U.A. Grossman (1967) J. Inst. Wood. Sci. 18 p.44 "The Effect of Frequency of Vibration on the Viscoelastic Properties of Wood".

(31) Becker, H., and D. Noack (1968) Wood Sci. & Technol. 2 p.213 "Studies on Dynamic Torsional Viscoelasticity of Wood".

Kollman & Côté (32) state that "although generally the moduli of elasticity obtained by vibration tests are somewhat higher than those from static experiments, the differences are small and mostly negligible".

On the basis of the above reports, it seems reasonable to assume that the elastic stiffness constants of cellulose, hemicellulose and lignin, at all moisture contents, do not vary significantly with strain rate. Therefore, equations 3 will be true at all strain rates.

4:3 Variation of Matrix Strength with Strain Rate

Bulk strengths of airdry and saturated samples of summerwood have been measured over a wide range of strain rates. These are tabulated below (in Table 5), along with the corresponding "matrix strengths" obtained via equations 3.

---

(32) Kollmann, F.P., and W.A. Côté, Jr. (1968) "Principles of Wood Science and Technology, Part 1, Solid Wood" (George Allen & Unwin Ltd, London, Springer Verlag, Berlin) p.302.

	Airdry Summerwood			Saturated Summerwood		
Nominal Strain Rate (sec^{-1})	Failure Time (sec)	Bulk Wood Strength (Kg/mm^2)	Matrix Strength (Kg/mm^2)	Failure Time (sec)	Bulk Wood Strength (Kg/mm^2)	Matrix Strength (Kg/mm^2)
$2x10^{-6}$	$(8.4\pm.5)x10^{3}$	$.90\pm.08$	$1.84\pm.16$	$(6.7\pm1.1)x10^{3}$	$.21\pm.06$	$.39\pm.11$
10^{-5}	$(2.2\pm.3)x10^{3}$	$1.01\pm.11$	$2.07\pm.22$	$(1.4\pm.4)x10^{3}$	$.33\pm.08$	$.61\pm.15$
10^{-4}	$(1.6\pm.4)x10^{2}$	$.84\pm.17$	$1.72\pm.34$	$(1.9\pm.3)x10^{2}$	$.39\pm.04$	$.72\pm.07$
10^{-3}	$(2.0\pm.5)x10$	$.98\pm.19$	$2.01\pm.38$	$(1.7\pm.1)x10$	$.47\pm.05$	$.87\pm.09$
10^{-2}	$1.0\pm.2$	$1.14\pm.08$	$2.34\pm.16$	$1.5\pm.2$	$.70\pm.11$	$1.30\pm.20$
10^{-1}	$(1.1\pm.1)x10^{-1}$	$1.09\pm.17$	$2.23\pm.34$	$(1.1\pm.5)x10^{-1}$	$.76\pm.07$	$1.41\pm.13$
1	$(1.2\pm.04)x10^{-2}$	$1.11\pm.05$	$2.27\pm.10$	$(1.6\pm.1)x10^{-2}$	$.86\pm.04$	$1.60\pm.07$
10	$(1.8\pm.3)x10^{-3}$	$1.01\pm.13$	$2.07\pm.26$	$(2.4\pm.3)x10^{-3}$	$1.02\pm.11$	$1.89\pm.20$
10^{2}	$(1.0\pm.2)x10^{-4}$	$1.17\pm.08$	$2.40\pm.16$	$(1.2\pm.1)x10^{-4}$	$1.04\pm.12$	$1.93\pm.22$

($1\ Kg/mm^2 \doteq 10^7\ N/m^2$)

Table 5 : Summerwood strengths at Various Strain Rates.

(The above bulk wood strengths are shown graphically in Fig. 34 and matrix strengths in Fig. 61.)

4:4 Matrix Failure Strains

At low strain rates, the strength of wet matrix lies in the range 0.4 to 0.8 Kg/mm^2, and the strength of dry matrix is approximately 1.9 Kg/mm^2. Assuming uniaxial loading, and that Hooke's Law is obeyed until failure, the failure strain of matrix is given by matrix strength/matrix Young's modulus. Possible values of matrix Young's modulus are listed in Table 14, and these, together with the above strengths, give rise to the matrix failure strains of Table 6.

	Shear Modulus (Kg/mm^2)	Young's Modulus (Kg/mm^2)	Failure Strain (%)
Wet Matrix	2	6	6.6 → 13
Strength :	10	36	1 → 2
0.4 → 0.8	50	137	0.3 → 0.6
Kg/mm^2	100	250	0.15 → 0.3
Dry Matrix	50	137	1.4
Strength :	100	250	0.8
1.9 Kg/mm^2	200	430	0.5
	500	760	0.3

Table 6: Dependence of Matrix Failure Strain on Matrix Young's Modulus.

Measured low-rate failure strains of wood are generally in the range 0.5 to 1.5%, with wet wood having somewhat higher values than dry wood. It is probable that matrix itself will fail at similar strains,

in which case the most likely values for the matrix shear moduli are 10 Kg/mm^2 for wet matrix, and 100 or 200 Kg/mm^2 for dry.

To save repetition in future calculations only two values of matrix shear modulus will be used, 10 Kg/mm^2 for wet matrix and 200 Kg/mm^2 for dry.

Summary (1)

The relatively good tangential and radial alignment of summerwood tracheids suggested the approximation of perfect alignment as shown in Fig. 37. Such a situation is similar to a problem treated by Timoshenko (26), because the tracheid walls at right angles to the applied load approximate to continuous plates, which are joined in pairs by thin layers of middle lamella. Plates are loaded by those regions of tracheid wall which lie parallel to the applied load.

The following results arose -

(i) Only a small proportion of the total load is carried by that part of the middle lamella which is not directly beneath the loaded region of a "plate". In springwood, stresses in the middle lamella become negligible less than 6 μm from the centre of a loaded region, so it is only in tracheids of less than 12 μm diameter that the stress waves radiating from adjacent loaded regions will interfere, and increase the likelihood of intrawall failure. Since very few tracheids have tangential diameters of less than 12 μm , tracheid

diameter must have little influence on the occurrence of transwall failure.

(ii) The ratio "maximum middle lamella stress"/"radial wall stress" increases as one goes from springwood to summerwood, which implies that the springwood tracheid wall is the more highly stressed when intrawall failure occurs. Therefore, transwall failure is more likely to occur in springwood than in summerwood.

However, variations in springwood wall thicknesses are far too small to have any significant influence on the occurrence of transwall failure, so this cannot be the reason why some springwood tracheids fail, but others do not.

(iii) For summerwood, the following very useful relationships were obtained -

Wet matrix strength = 1.8 x wet summerwood strength

Dry matrix strength = 2.0 x dry summerwood strength

These are valid at strain rates from 2×10^{-6} sec^{-1} to 10^{2} sec^{-1}.

(iv) Consideration of matrix failure strains suggested that the shear modulus of matrix has the following values: 10 Kg/mm^2 for wet matrix, and 100 or 200 Kg/mm^2 for dry.

Middle Lamella Shear Stresses

4:5 General

When samples of springwood are broken in transverse tension, some tracheids split in transwall failure but others do not. The

remainder of this chapter attempts to explain why this is so.

The simplest model of springwood is that shown in Fig. 44, all tracheids being identical and regularly arranged with 50% overlap when viewed along a tangential direction, (i.e. 50% tangential overlap). This model would lead to percent transwall failures of 0, 50 or 100%, depending on the relative strengths of the tracheid walls and the middle lamella matrix material bonding adjacent tracheids together. It is, therefore, inadequate.

An obvious improvement would be to allow wall thicknesses and tracheid diameters to vary. However, microscopic examination of fractured specimens and the theoretical results of section 4:1 do not reveal any tendency for thin walled and/or large diameter tracheids to break preferentially.

Another possibility is that some tracheid walls are stronger than others through the possession of higher than average values of S_2 microfibril angle. (See Fig. 45 for definition of S_2 microfibril angle.) Microfibril angle can vary by as much as 20° from one tracheid to another in the same sample of wood. One would expect tracheids having high values of microfibril angle to be stronger than those having low values, since when microfibril angle is high the reinforcing microfibrils are more nearly aligned with applied transverse loads.

An obvious corollary to this is that the average of the microfibril

angles of those tracheids broken in transwall failure should be lower than that of the sample as a whole. The method outlined in appendix 3 was devised in order to test this hypothesis. A single layer of tracheids was removed from the surface of the fractured specimen, and it was possible to measure the microfibril angles of those tracheids which were broken in transwall failure. The same was done to a surface which had been prepared by a knife cut, and, in this case, the average microfibril angle of all tracheids was obtained. Results showed that tracheids broken in transwall failure did not have lower than average microfibril angles. Therefore, the hypothesis is false, and the microfibril angle of a tracheid cannot be the factor which determines whether or not it will fail in the transwall mode.

4:6 Tracheid Overlap and Middle Lamella Shear Stresses

Fig. 46 is a cross-sectional view of a typical springwood specimen. It can be seen that the degree of tangential overlap varies greatly from tracheid to tracheid, and it is, therefore, possible that it is the degree of overlap which will determine whether or not a tracheid will fail in the transwall mode. Tracheids A and B of Fig. 47 show different degrees of overlap. Obviously, more middle lamella material must be broken to pull A away from its neighbours, than to pull B away. Because applied loads are transmitted along the tracheid radial walls, A is going to have more highly stressed radial walls than B when separation occurs, and will be more likely to fail in the transwall mode.

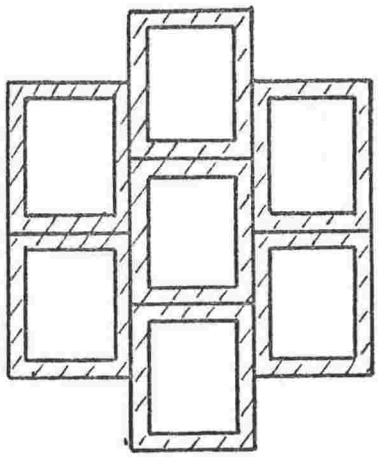

Fig. 44 : Springwood Tracheids

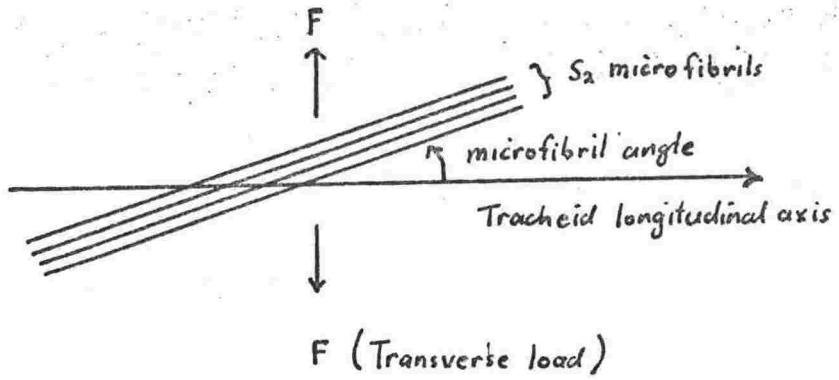

Fig. 45 : Orientation of S_2 Microfibrils

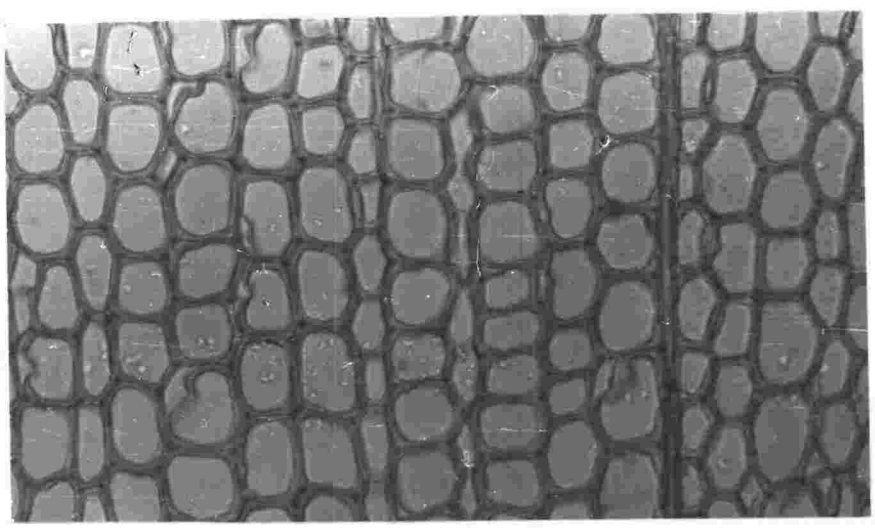

Fig. 46 : Cross-section of Springwood (x 200)

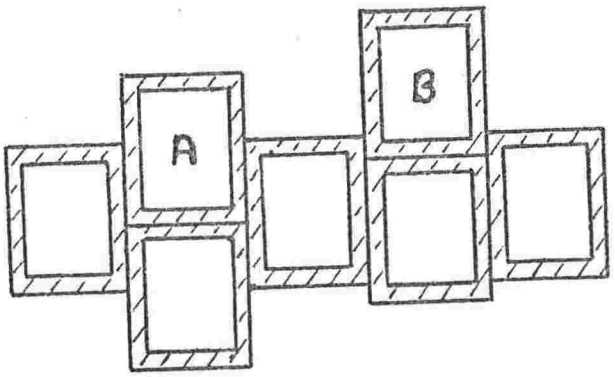

Fig. 47 : Variable degree of overlap.

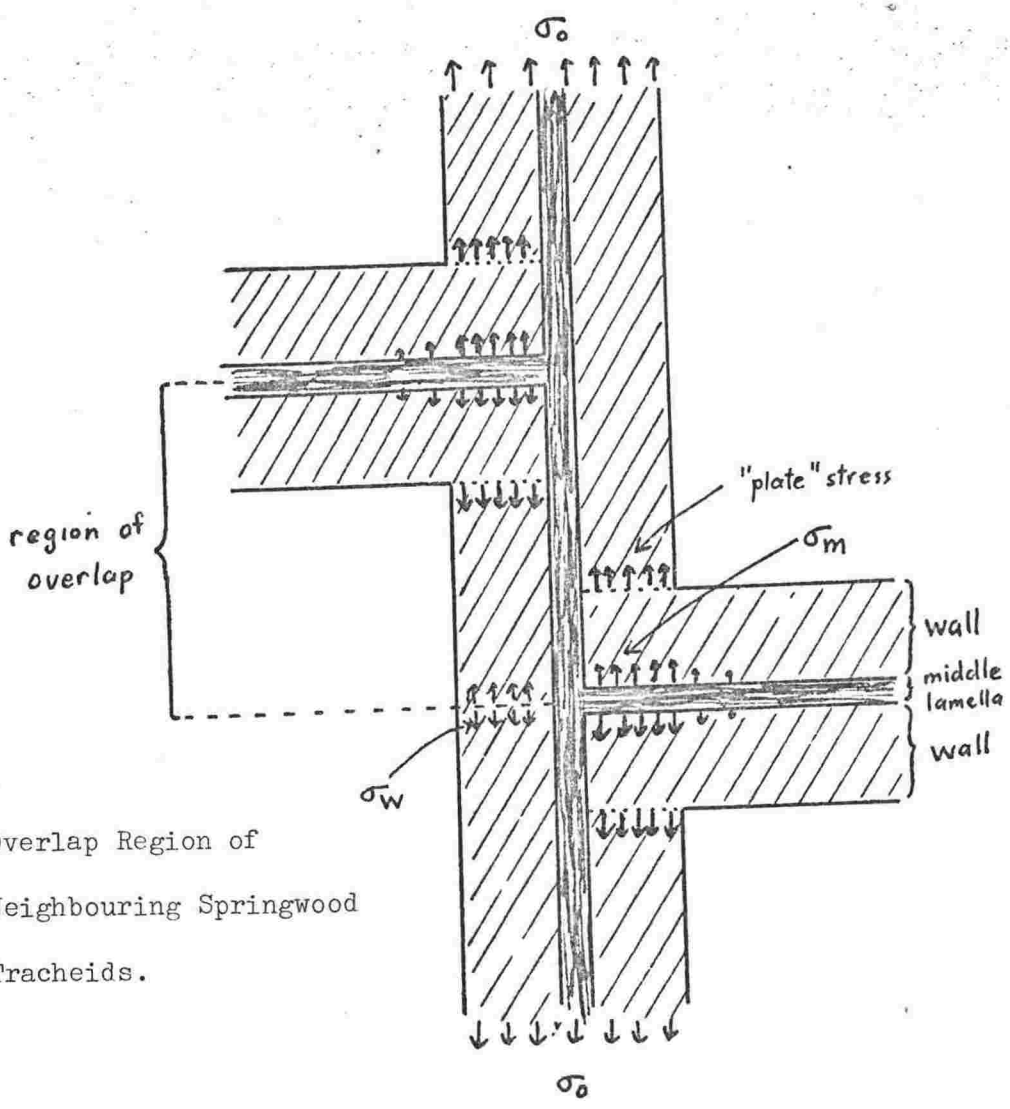

Fig. 48 : Overlap Region of Neighbouring Springwood Tracheids.

To determine whether or not variations in overlap result in significant changes in middle lamella stresses, it is necessary to carry out a stress analysis on a somewhat simplified model of the overlap region. A suitable one is illustrated in Fig. 48. The tracheid walls are lightly shaded, and the middle lamellae are darker. When tensile loads are applied to the radial walls the tangential segments of middle lamella will experience tensile loads in the directions indicated by the arrows. If the walls are imagined to be divided along the dashed lines, then the tangential portions of wall and middle lamella will form "bent-plates on elastic foundations" and the results of section 4:1 may be applied. If "plate stress" is the uniform stress applied to the "bent-plate", and "maximum middle lamella stress" is the maximum tensile stress experienced by the tangential segment of middle lamella, then the useful springwood relations are -

(i) wet wood : maximum middle lamella stress = 0.68 x plate stress

(ii) dry wood : maximum middle lamella stress = 0.84 x plate stress.

The radial portion of middle lamella is in shear. This section of the problem bears some similarity to a glue lap joint, but the presence of the tangential walls means that lap joint stress formulae are not applicable. Instead, a finite element technique is necessary. A very simple one is developed in appendix 4, and is first applied to a glue lap joint. The glue shear stresses that it gives are compared with those obtained by the use of an existing formula. Good agreement is obtained between the finite element technique and the formula, which is

applicable to a lap joint in which no bending is allowed. Since no bending can occur in the simplified model of the overlap situation being studied, it seems that application of the finite element technique is justified.

The results of the calculations are illustrated in Fig. 49. As is to be expected, the maximum stress which must be carried by the tangential middle lamella (σ_m) decreases as the degree of overlap increases. At the same time the maximum stress (σ_w) in the opposing radial wall, increases. In wet wood, the changes in σ_m and σ_w are nearly 20% of their values at zero overlap. The changes in dry wood are smaller, only 8%. (σ_o is the average stress applied to the radial walls.)

Peak shear stresses in the radial middle lamella (τ_m) are always much lower than the above tensile stresses. Therefore, shear failure of the radial middle lamella is unlikely to occur before tensile failure of either the tangential middle lamella or its opposing tracheid wall.

Note that in each case most of the stress change takes place in the range 0 → 20% overlap. The stress changes are summarised in Table 7 (below).

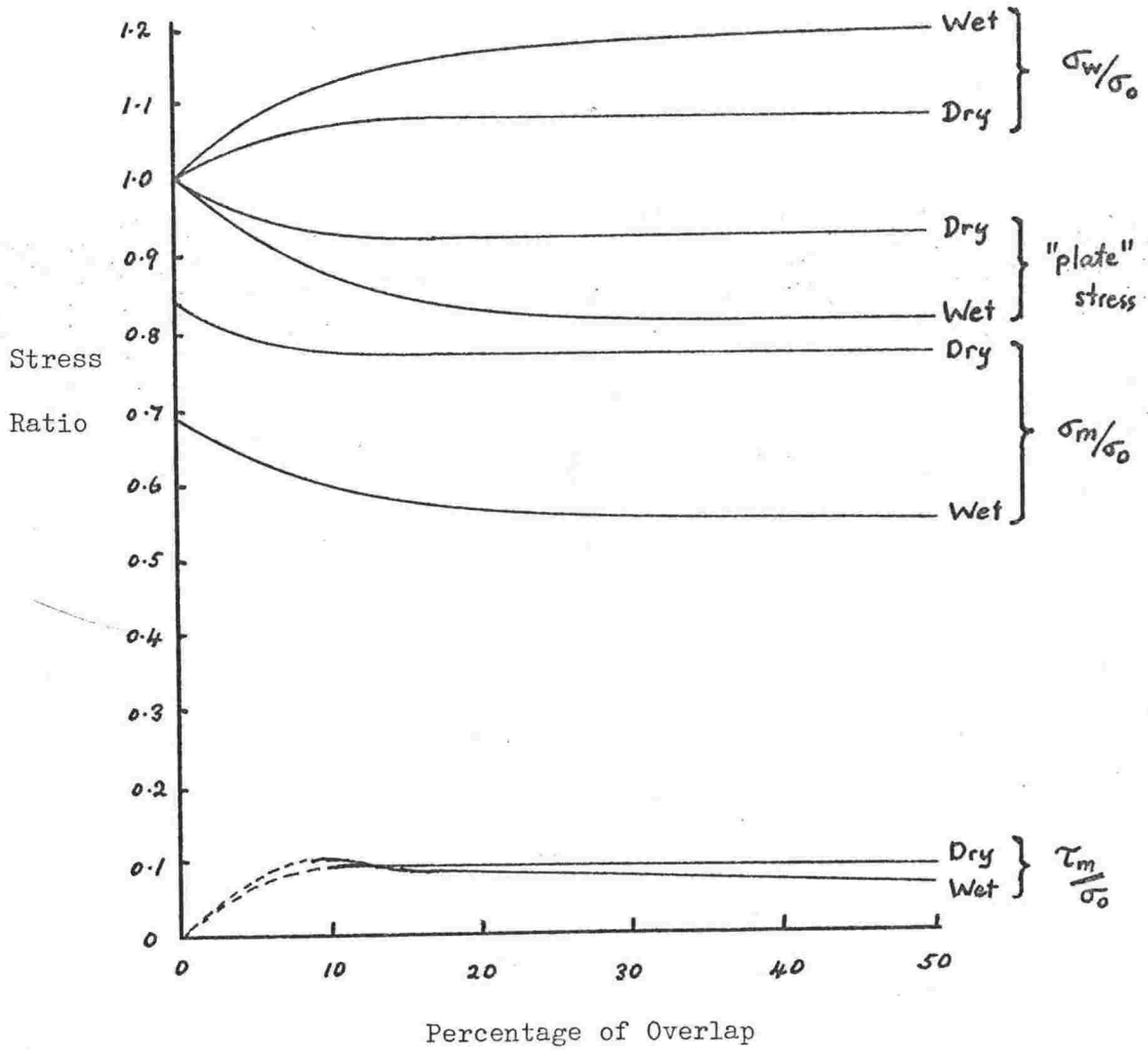

Fig. 49 : Effect of Degree of Overlap on Various Wall Stresses.

Percentage of Overlap	0	20	50
Wet Wood	1.5	2.1	2.2
Dry Wood	1.2	1.4	1.4

Table 7 : Variation of σ_w/σ_m with the Degree of Overlap.

4:7 Shear Stresses After Initial Splitting

Radial wall and tangential middle lamella tensile stresses are very much greater than radial middle lamella shear stresses. Therefore, either the radial tracheid wall, or the tangential middle lamella, will be the first to fail. The first possibility results in the transwall failure of at least one tracheid wall. However, the second possibility does not necessarily lead to complete intrawall failure. It is studied further in this section.

Assuming complete failure of the tangential middle lamella, the situation shown in Fig. 50 arises. Intertracheid bonding has been reduced to two lap joints, labelled A and B.

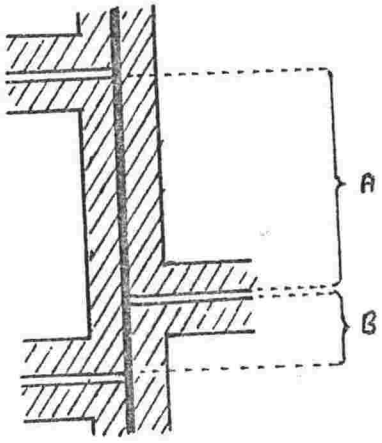

Fig. 50 Tracheid Lap Joints

Calculations in appendix 4 show that peak shear stresses will be higher in the shorter lap joint. Its length will depend on the degree of overlap. At 50% overlap, each lap joint will be equal

in length to half of the tracheid radial diameter, and at 0% overlap, one will be 45 μm long and the other non-existant. To determine the way in which the peak shear stress (τ_m) varies with the degree of overlap, Volkersen's formula (see appendix 4) can be applied to tracheid wall lap joints ranging in length from 2 to 22 μm. The results of these calculations are shown in Fig. 51 in which τ_m/σ_o is plotted as a function of lap joint length, or percentage overlap. It can be seen that the maximum shear stress in the middle lamella "glue" decreases as the degree of overlap increases. Obviously, middle lamella failure is less likely, and transwall failure more likely, when the degree of overlap is high.

4:8 Limitations on Tracheid Wall Transverse Strength

The results of the previous two sections have some interesting implications -

(1) Dry Wood. About 20% transwall failure occurs during fracture. Fig. 51 shows that once failure of the tangential middle lamella has occurred, peak shear stresses in radial middle lamella are never less than 56% of the radial wall stress. Therefore, if transwall failure is ever to occur, the tracheid wall tensile stress must exceed the tracheid wall tensile strength before the middle lamella shear stress exceeds middle lamella shear strength. In other words -

$$\frac{\text{wall tensile stress}}{\text{wall tensile strength}} \text{ must be greater than } \frac{\text{middle lamella shear stress}}{\text{matrix shear strength}}$$

$$\text{which is not less than } \frac{0.56 \times \text{wall tensile stress}}{\text{matrix shear strength}}$$

Since the dry matrix shear strength is unlikely to be greater than

its tensile strength of 2.0 Kg/mm^2, the wall tensile strength must be less than 3.6 Kg/mm^2.

From Table 7, tangential middle lamella tensile stresses are always greater than 71% of the radial wall tensile stresses. If transwall failure is ever to occur before tangential middle lamella splitting, then the wall strength must be less than 2.8 Kg/mm^2. This seems to be of less significance than the previous limit.

A lower limit to wall strength is 2.0 Kg/mm^2, which is the tensile strength of the weaker of its components, matrix material. Therefore, the transverse tensile strength of the dry tracheid wall must lie within the range 2.0 Kg/mm^2 to 3.6 Kg/mm^2.

(2) Wet Wood. Similar arguments applied to the wet tracheid wall show that its transverse tensile strength must lie within the range 0.6 Kg/mm^2 to 3.4 Kg/mm^2.

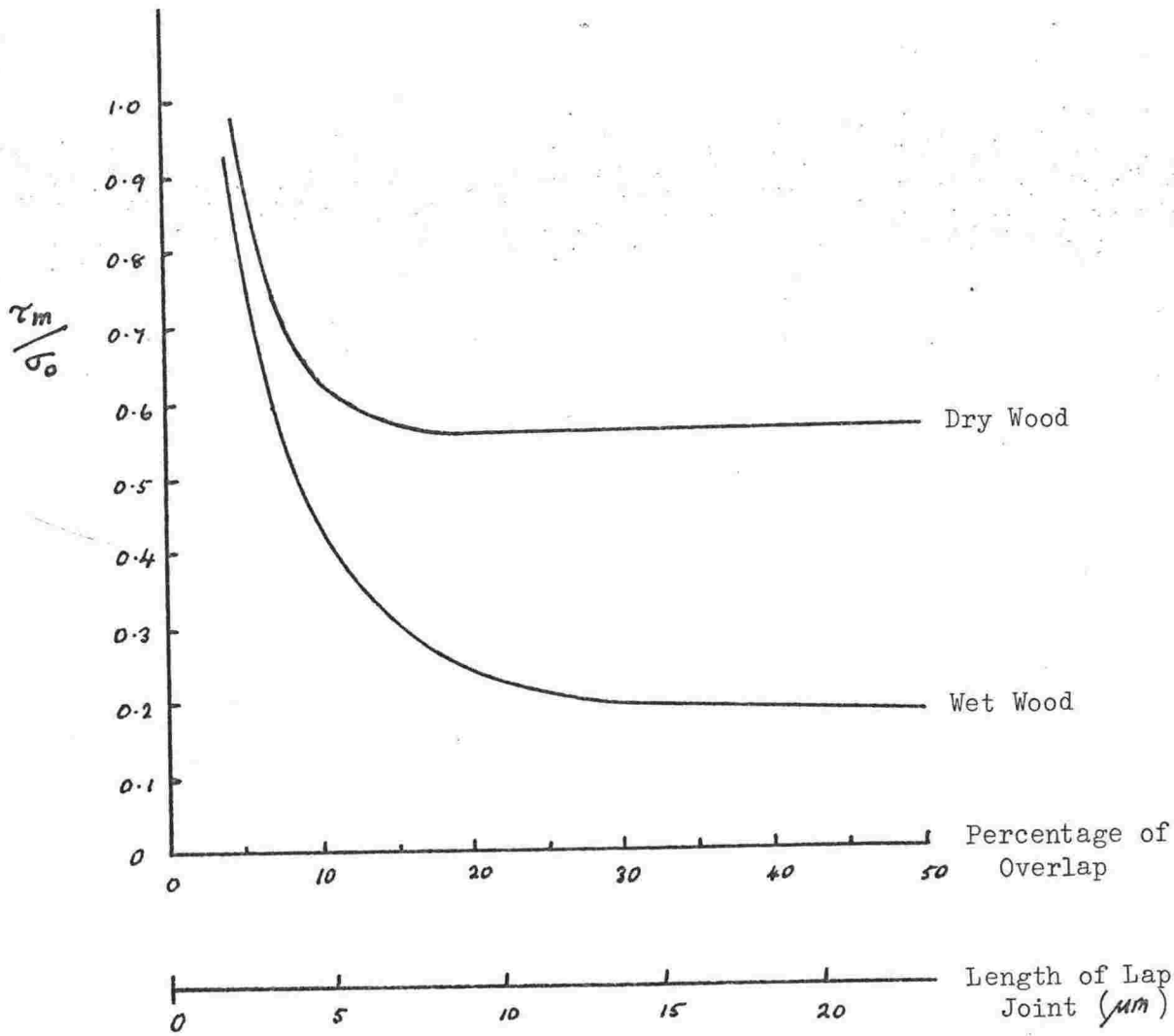

Fig. 51 : Effect of Overlap on Middle Lamella Shear Stresses after splitting has occurred in the Tangential walls.

Summary (2)

Possible reasons for the transwall failure of some springwood tracheids are -

(a) large tangential diameter,

(b) thinner than average walls,

(c) low S_2 microfibril angle, and

(d) high degree of tracheid overlap.

Reasons (a) and (b) were considered in section 4:1, and appeared to be of little importance. Reason (c), low microfibril angle, has been examined experimentally and also seems to be unimportant. However, the fourth possibility, high degree of overlap, leads to sufficiently large increases in wall stresses to account for the occurrence of transwall failure. The effects of degree of overlap were examined by means of a finite element technique. The important results are as follows-

(i) Shear stresses in radial middle lamella (parallel to applied stresses) are always much lower than either radial wall tensile stresses or tangential middle lamella tensile stresses. Therefore, either the tracheid radial wall, or the tangential middle lamella will be first to fail.

(ii) As the degree of overlap is increased from 0% to 20% (in a springwood tracheid of 45μm radial diameter) the ratio radial wall tensile stress/tangential

middle lamella tensile stress increases by 40% in wet wood, and by 17% in dry. From 20% to 50% overlap, little further increase occurs.

These changes seem sufficiently large to account for the observed transwall failure. However, quantitative estimates of the amounts of transwall failure cannot be made without knowledge of -

(a) wall strengths, and

(b) the distribution of degrees of overlap.

(iii) If tangential middle lamella failure occurs first, middle lamella lap joints still link adjacent tracheids, and wall failure is still likely at high degrees of overlap. (Note that to be in agreement with experimental observations, middle lamella "failure" would have to occur at the edge of the middle lamella region in either the P or the S_1 layers of the tracheid wall. The reasons for this are not clear, but since this type of splitting will result in the fracture of mainly matrix material, the above results are thought to give a valid indication of the stresses required to initiate intrawall failure.)

(iv) Calculations suggest that the transverse tensile strengths of the tracheid wall must lie in the following ranges -

airdry springwood : 2.0 → 3.6 Kg/mm^2

wet springwood : 0.6 → 3.4 Kg/mm^2

The upper limits are the strengths beyond which no transwall failure can occur, and the lower limits are simply matrix tensile strengths.

Chapter 5 THE TRANSVERSE STRENGTH OF THE TRACHEID WALL

5:1 The Strength Criterion

A considerable amount of research, both theoretical and experiental, has been carried out on the strength of fibre-reinforced materials. Theories of strength range from applications of semi-empirical yield conditions (e.g. Tsai (33,34), Shu and Rosen (35), Lance and Robinson (36)) to statistical treatments (Zweben and Rosen (37)). The work that is most applicable to the wood cell wall is that of Tsai, who considered the brittle fracture of glass fibre reinforced composites. Tsai suggested that "strength" and "yield" be considered synonymous, and applied Hill's yield critereon (Hill (38)) to orthotropic material. Assuming a state of plane stress (since the composite material is in the form of thin plates) the yield condition becomes

$$\left(\frac{\sigma_3'}{\Gamma_3}\right)^2 - \left(\frac{\sigma_2'\sigma_3'}{\Gamma_3^2}\right) + \left(\frac{\sigma_2'}{\Gamma_2}\right)^2 + \left(\frac{\sigma_4'}{\Gamma_4}\right)^2 = 1 \quad , \qquad \ldots\ldots(4)$$

Where σ_2', σ_3', σ_4', and Γ_2, Γ_3, Γ_4 are, respectively, the transverse longitudinal, and shear stresses and strengths in the unidirectional

---

(33) Tsai, S.W. (1965) N.A.S.A. Contractor Report CR-224 "Strength Characteristics of Composite Materials".

(34) _____ D.F. Adams, and D.R. Doner (1966) N.A.S.A. Contractor Report CR-620 "Analysis of Composite Structures".

(35) Shu, L.S., and B.W. Rosen. (1967) J. Composite Materials 1 p.366 "Strength of Fibre-reinforced Composites by Limit Analysis Methods".

(36) Lance, R.H. and D.N. Robinson (1971) J. Mech. Phys. Solids 19 p.49 "A Maximum Shear Stress Theory of Plastic Failure of Fibre-reinforced Materials".

(37) Zweben, C., and B.W. Rosen. (1969) J. Mech. Phys. Solids. 18 p.189 "A Statistical Theory of Material Strength with Application to Composite Materials".

(38) Hill, R. (1960) "The Mathematical Theory of Plasticity". (O.U.P.)

composite. The stresses are referred to the co-ordinate system coincident with that of material symmetry, so any other stresses must be transformed to this co-ordinate system before application of the yield criterion. In a plane stress situation, the transformation process is simply an in-plane rotation about the "1" axis. The relations are given below, in matrix form -

$$\begin{bmatrix} \sigma_2' \\ \sigma_3' \\ \sigma_4' \end{bmatrix} = \begin{bmatrix} c^2 & s^2 & 2cs \\ s^2 & c^2 & -2cs \\ -cs & cs & c^2-s^2 \end{bmatrix} \begin{bmatrix} \sigma_2 \\ \sigma_3 \\ \sigma_4 \end{bmatrix} \quad \cdots\cdots(5)$$

Where $c = \cos\theta$,

$s = \sin\theta$,

and positive θ is shown in Fig. 52.

Fig. 52.

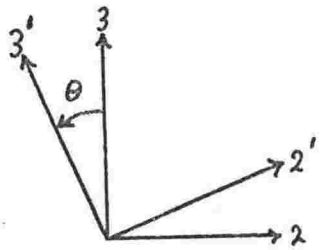

5:2 Yield Stresses

The yield stresses Γ_2, Γ_3, Γ_4, generally have to be measured experimentally for the composite under consideration. In the case of a parallel fibre-reinforced composite (such as a single layer of the wood cell wall) Γ_3 is the measured strength when stresses are applied in a direction parallel to the reinforcing fibres, Γ_2 when stresses are perpendicular to the fibres, and Γ_4 when shear stresses lie parallel to the "2" and "3" axes.

Measurement of the yield stresses of the S_1 and S_2 layers of the

wood tracheid wall did not prove possible, but estimates were made from available data. These are tabulated below in Table 8. The origin of each of these figures is outlined in appendix 5.

	S_1 Layer		S_2 Layer	
	Γ_3	Γ_2, Γ_4	Γ_3	Γ_2, Γ_4
Airdry	50	2.0	100	2.0
Saturated	50	0.6	100	0.6

Units = Kg/mm^2

Table 8 : Yield Stress of the Layers of the Tracheid Wall.

Applications of the Strength Criterion

5:3 Parallel-Fibre-Reinforced Composite : Uniaxial Loading

A parallel-fibre-reinforced composite is shown in Fig. 53. The primed axes are the material symmetry axes. A tensile stress, σ_3 is applied parallel to the "3" axis (i.e. at an angle θ to the reinforcing fibres).

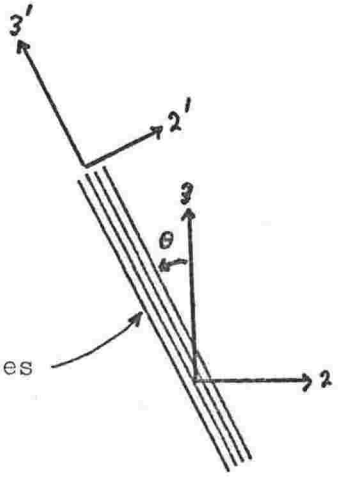

Fig. 53 Parallel-fibre-reinforced composite

From equations 4 and 5 the strength of the composite($\sigma_{3\,max}$) is given by

$$\sigma_{3max}^{2} = \left[\frac{c^4 - c^2 s^2}{\Gamma_3^2} + \frac{s^4}{\Gamma_2^2} + \frac{c^2 s^2}{\Gamma_4^2} \right]^{-1} \quad \ldots\ldots (6)$$

As an illustration, equation 6 may be applied to individual layers of the tracheid wall. For instance, the dependence of strength on θ is illustrated in Fig. 54 for both wet and dry S_2 layers. (Tsai (33,34) obtained similar curves for his glass fibre-reinforced composites, and verified them experimentally.) They show that as θ increases from zero, strength decreases very rapidly at first ($0^\circ \leq \theta \leq 20^\circ$) but much more slowly later ($40^\circ \leq \theta \leq 90^\circ$).

These trends agree with the relationship between tracheid longitudinal strength and microfibril angle observed by Cave (39). In this case θ would be the angle between the applied (longitudinal) load and microfibril direction. (The S_1 layer makes very little contribution to longitudinal strength).

Also, when transverse loads are applied to a tracheid, the angle between the S_2 microfibril directions and applied loads will be large, in the range 50 to 90°. The dependence of strength on angle in this range is slight, which agrees with previous observations that cells with low microfibril angles do not break preferentially. (See section 4:5.)

5:4 Complete Tracheid Wall : Transverse Loading

In a complete double tracheid wall (Fig.55) there are two S_2 layers

---

(39) Cave, I.D. (1969) Wood Sci. & Techno. 3 p.40 "The Longitudinal Young's Modulus of Pinus Radiata".

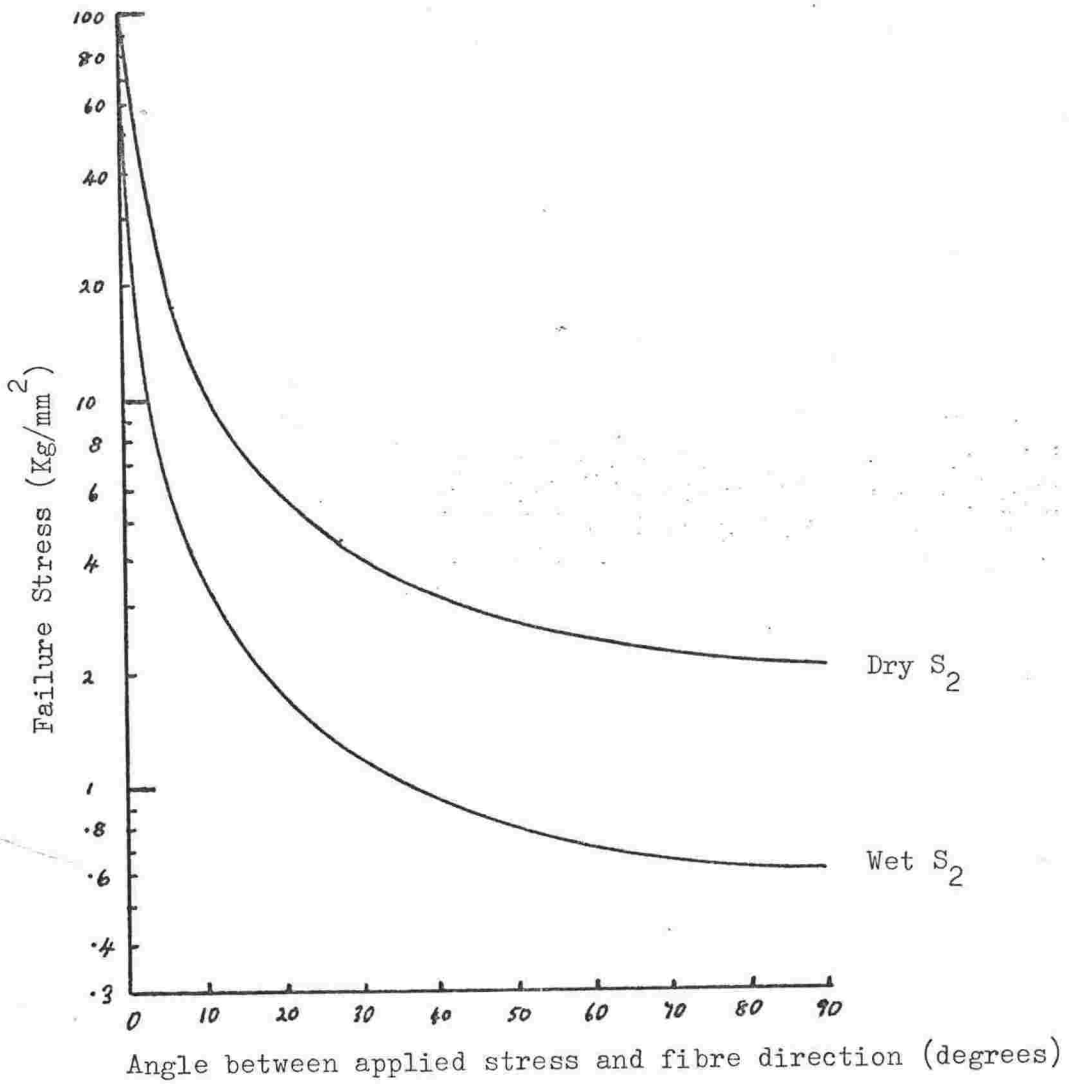

Fig. 54 : Dependence of composite strength on the angle between applied tensile loads and the reinforcing fibre direction.

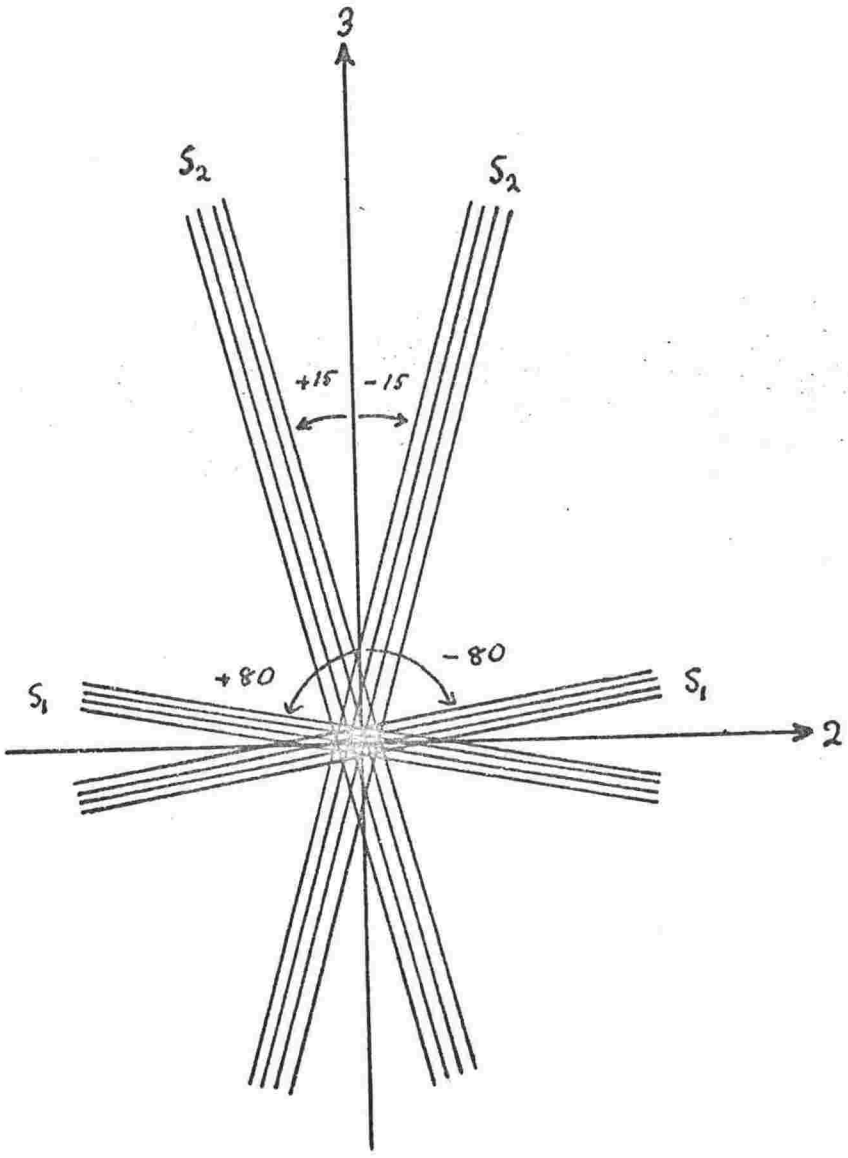

Fig. 55 : Microfibrillar Orientations viewed along the "1" axis.

two S_1 layers, and a middle lamella. In one of the S_2 layers the microfibrils will be oriented at 15^o to the "3" axis, in the other at -15^o. A completely balanced structure results. All layers are firmly attached to one another, so are constrained to undergo identical in-plane strains in response to any applied loads. This immediately means that no shear strains can result from applied axial tensile loads.

To simulate transverse loading, apply a stress σ_2 to the wall (i.e. $\sigma_2 > 0$, $\sigma_1 = \sigma_3 = \sigma_4 = 0$). The strains in the cell wall will be $\varepsilon_1 = S_{12}\sigma_2$, $\varepsilon_2 = S_{22}\sigma_2$, $\varepsilon_3 = S_{23}\sigma_2$, $\varepsilon_4 = 0$, where the S_{ij} are compliances of the tracheid double wall. All layers must undergo these strains. Therefore, the stresses in each layer are given by -

$$\begin{pmatrix} \sigma_1^* \\ \sigma_2^* \\ \sigma_3^* \\ \sigma_4^* \end{pmatrix} = \begin{pmatrix} C_{11} & C_{12} & C_{13} \\ C_{12} & C_{22} & C_{23} \\ C_{13} & C_{23} & C_{33} \\ C_{14} & C_{24} & C_{34} \end{pmatrix} \begin{pmatrix} S_{12}\sigma_2 \\ S_{22}\sigma_2 \\ S_{23}\sigma_2 \end{pmatrix} \quad , \ldots\ldots\ldots (7)$$

where the C_{ij} are stiffness of the layer under consideration.

Since there are no restraints in the "1" direction σ_1^* must be zero always, i.e. $C_{11}S_{12} + C_{12}S_{22} + C_{13}S_{23} = 0$,

The other stresses are non zero and may be written as

$\sigma_2^* = A\sigma_2$, where $A = C_{12}S_{12} + C_{22}S_{22} + C_{23}S_{23}$

$\sigma_3^* = B\sigma_2$, where $B = C_{13}S_{12} + C_{23}S_{22} + C_{33}S_{23}$

$\sigma_4^* = C\sigma_2$, where $C = C_{14}S_{12} + C_{24}S_{22} + C_{34}S_{23}$

Applying equation 5 gives -

$\sigma_2' = D\sigma_2$ $\qquad D = c^2A + s^2B + 2csC$

$\sigma_3' = E\sigma_2$, where $\qquad E = s^2A + c^2B - 2csC$

$\sigma_4' = F\sigma_2$ $\qquad F = cs(B-A) + (c^2-s^2)C$

The strength criterion, equation 4 then gives -

$$\sigma_{2\,max}^{2} = \left[\frac{E^2 - DE}{\Gamma_3^2} + \frac{D^2 + F^2}{\Gamma_2^2} \right]^{-1} \qquad \ldots\ldots\ldots (8)$$

Equation 8 gives the transverse stress σ_2 that is required to cause failure of S_1 and S_2 layers, provided no previous failures have occurred. The results for wet and dry springwood are tabulated in Table 9.

	S_2	S_1
Dry	3.33	2.00
Wet	1.85	.34

(Units = Kg/mm^2)

Table 9 : Transverse stresses required to cause failure of S_1 and S_2 layers in a complete double cell wall.

Note that the S_1 layer always fails first, making the S_2 figures invalid, and that "dry" stresses are greater than "wet" stresses.

The type of failure in each case may be determined in the manner described by Chiu (40). If $\frac{\sigma_3}{\sigma_2} > \frac{\Gamma_3}{\Gamma_2}$, and $\frac{\sigma_3}{\sigma_4} > \frac{\Gamma_3}{\Gamma_4}$,

---

(40) Chiu, K.D. (1969) J. Composite Materials 3 p.578 "Ultimate Strengths of Laminated Composites".

the yield condition is categorised as longitudinal. Otherwise it is categorised as transverse or shear. Applying these relations shows that failure of both S_1 and S_2 layers is transverse or shear, i.e. splits form in a direction parallel to the microfibrils.

The first layer to fail is the S_1. However, because of its microfibrillar orientation it still retains some of its strength in the loading direction, and cannot be ignored. After initial splitting the non-zero stiffness constants of the S_1 layer (referred to the symmetry axes) are C_{11}, C_{13} and C_{33}. All others are zero. Using these in place of the appropriate constants of Table 15, it is possible to calculate the stiffness constants for springwood and summerwood tracheid walls which contain split S_1 layers. These are tabulated in Table 21, (appendix 2). It can be seen that the new stiffness constants are very little different from the previous values, especially for summerwood.

Repeating the strength calculations shows that wet and dry S_2 failures now occur when applied stresses are 1.05 and 3.22 Kg/mm^2 respectively. Once again, failure is a splitting of the matrix in a direction parallel to the microfibrils.

If complete wall failure follows S_2 splitting without further increases in stress, then the above figures are the transverse strengths of springwood cell walls. Since they lie within the ranges specified in section 4:8, it would follow that transwall failure occurs when tracheid overlap is high, but not when it is low.

Unfortunately it is not possible to determine from the present theory whether or not fibre failure will follow matrix splitting. If microfibrils are separate fibres with finite lengths (about 10μm), then fibre separation and complete wall failure is likely to follow matrix splitting. But if they can be regarded as having infinite length, complete failure may require higher stresses. However, the above figures will provide a lower limit to strength, so wet and dry wall transverse strengths must lie in the ranges 1.1 → 3.4 and 3.3 → 3.6 Kg/mm^2 respectively.

The methods used in this chapter may also be applied to the summerwood tracheid wall. In this case, since a negligible amount of transwall failure occurs the only prior requirements are that the wet and dry transverse strengths exceed .72 and 2.15 Kg/mm^2 respectively. The transverse stresses at which matrix splitting occurs are tabulated below, and it can be seen that those pertaining to the S_2 layer do satisfy these requirements.

	S_2	S_1
Dry	2.59	1.55
Wet	0.99	0.17

(Kg/mm^2)

Table 10 : Transverse stresses required to cause matrix splitting in the S_1 and S_2 layers of summerwood.

5:5 Variations in S_1 Thickness and Tracheid Wall Strength

So far calculations have been based on the assumption of constant S_1 layer thickness, despite the fact that Fengels' figures (table 1) indicate a variation of approximately 30%. That the S_1 layer makes an important contribution to cell wall strength can be illustrated by comparison of stresses required to cause failure of a parallel-fibre-reinforced composite when loading is at 85° to the fibre direction, and those leading to S_2 splitting in the complete cell wall. One might, therefore, expect variations in the thickness of the S_1 layer to lead to variations in wall strength. Such variation has not been considered explicitly, but a good estimate of its importance can be obtained by comparison of the springwood and summerwood "strengths" calculated in section 5:4. The relevant figures are (Table 11) -

	Ratio of S_1 thickness : S_2 thickness	Dry Wood	Wet Wood
Springwood	3 : 17	3.3	1.1
Summerwood	1 : 19	2.6	1.0

Table 11 : Stresses Required to Cause S_2 Splitting (Units Kg/mm^2)

The above figures may also be regarded as pertaining to cell walls having equal thicknesses, but different percentage layer compositions. That is, the figures labelled "springwood" belong to a wall comprising 15% S_1, whilst those labelled "summerwood" belong to one comprising 5% S_1, but which has the same thickness as the first. The range 15% S_1 to 5% S_1 is slightly greater than that indicated by Fengel, and leads to variations in S_2 splitting stresses of 6% for wet wood, and 22% for dry. The wet wood "strength" variation is much smaller than

variations in the ratio "radial wall stress/maximum middle lamella stress" that result from changes in cell overlap, so the latter is likely to be the dominant factor in controlling fracture behaviour. In dry wood, "strength" variation is comparable to variations in "radial wall stress/maximum middle lamella stress", so cannot be ignored. Also, bearing in mind the very narrow limits set on wall strength by -

(a) matrix splitting (3.3 Kg/mm^2), and

(b) the strength beyond which no transwall failure can occur (3.6 Kg/mm^2),

it seems very likely that at least some of the observed transwall failure results from the failure of thinner than average S_1 layers.

Summary

A semi-empirical criterion of strength of a parallel-fibre-reinforced composite was applied to the tracheid wall. Transverse loads were applied to the wall, and the stresses at which failures occurred in the various layers were calculated.

Results

(i) The S_1 layer is always the first to fail. Splits form in the matrix in a direction parallel to the reinforcing microfibrils, which themselves do not break. Assuming that the S_1 microfibrils are still intact, it is possible to calculate the elastic constants for a wall containing a split S_1 layer. These turn out to be very little different from the original values.

Continuing the analysis shows that the next failure is a matrix splitting in the S_2 layer, again parallel to the microfibrils.

The transverse stresses at which matrix splitting occurs are tabulated below -

	Springwood		Summerwood	
	S_1	S_2	S_1	S_2
Dry Wood	2.0	3.3	1.6	2.6
Wet Wood	0.34	1.1	0.17	1.0

(Units : Kg/mm^2)

(ii) Unfortunately, the theory gives no indication of when fibre failure is likely to occur. It may be that complete fibre failure requires a further increase in stress. Therefore, all that can be said is that the above S_2 splitting stresses represent lower limits to tracheid wall transverse strengths. This restricts wall strengths to the following ranges -

dry springwood $3.3 \rightarrow 3.6$ Kg/mm^2, and

wet springwood $1.1 \rightarrow 3.4$ Kg/mm^2.

(iii) It was also shown that in dry wood only, changes in the thickness of the S_1 layer can lead to significant variations in wall transverse strength. Therefore, dry cells with

thinner than average S_1 layers will be more likely to fail in the transwall mode.

Chapter 6 A HYDROGEN-BOND EXPLANATION FOR THE STRAIN RATE SENSITIVITY OF HEMICELLULOSE AND LIGNIN

The purpose of this chapter is to explain why the strength of matrix (hemicellulose and lignin) increases as the strain rate is increased.

Since the explanation involves the properties of hydrogen bonds, and the use of reaction-rate theory, these will be briefly reviewed in sections 6:1 and 6:2.

6:1 Hydrogen Bonds

A hydrogen bond is a low energy bond resulting from electrostatic attraction between certain molecules. For example, in water, the probability distribution of the valence electrons is such that the oxygen atom has a small residual negative charge, and the hydrogen atoms have small residual positive charges. As a result, correctly orientated molecules will be attracted to one another as shown in Fig. 56.

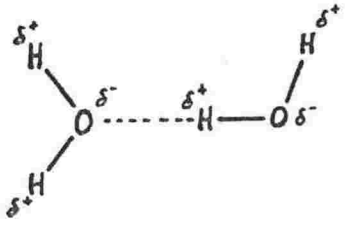

Fig. 56 : Hydrogen bonds between water molecules.

Only molecules containing strongly electronegative atoms such as O, N, Cl, F, are able to form hydrogen bonds. Therefore, in carbohydrate molecules such as cellulose, hemicellulose and lignin,

hydrogen bonds will form between adjacent "OH" groups, but not between "CH" groups.

Because the residual charges are small, the hydrogen bond is much weaker than a covalent bond. Typical bond energies are :- covalent bonds, 2 to 3 electron volts, hydrogen bonds, .2 electron volts. This means that at room temperature, many hydrogen bonds will have sufficient thermal energy to rupture.

6:2 Reaction-Rate Theory

(References: Glasstone (41), Glasstone, Laidler & Eyring (42))

Consider a simple chemical reaction -

$$AB + C \rightarrow A + BC + \Delta G$$

where ΔG is the free energy evolved during the reaction.

Before any reaction can occur between an atom C and a molecule AB, the two must be brought into very close contact, to form what is known as an activated complex. Because of repulsion between the electron clouds of AB and C, this process requires a definite amount of energy, called the "activation energy". This is represented by

---

(41) Glasstone, S. (1946) "Textbook of Physical Chemistry". (Van Nostrand Co., N.Y.) p.1087.

(42) _____ K.J. Laidler, and H. Eyring. (1941) "Theory of Rate Processes" (McGraw Hill, N.Y.).

G_1 (the Gibbs free energy of activation) in the potential energy diagram, Fig. 57.

The activated complex, A...B...C may then decompose to form products A and BC with the release of energy G_2. The free energy of the reaction ΔG is the difference between G_2 and G_1.

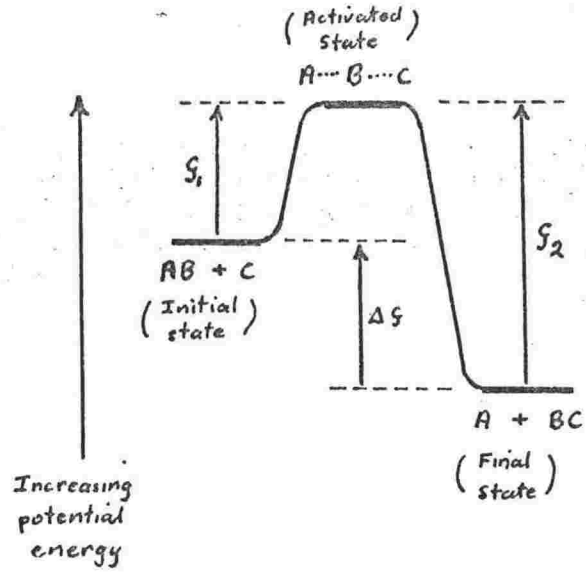

Fig. 57 Potential Energies

Let M_1 be the molar concentrations of AB and C, and M_2 be the concentrations of A and BC. Then, the rate of increase in M_2 is given by $\frac{dM_2}{dt} = k_1 M_1^{\,2}$ .....(9a)

Constant k_1 is called the rate constant of the reaction, and is given from the theory of absolute reaction rates (Glasstone, Laidler & Eyring (42)) to be $k_1 = \frac{kT}{h} e^{(-G_1/RT)}$ .....(9b)

In equation 9a, the exponent of M_1 is called the order of the reaction, and represents the number of molecules which must simultaneously be activated before the reaction can take place.

For the reverse reaction, A + BC $\rightarrow$ AB + C $-\Delta G$, the rate of

increase in M_1 is given by - $\frac{dM_1}{dt} = k_2 M_2^2$,

where $k_2 = \frac{kT}{h} e^{(-S_2/RT)}$

k = Boltzmanns constant

h = Plancks constant

R = Universal gas constant

T = Absolute temperature

When an equilibrium state is reached and there is no further change in either M_1 or M_2, the rate of the forward reaction (formation of products) must equal the rate of the reverse reaction (break up of products).

That is, $\frac{dM_1}{dt} = \frac{dM_2}{dt}$ which implies $k_1 M_1^2 = k_2 M_2^2$.

6:3 Application of Rate Theory to the Formation and Rupture of Hydrogen Bonds in Wood

The formation and rupture of hydrogen bonds in wood may be represented by the equation -

$$nA + nB \underset{(2)}{\overset{(1)}{\rightleftharpoons}} n\,A...B + n\Delta G.$$

A and B represent any possible hydrogen bond forming regions of cellulosic molecules, which may combine to form the hydrogen bonded molecule A...B. Let the concentrations of A and B each be M_1 (moles/litre), and the concentration of A...B be M_2.

The rate of the formation reaction (1) is given by $\frac{dM_2}{dt} = k_1 M_1^{2n}$,

and the rate of the reverse reaction (2) by $\frac{dM_1}{dt} = k_2 M_2^{\,n}$.

In an unstrained sample of wood, there can be no net breakage or formation of bonds, therefore, $\frac{dM_1}{dt} = \frac{dM_2}{dt}$, and $k_1 M_1^{\,2n} = k_2 M_2^{\,n}$.

The exponent n represents the number of bonds that must simultaneously be activated, and it arises as follows. In hemicellulose and lignin, touching molecules must have an area of contact at least as large as one pyranose ring. Also, as a result of the random orientations of molecules, contact areas will probably be no larger than three or four pyranose rings. Over this area there are several possible hydrogen bond sites so it is likely that there will be several hydrogen bonds linking adjacent molecules at all points of contact. Therefore, hydrogen bonds will not occur singly, but in separated groups, each of which contains several bonds. Such a group of bonds is illustrated in Fig. 58(a).

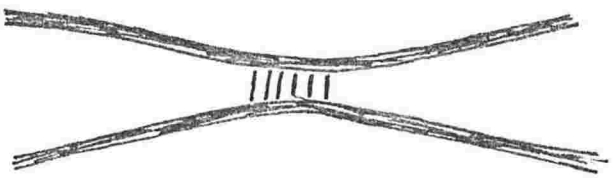

Fig. 58(a) Hydrogen Bonding between adjacent hemicellulose or lignin molecules.

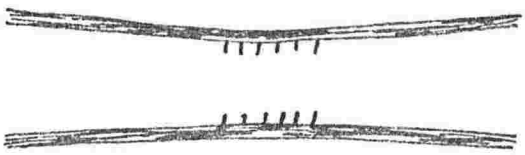

Fig. 58(b) Ruptured hydrogen bonds.

Rupture of any single bond requires the separation of the parent molecules that form it. This is possible only if the group of hydrogen bonds is ruptured as a whole. That is, if there are n hydrogen bonds in a group, all must be activated simultaneously

before rupture can occur.

Similar arguments can be applied to the reformation process. 2n potential hydrogen bond sites must be brought into close contact to form n hydrogen bonds. (Fig. 58(b).)

6:4 Activation Energies

Activation energies and heats of reaction have been measured for many reactions involving the rupture and formation of hydrogen bonds. The most readily available figures are for G_2 and ΔG. These are listed in appendix 6, together with a brief description of the origin of each figure.

For lack of any better information, the means of the values given for G_2 and ΔG will be assumed to govern the rupture and formation of hydrogen bonds in wood. Therefore, the activation energies of hydrogen bond reactions in wood are -

G_1 = 3.1 Kcal/mole (.13 e.v./bond)

G_2 = 5.2 Kcal/mole (.23 e.v./bond)

6:5 Effects of Applied Stresses in Hemicellulose and Lignin

Assume that hemicellulose and lignin consist of rigid polymer molecules bonded together by hydrogen bonds. On a large scale the bonds appear to be uniformly distributed, even though on a molecular scale they occur in separated groups. Assume that one third of the bonds is aligned along each of the cartesian reference axes . Then, if a tensile load is applied in a direction parallel

to one of the axes, that third of the bonds parallel to it will be stressed, whilst the remaining two thirds will be unstressed. It is convenient to assume that all stressed bonds carry the same load. (This is not true in a real material and possible effects of varying loads will be considered later.)

Let there be N load carrying hydrogen bonds per cubic metre of matrix material. Then the density of bonds in a plane perpendicular to their direction is $N^{2/3}$ bonds/m^2. If a tensile stress of σ newtons/m^2 is applied to the material, the load carried by each bond will be $\sigma/N^{2/3}$ newtons. Therefore, the strain energy per bond will be $\sigma^2/2N^{4/3}K_b$ joules, where K_b is the spring constant of one hydrogen bond. (K_b is given by Jaswon, Gillis, & Mark (43) to be 50N/m.)

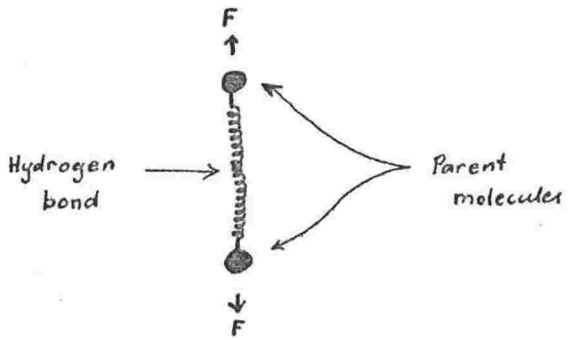

Fig. 59 Hydrogen bond (diagramatic)

Consider a typical hydrogen bond (Fig. 59). For it to rupture, its parent molecules must move apart, until it has sufficient strain energy to break. Normally this energy is supplied by thermal motion, but if a static load is applied to the bond in the correct direction,

---

(43) Jaswon, M.A., P.P. Gillis, & R.E. Mark (1968) Proc. Roy. Soc. A.306 p.389 "The Elastic Constants of Native Crystalline Cellulose".

as is indicated by the arrows in Fig. 59, the amount of strain energy to be supplied by thermal motion for rupture is decreased. Since a smaller amount of energy is more likely to be available than a larger amount, the breakage of the bond becomes more probable.

The recombination process too will be affected. The parent molecules will be further apart than in the unstrained state, so more thermal energy will be required to bring them together for bond formation.

In summary, the effect of the bond strain energy is to decrease the activation energy of the rupture reaction (G_2) by an amount Gs, and to increase that of the formation reaction (G_1) by an amount G'_S. (See Fig. 60.)

Postulate

G_S and G'_S are numerically equal to the strain energy of the loaded hydrogen bonds when all energies are expressed in the same units i.e.

$$G_S = G_S' = C\sigma^2/2N^{4/3}K_b \qquad \ldots\ldots(10)$$

(C is a conversion factor, joules/bond → calories/mole.)

The rate of breaking of hydrogen bonds now becomes -

$$\frac{dM_1'}{dt} = M_2^n \frac{kT}{h} \exp\left(\frac{-G_2 + G_S}{RT}\right) = k_2 M_2^n \exp\left(\frac{G_S}{RT}\right),$$

and the rate of reformation -

$$\frac{dM_2'}{dt} = M_1^{2n} \frac{kT}{h} \exp\left(\frac{-G_1 - G_S}{RT}\right) = k_1 M_1^{2n} \exp\left(-\frac{G_S}{RT}\right).$$

There is now no longer an equilibrium situation. The rate of breaking of bonds exceeds the rate of formation, so that there is a net breakage of bonds. The rate of breaking is given by

$$R_b = k_2 M_2^{\,n} \exp\left(\frac{G_s}{RT}\right) - k_1 M_1^{\,2n} \exp\left(-\frac{G_s}{RT}\right), \quad \ldots\ldots(11)$$

where G_s is given by equation 10.

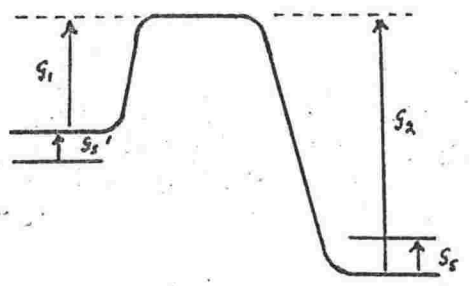

Fig. 60 Potential energy diagram.

Application

Let the intial concentration of undissociated bonds be M_{2i}. Then the initial concentration of dissociated bonds will be given by -

$$k_1 M_{1i}^{\,2n} = k_2 M_{2i}^{\,n},$$

and total concentration of bonds by

$$M_o = M_{2i} + M_{1i}.$$

If at time t = 0 a stress σ is applied and maintained constant, the concentration of whole bonds will decrease as time t increases, and will be given by

$$M_2 = M_{2i} - \int_0^t R_b \, dt \qquad \ldots\ldots(12)$$

M_1, the concentration of dissociated bonds, will be equal to $M_o - M_2$. If the concentration of bonds at which catastrophic failure occurs, is known, equation 12 leads to the time to failure for any given stress σ. Thus the relationship between strength and failure time may be built up. (It will be shown later that $M_2 = 0$ is a reasonable

criterion for failure.)

In the experiments reported in this thesis, the method of loading was not static stress, but ramp loading. This may be simulated by replacing σ by αt where "α" is a constant. Equation 12 will then give rise to both failure times and failure stresses.

As yet there are two unknown quantities in equation 11 :- M_{2i}, the initial concentration of whole bonds and n, the order of the reaction. Sometimes their values may be derived from other sources, but failing this they may be obtained by comparing the strength versus failure time relationship obtained from equation 11 with experimental data. (This is a simple process, since the two

In the case of wet wood, the parameters giving the best fit curves lie in the range $M_{2i} = 1.0 \times 10^{-3}$, $n = 5.0$, to $M_{2i} = 1.2 \times 10^{-3}$, $n = 4.8$. Both resulting curves are shown in Fig. 61. Also plotted (in Fig. 62) are curves for the following parameter values -

$$n = 4.0 \qquad \begin{cases} M_{2i} = 1.5 \times 10^{-3} \\ M_{2i} = 1.0 \times 10^{-3} \\ M_{2i} = 7.5 \times 10^{-4} \end{cases}$$

6:6 Discussion

The dry wood order of reaction (8.5) is somewhat higher than the value of 6.0 given for paper by Nissan (17). However, it is still a reasonable value since two overlapping cellobiose units may easily be linked by this number of hydrogen bonds.

In wet wood, the order of reaction is lower, which indicates that the adsorbed water has had a plasticising effect. At the same time the concentration of load bearing hydrogen bonds has increased. This is not unreasonable since water molecules may penetrate the open network of polymer molecules and form intermolecular links where previously there were none.

One important point to note is that the term "hydrogen bond" as used so far refers to some kind of load bearing entity which links two adjacent polymer molecules. There is no reason why such an entity should not in fact be composed of several hydrogen bonds in series. So far as the arguments used in this chapter are concerned, such a structure would be indistinguishable from a single

hydrogen bond.

In oven dry wood, all intermolecular links will be single hydrogen bonds. In airdry wood, which contains 12% of its weight of water, most intermolecular links will still be single hydrogen bonds, but some will be structures like

polymer molecule ... H_2O ... polymer molecule

i.e. containing two hydrogen bonds in series. Finally, when wood is saturated, almost all linkages between adjacent polymer molecules will be via one or more water molecules, and will, therefore, consist of two or more hydrogen bonds, in series. As a result of this it is not possible to state the number of hydrogen bonds actually taking part in intermolecular linkages. Only the number of intermolecular links may be determined.

The only estimate for the concentration of load bearing entities in wood is due to Kauman (9) who shows via a probability argument that the number of intermolecular linkages is near 1.8×10^{-2} moles/l. This is approximately 20 times the value for M_{2i} but is close to values for M_o. These are tabulated below -

	n	M_{2i}	M_o
Dry Wood	8.0	7.5×10^{-4}	2.28×10^{-2}
	9.0	6.0×10^{-4}	2.08×10^{-2}
Wet Wood	4.8	1.2×10^{-3}	2.53×10^{-2}
	5.0	1.0×10^{-3}	2.33×10^{-2}

Table 12:

It is interesting to note that on addition of moisture, M_0 increases only slightly, but as a result of the change in the order of reaction, M_{2i} increases considerably. Both changes result in striking variations in the properties of wood.

Failure Criterion

So far, the criterion for failure has been $M_2 = 0$. That this is a reasonable value to choose is shown by Fig. 63, in which M_2 is plotted as a function of time. For all but the lowest loading rates in wet wood, M_2 does not begin to decrease until times (and stresses) have very nearly reached their final values. Also, the final decrease in M_2 is generally very rapid. In all cases the failure criterion could have been set at $M_2 = 0.7M_{2i}$ without substantially altering the results. The only effect would have been to delay the "levelling off" that occurs at the lower right ends of the "wet wood" curves of Figs. 61 and 62.

6:7 Rupture of Covalent Bonds in Crystalline Cellulose

Strain Rate and Transwall Failure in Wet Wood

Mark (44) shows that rupture of the C-O-C bridge between adjacent pyranose rings is the most likely means of failure of crystalline cellulose. Therefore, the relationship between the strength of this bond and the rate of breaking will be the same as the behaviour

---

(44) Mark, R.E. ~~(1965) in W.A. Côté, Jr. (Ed.)"Cellular Ultrastructure of Woody Plants" (Syracuse Univ. Press, Syracuse).~~ (1967) "Cell Wall Mechanics of Tracheids" (Yale Univ. Press, New Haven & London)

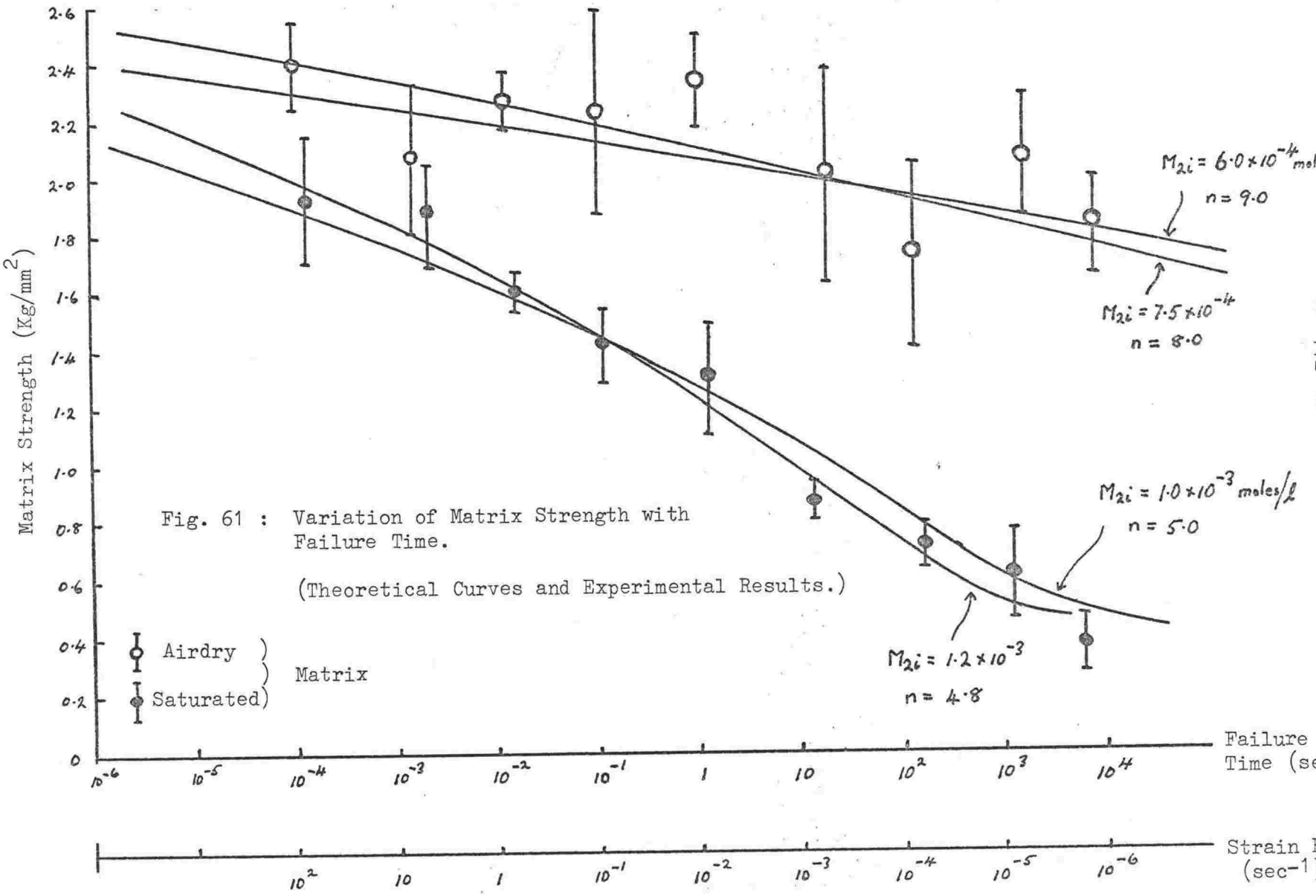

Fig. 61 : Variation of Matrix Strength with Failure Time.

(Theoretical Curves and Experimental Results.)

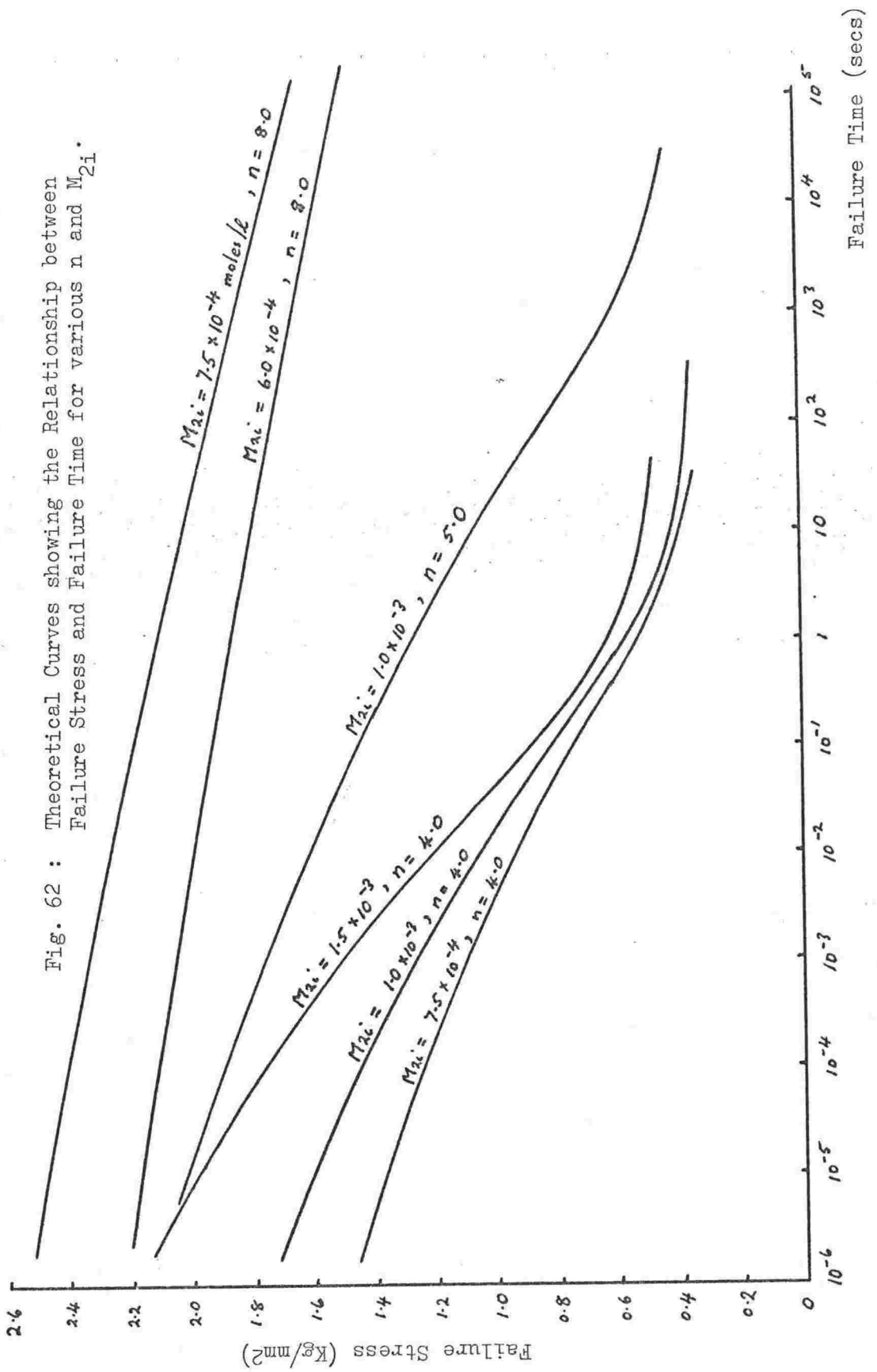

Fig. 62 : Theoretical Curves showing the Relationship between Failure Stress and Failure Time for various n and M_{2i}.

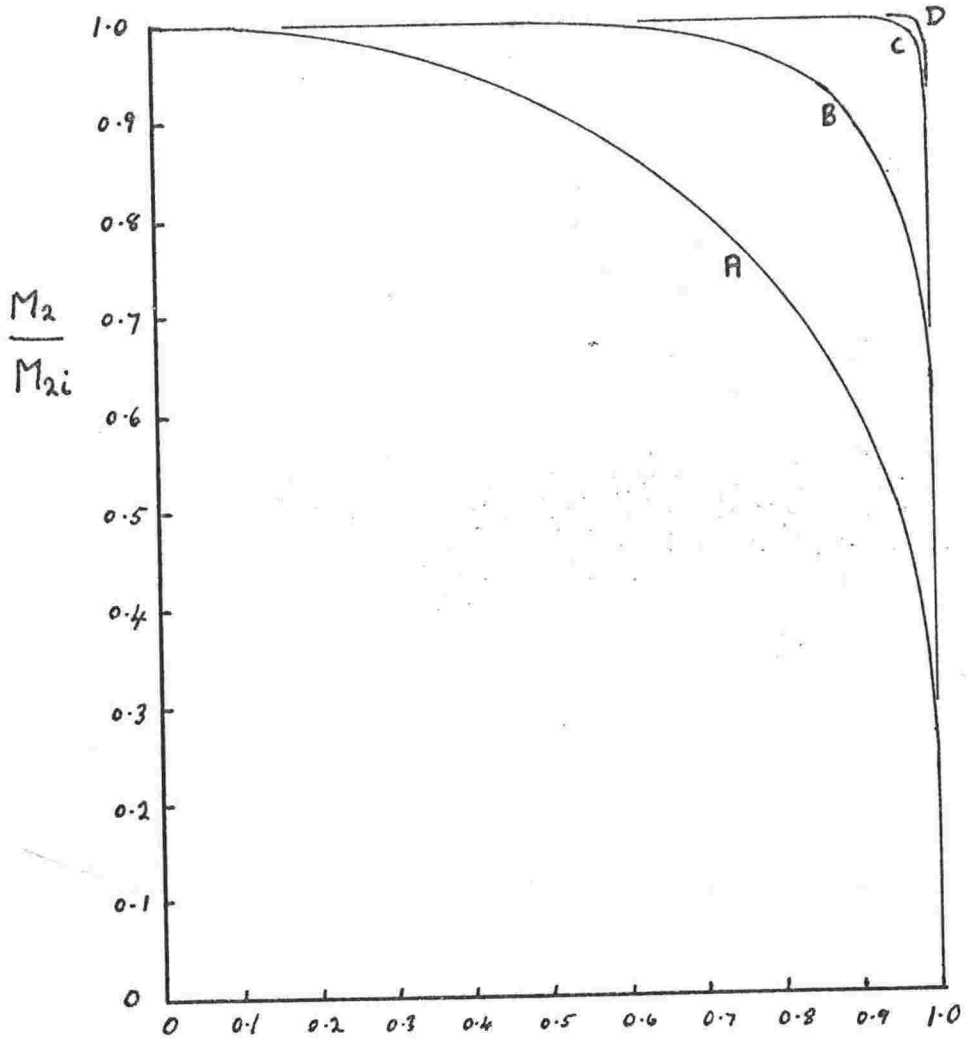

A n = 5 $M_{2i} = 1.0 \times 10^{-3}$ $t_f = 4.35 \times 10^{4}$

B n = 5 $M_{2i} = 1.0 \times 10^{-3}$ $t_f = 10.58$ } wet matrix

C n = 5 $M_{2i} = 1.0 \times 10^{-3}$ $t_f = 2.2 \times 10^{-7}$

D n = 8 $M_{2i} = 7.5 \times 10^{-4}$ $t_f = 1.6 \times 10^{5}$ dry matrix

(moles/litre) (seconds)

Fig. 63 : Variation of the Concentrations of Load-bearing bonds with time.

of crystalline cellulose.

In determining the strength versus failure-time behaviour of the C-O bond, the following points should be noted -

(1) The dissociation energy of the C-O bond is 90 Kcal/mole (Mark (44)). As an approximation set this equal to G_2.

(2) Recombination of broken bonds can be neglected, since applied stresses will be high.

(3) It is likely that bonds will break singly, since intermolecular links are via the much weaker hydrogen bonds. Therefore, n = 1.

(4) There are three bridges per unit cell of crystalline cellulose, which gives a concentration of roughly 5 moles/l.

Ignoring recombination, the rate of permanent breaking of bonds becomes :- $R_b = k_2 M_2 \exp\left(\frac{G_s}{RT}\right)$. From this equation it can be shown that decreasing G_s by 10% results in a $10^{6.5}$ fold increase in failure times. Therefore, over the range of failure times covered in Fig. 61, the relative strength variation of crystalline cellulose is very much less than variations in the strength of wet matrix. In other words, as breaking rate is increased, the strength of crystalline cellulose will remain very nearly constant, whilst the strength of wet matrix increases greatly. Therefore, if the transverse strength of the wet cell wall ultimately depends in some way on the strength of crystalline cellulose, the reason for

increased transwall failure at high strain rates becomes clear.

The transverse strength of wet wood has been restricted to the range 1.1 → 3.3 Kg/mm^2. The lower limit is the stress at which matrix splitting occurs, and the upper limit the strength beyond which transwall failure cannot occur. Therefore, it is possible that the ultimate transverse strength is higher than the matrix splitting stress, and dependent on the strength of crystalline cellulose.

(Note: The calculations of this section have been very approximate, but the major result obtained, that crystalline cellulose strength varies only slightly over the range of failure times, is likely to be reliable.)

6:8 Relative Amounts of Transwall Failure in Wet and Dry Woods at High Strain Rates

So far there has been no indication of what the relative amounts of transwall failure in wet and dry woods should be. These will be difficult to determine exactly without more precise values of wet wall transverse strengths, but a qualitative estimate is easily obtained.

At high strain rates, when wet and dry matrix have similar strengths, the reduction of middle lamella stresses that occurs at high degrees of cell overlap will still be much greater in wet wood than in dry, since elastic constants are independent of strain rate. Even including the effects of varying S_1 thickness in the worst possible

way cannot make up the difference. Therefore, one would expect to see a greater amount of transwall failure in wet wood, as is in fact observed.

6:9 Stress Relaxation

Stress relaxation in the matrix is likely to be quantitatively very similar to that of bulk wood, and should be predicted by the hydrogen bond model of matrix described in sections 6:3 and 6:5. Derivation of stress relaxation behaviour from this model simply necessitates the additional assumption that all matrix strain is due to the extension of its component hydrogen bonds. It then follows that $\sigma = \varepsilon N^{1/3} \kappa_b$, and the time variation of σ can be obtained by use of equations 11 and 12. Unfortunately, the resultant "stress relaxation" in matrix is nothing like that which is seen in bulk wood. The initial decrease in stress is much too slow, which is a consequence of the previous assumption that all hydrogen bonds bear identical loads.

In real matrix a significant proportion of bonds must bear such high loads that they will fail rapidly, even though the material as a whole is only lightly stressed. Failure of these will give rise to an initial rapid decrease in stress. Then, as time increases and more and more of the highly stressed bonds fail (leaving only the bonds which carry lower loads) the rate of breaking of bonds will tend to decrease, and the rate of reduction of stress will become smaller, as is observed. Therefore, it seems that although

the assumption of uniformly loaded bonds leads to a good description of the strength-time behaviour of matrix, some kind of distribution of varying bond loads must be an integral part of any theory which attempts to explain stress relaxation in the above manner.

Chapter 7 SUMMARY AND CONCLUSIONS

(1) Experimental

Small rectangular blocks of Pinus Radiata were broken in transverse tension. Initially, both radial and tangential loads were applied, but after a few preliminary tests it became apparent that tangential loading (leading to failure in the radial - longitudinal plane) was giving less useful results, so that thereafter only radial loading was considered. The conditions of fracture were varied as follows -

(i) strain rate : at 2×10^{-6} sec^{-1}, and in decade steps from 10^{-5} sec^{-1} to 10^{2} sec^{-1},

(ii) moisture content : 12.7% (airdry), saturated, and

(iii) structure : springwood and summerwood.

Two types of failure were observed, transwall and intrawall. (Transwall failure is the longitudinal splitting of a tracheid wall, and intrawall failure is a splitting between adjacent tracheids.) The proportion of fracture surface tracheids broken in transwall failure was not constant, but varied as follows. In summerwood there was always very little transwall failure. In dry springwood 20% of the surface tracheids were broken, at all strain rates; but in wet springwood the percentage varied with strain rate, ranging from nearly zero at 10^{-5} sec^{-1} to 55% at 10^{2} sec^{-1}.

The transverse strength of Pinus Radiata also was dependent on

strain rate and moisture content. At the lowest rate of 2×10^{-6} sec^{-1}, the strength of dry summerwood was 0.9 Kg/mm^2, and that of wet summerwood 0.2 Kg/mm^2. Both wet and dry strengths increased as strain rate was increased, until at 10^2 sec^{-1} they were nearly equal at 1.1 Kg/mm^2.

Springwood strengths followed similar trends.

Failure strain decreased as strain rate was increased. Over the range of rates covered, the decreases were approximately 40% for dry wood and 20% for wet. Springwood and summerwood strains were very similar, as is to be expected on the basis of specimen size. (Failure strains were generally near 1%.)

The energy absorbed during the fracturing process varied with strain rate and moisture content. As strain rate was <u>increased</u>, the energy absorbed by dry wood <u>decreased</u>, but that absorbed by wet wood <u>increased</u>. When expressed as specific surface energies (energy absorbed divided by nominal area of surfaces produced) measured values were in the range 1.0×10^2 to 4.0×10^2 $joules/m^2$.

<u>Theoretical</u>

A. <u>Surface Morphology</u>

Two major problems arose from the observed variations in fracture surface morphology -

(a) why did some tracheids fail in the transwall

mode, but others not, and

(b) why did the percentage of tracheids broken in transwall failure depend on tracheid structure, moisture content, and strain rate?

(1) Comparison of dry springwood and dry summerwood results shows that, respectively, 20%, and less than 5%, of the tracheids in the fracture surface were broken. The major structural differences between springwood and summerwood are -

(a) the summerwood tracheid wall is much thicker,

(b) the degree of tangential overlap is less in summerwood, and

(c) the radial diameter is much smaller in summerwood.

The effects of variations in wall thickness were examined in the first part of Chapter 4 by calculation of radial wall and tangential middle lamella tensile stresses in a regular array of tracheids such as that shown in Fig. 66. The tangential portions of tracheid wall were assumed to be continuous plates, which were loaded by the intersecting radial walls. The middle lamella joining adjacent plates was considered to be an "elastic foundation".

Fig. 66

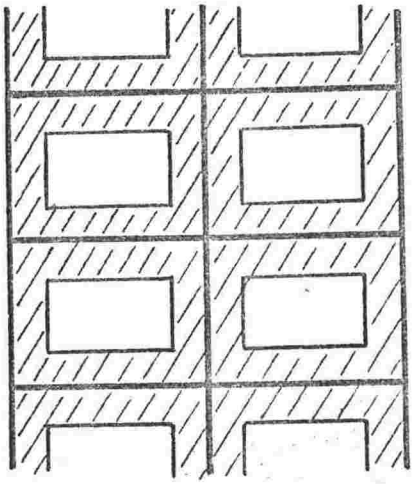

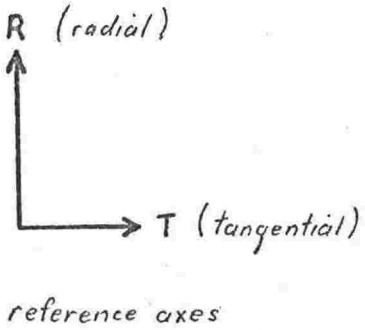

reference axes

Treatment of this problem followed the method of Timoshenko (26). The results obtained showed that because of the greater thickness of the summerwood tracheid wall, the radial wall stresses required to initiate middle lamella splitting are greater in springwood than in summerwood. Therefore, transwall failure is more likely to occur in springwood.

However, the springwood to summerwood transition results in a fourfold increase in wall thickness, for a stress change of only 18%. Therefore, the relatively small variations in springwood wall thickness cannot lead to stress changes that are sufficiently large to explain why some springwood tracheids fail, but others do not.

Other results that arose from the above calculations are -

(a) Variations in tracheid tangential diameter probably have little influence on the occurrence of transwall failure. Stresses in the tangential part of the middle lamella rapidly decay to zero as one moves away from the stressing radial walls. Therefore, it is only in very narrow tracheids (less than 12 μm diameter) that stress waves arising from adjacent radial walls will add and increase the likelihood of middle lamella failure. (Tracheids having tangential diameters of less than 12 μm are extremely rare in Pinus Radiata.)

(b) In the case of summerwood, for which tracheids exhibit very good alignment in both radial and tangential directions, the following very useful relationships were obtained -

Wet matrix strength = 1.8 x wet summerwood strength, and dry matrix strength = 2.0 x dry summerwood strength.

Since evidence suggests that the elastic constants of wood are independent of strain rate, the above results are likely to be true over the range of rates covered in this thesis. Therefore, it

seems that matrix material (hemicellulose and lignin) is responsible for the rate sensitivity of wood.

(c) Consideration of middle lamella failure strains suggested that the shear modulus of matrix material is likely to have the following values -

wet matrix : 10 Kg/mm^2, and
dry matrix : 100 to 200 Kg/mm^2.

(2) A second possible reason for the transwall failure of tracheids is the possession of a lower than average S_2 microfibril angle. One might expect that tracheids having a high microfibril angle would be more difficult to break transversely than those having a low angle, since the reinforcing microfibrils would then be more aligned with applied loads. However, an experimental investigation showed that split tracheids did not have lower than average microfibril angles. Therefore, variations in S_2 microfibril angle must have very little effect on tracheid transverse strength.

(3) Another important structural variable is the degree of tracheid overlap. At high degrees of overlap, radial tracheid walls opposite the less stiff regions of tangentially oriented middle lamella will carry more than half of the total load. (A case of maximum, or 50%,

overlap is illustrated in Fig. 67.)

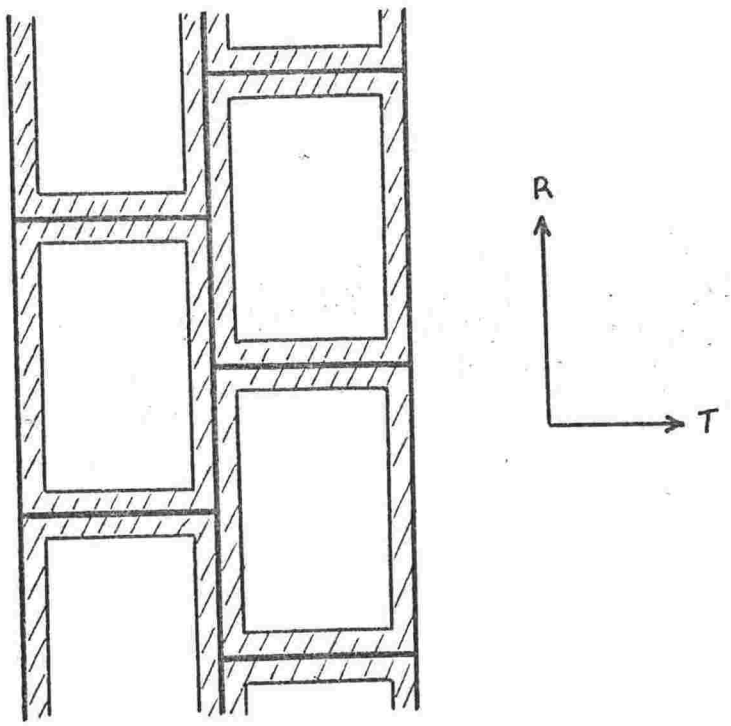

Fig. 67

Although the overlap regions have some of the characteristics of lap joints, they are sufficiently different that formulae applicable to lap joints cannot be used. Therefore, a finite element technique was developed. The tracheid radial walls were divided into many tensile springs, and the sheared (radial) middle lamella was replaced by a series of sheared blocks of matrix. Tangential middle lamella was replaced by a single tensile spring.

Calculation of shear and tensile stresses yielded the following results -

(a) Middle lamella shear stresses (in the radial region of middle lamella) are always much smaller than either tracheid radial wall stresses or tensile stresses in the tangential portions of the middle lamella. Therefore, either the tracheid wall, or the tangential middle lamella, is likely to be the first to fail.

(b) As the degree of overlap is increased from 0% to 50% (in a typical springwood tracheid with a radial diameter of 45 μm) the ratio maximum wall stress/maximum middle lamella tensile stress increases by 47% in wet wood, and by 17% in dry. These changes seem sufficiently great to account for the observed transwall failure. Therefore, tracheids exhibiting a high degree of overlap will be more likely to fail than those with a lesser degree.

(c) Theory suggests that the transverse tensile strengths of the tracheid wall cannot be greater than the following values -

wet springwood : 3.4 Kg/mm^2, and

dry springwood : 3.6 Kg/mm^2.

If strengths are greater than these values, transwall failure is not able to occur.

(4) In an attempt to obtain an estimate of the wall's transverse strength a semi-empirical criterion of strength of a parallel - fibre - reinforced composite was applied to the tracheid wall. (The wall can be regarded as a composite consisting of crystalline cellulose microfibrils embedded in an amorphous matrix of hemicellulose and lignin.) Analysis showed that under transverse loading the matrix is first to fail, and that in each wall layer splitting occurs in a direction parallel to the microfibrils. The stresses at which both the S_1 and S_2 layers have split are lower limits to tracheid wall's transverse strengths. They are -

wet springwood : 1.1 Kg/mm^2, and
dry springwood : 3.3 Kg/mm^2.

If complete wall failure automatically follows matrix splitting without further increases in load, then the above figures are valid wall strengths. Unfortunately, the theory does not indicate whether or not this is so.

It was also shown that in dry wood only, variations in S_1 layer thickness are likely to cause significant changes in the wall's transverse strength. Decreasing the proportion of S_1 in the wall

from 15% to 5% resulted in a 17% decrease in transverse strength. Figures quoted for S_1 thicknesses showed a variation of nearly this magnitude, therefore S_1 thickness and tangential overlap appear to play equal roles in determining whether or not a dry springwood tracheid will fail in the transwall mode.

In summary, (1) wall thickness and the lack of tangential overlap appear to be the reasons for the lack of transwall failure in summerwood, and (2) it is primarily variations in the degree of tangential overlap that determine whether or not a springwood tracheid will fail, although in dry wood the thickness of the S_1 layer is likely to be of equal importance.

B. Strength

Perhaps the most important phenomenon to be explained was the variation of matrix strength with breaking rate and moisture content. As has been stated above, this is the source of the variations in the strength of wood. A theory which accounts for the properties of matrix has been developed and it is briefly reviewed below.

In hemicellulose and lignin (matrix) the only important intermolecular bonding is hydrogen bonding. Since hydrogen bonds are much weaker than covalent bonds, they can be assumed to have a far greater probability of rupture. Because of their low dissociation energies, many break each second as a result of thermal excitation. However,

since in the unstressed state there can be no net breakage of bonds, the rate of breaking must be countered by an equal rate of recombination. When a tensile load is applied, the rate of breaking increases and the rate of recombination decreases, so that there is a net breakage of bonds.

The assumption that bond strain energy is equal to a change in the free energy of activation leads to the following expression for R_b the net rate of breaking of bonds.

$$R_b = k_2 M_2^{\,n} \exp\left(\zeta_c/RT\right) - k_1 M_1^{\,2n} \exp\left(-\zeta_s/RT\right)$$

where

$$\zeta_s = C\sigma^2 / 2 K_b N^{4/3}$$

k_1, k_2	=	reaction rate constants
M_2	=	molar concentration of load bearing H-bonds
M_1	=	molar concentration of dissociated H-bonds
n	=	number of H-bonds that must break simultaneously
R	=	universal gas constant
T	=	absolute temperature
σ	=	applied stress
K_b	=	H-bond spring constant
N	=	density of H-bonds.

The higher the stress σ, the greater the rate of breaking of bonds and the shorter the time to failure.

The above equations lead to a failure stress - failure time

relationship that is in good agreement with experimental data. Evidence has also been obtained which indicates that the rupture of matrix hydrogen bonds must be a co-operative process. In dry wood, bonds must break in groups of 8 or 9, or not at all, and in wet wood, in groups of 5. Thus it appears that adsorbed moisture has a plasticising effect on the matrix.

The concentrations of intermolar linkages were estimated to be -

2.1×10^{-2} moles/litre in dry wood, and
2.4×10^{-2} moles/litre in wet wood.

However, many of these are dissociated at any instant of time, and the concentrations of bonds actually carrying loads are -

7.0×10^{-4} moles/litre in dry wood, and
1.1×10^{-3} moles/litre in wet wood.

(Note that there are more load carrying bonds in wet wood, but that they are easier to rupture.)

Application of the same reasoning to crystalline cellulose (this time, however, considering the rupture of its covalent bonds) suggests that its strength does not vary greatly with strain rate. If also the strength of the wet tracheid wall ultimately depends on the strength of crystalline cellulose then its strength too will not

vary greatly with rate, and the reason for the rate dependence of percent transwall failure in wet wood becomes clear. As strain rate is increased the strength of the wet wall will not vary greatly, but the stresses that it must bear in order to cause failure of the matrix will increase greatly. Therefore, the likelihood of transwall failure will also increase.

In dry wood, variations in matrix strength are not greatly different from those of crystalline cellulose, so the constancy of percent transwall failure is, therefore, to be expected.

Appendix 1 EXPERIMENTAL CONDITIONS AND TESTING EQUIPMENT

Conditions of Fracture

A1.1 Moisture Content

Tests were carried out at two specimen moisture contents, 12.7% and saturated. These are the moisture contents of airdry wood, and green wood respectively, although in these tests rewetted airdry wood was used instead of green wood.

The reasons for choosing these moisture contents are -

(a) they are easy to acheive and maintain throughout the experiment, and

(b) they are the conditions under which wood is normally cut or ground.

The 12.7% specimens were conditioned in a closed jar above a saturated solution of $NaNO_2$ for at least 72 hours before fracture. (The relative humidity above such a solution is 66% and the equilibrium moisture contents of the samples at this Rh were measured to be 12.7%.) During the tests each specimen was exposed to the air, but protected from draughts. The lowest rate Instron tests, which took three hours per specimen were carried out in a room with temperature controlled at 20°C and in which the Rh was approximately 60%, so that very little moisture content change occurred (less than 1.3%). During the higher rate tests (strain

rate 10^{-2} sec $^{-1}$ to 10^{2} sec^{-1}) the specimens were exposed to the room air for no longer than 15 sec, so again no significant loss of moisture could occur.

The "saturated" specimens were conditioned above a saturated solution of K_2SO_4 for 72 hours. (Rh = 97.5%, moisture content = 28%). They were then immersed in distilled water for five hours immediately before fracture and were kept wet throughout the test.

A1:2 Bulk Density

Because transwall failure is a splitting across the tracheid wall, its occurrence is likely to be influenced by the wall's thickness. Springwood and summerwood tracheids have greatly different wall thicknesses (Table 3), so in some specimens the fracture was located in the springwood region of the growth ring, and in the remainder in the summerwood region. To reduce variations in properties due to structural differences as much as possible, all "springwood" fractures were located in the same growth ring. (The specimen itself actually encompassed portions of three growth rings.) Similarly all "summerwood" fractures were located in one growth ring, which was only a short distance further from the centre of the tree. The two growth rings used were chosen because they were close together and their mean microfibril angles were nearly the same. Also, they were sufficiently far from the centre of the tree that their chemical compositions were likely to be similar. (Mean microfibril angle, which in all but very thin walled cells can be equated to the S_2 microfibrillar orientation, is readily measured by x-ray techniques, e.g. See Cave (45).)

---

(45) Cave, I.D. (1966) For. Prod. J. 16(10) p.37
"X-ray Measurement of Microfibril Angle".

The properties of the specimens near the plane of the fracture are summarised below in Table 13 -

Property	Springwood	Summerwood	Method of Measurement
Growth Ring	8	12	
S_2 Microfibril angle (degrees)	14 ± 2	16 ± 2	x-ray diffraction
Bulk Density (gm/cc)	0.36	0.62	Desch's Method (Desch (46))
Wall Thickness (μm)	1.9 ± 0.45	7.2 ± 1.9	Optical microscopy
Cell Diameter			
- Tangential (μm)	29 ± 7	31 ± 7	Optical microscopy
- Radial (μm)	45 ± 7	25 ± 5	Optical microscopy

Table 13 : Physical Properties of Specimens used in Fracture Tests

Tensile Testing Equipment

A1:3 Loading Machines

To cover the wide range of strain rates required, two different loading machines had to be used. For the low strain rates (2×10^{-6} sec^{-1} to 10^{-3} sec^{-1}) an Instron compression and tension testing machine was used. This loaded the specimen in tension and displayed the load versus time curve on a chart recorder. By relating chart speed to specimen extension rate, the load versus displacement curves of the specimen were obtained.

For the higher strain rates (10^{-2} sec^{-1} to 10^{2} sec^{-1}) a machine

---

(46) Desch, H.E. (1962) "Timber - its Structure and Properties" (MacMillan & Co. Ltd. London). p.90.

designed by the author was built in the instrument shop of the Physics and Engineering Laboratory of the D.S.I.R. This is illustrated in Figs. 68 and 69.

It consists of a steel frame, on which are mounted the various loading and measuring devices. At the left hand end is a load cell, to which one end of the specimen is pinned. The other end of the specimen is pinned to one of the two interchangeable loading mechanisms. The first is a worm drive, for strain rates of 10^{-2}, 10^{-1}, 10^{0} sec^{-1}. To obtain these strain rates the free end of the 0.01 m long specimen must move at velocities of 10^{-4}, 10^{-3}, 10^{-2} m/sec respectively.

The second mechanism is a pendulum impact device. One of two pendulums is pivoted directly above the initial position of the cross piece of the loading bar. As the pendulum swings down, two projecting pins strike the crosspiece, and accelerate the loading bar. The pendulums are shown in Fig. 69. In each case, the fall of the bob is 0.05 m so that its velocity at the time of impact is 1.00 m/sec. With the smaller pendulum the striking pins also have this velocity, and with the other, the pins have a velocity of 0.1m/sec. These give strain rates of 10^{2} and 10^{1} sec^{-1} respectively.

A1:4 Measurement of Load at the Higher Strain Rates

The load cell consists of two semiconductor strain gauges, mounted on either side of a steel bar as shown in Fig. 68. The bar extends as its free end is loaded, and the extension is indicated by the strain gauges. Using a steel bar with the dimensions shown, and having a

(a)

: Load Cell and Specimen

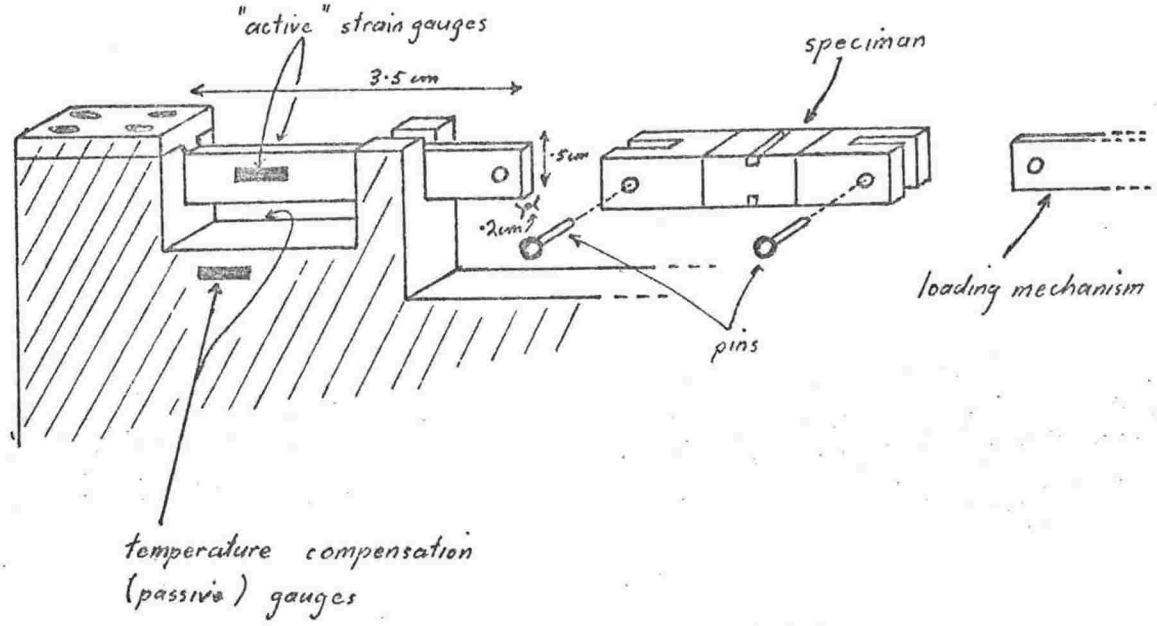

(b)

Worm Drive Loading Mechanism

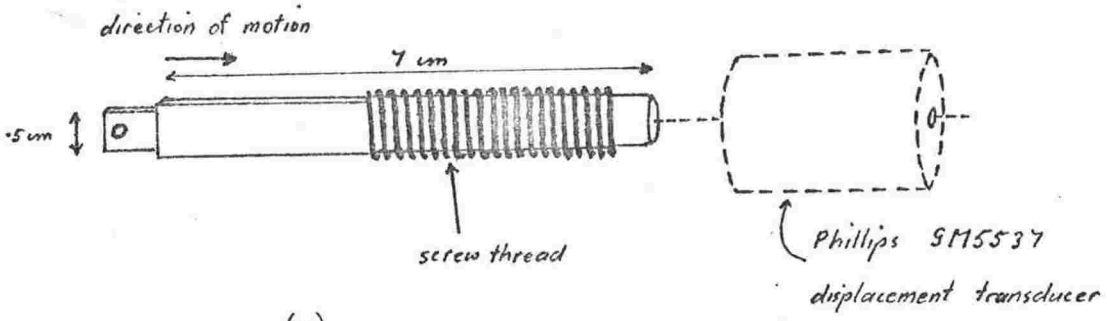

(c)

Pendulum Impact Loading Mechanism

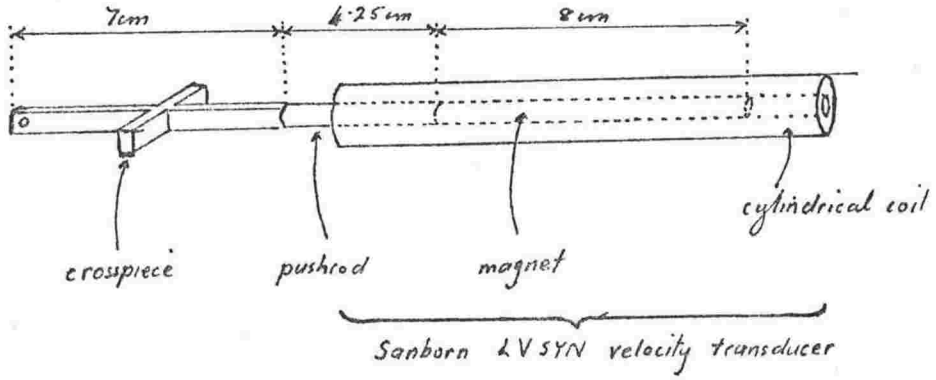

Fig. 68 : Tensile testing Machines for Strain Rates in Range $10^{-2} \rightarrow 10^{2}$ sec

(a)

Fig. 69 : Impact Pendulums

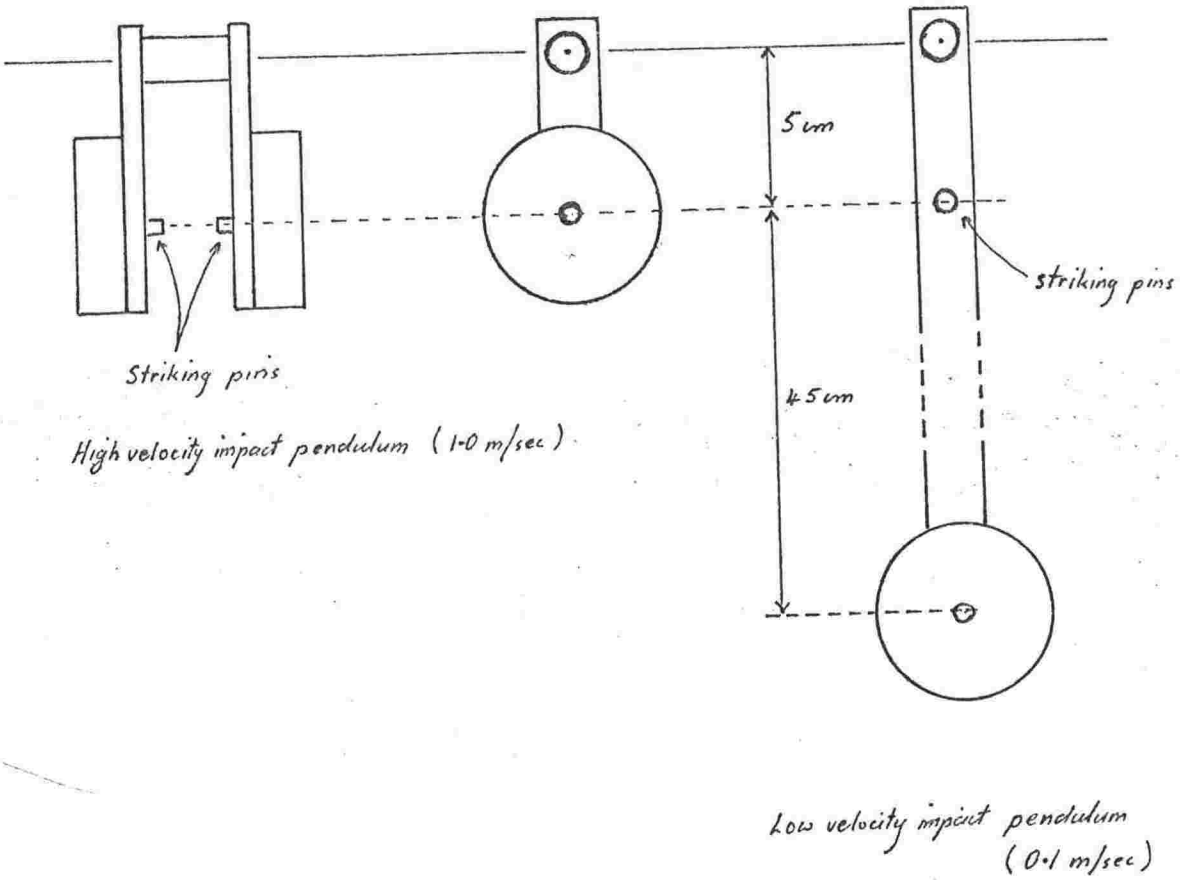

(b)
Layout of Pendulum Impact Loading Mechanism.

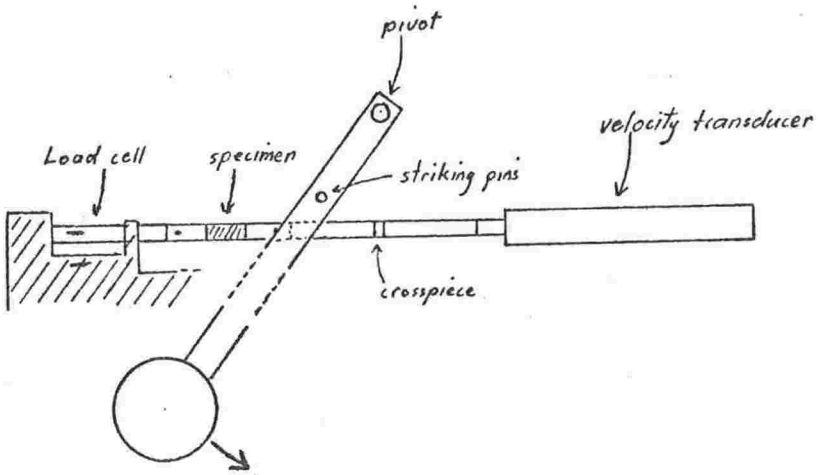

Young's modulus of 2.0 x 10^4 Kg/mm^2 (2.0 x10^{11} N/m^2) the strain induced by loading at the free end is 5.0 x 10^{-6} per kg load.

Two further gauges, for temperature compensation, were mounted on the frame of the machine, near the active gauges.

The gauges used were all Kyowa KSPH4-2000 E3 with gauge factors of 174. They were connected in the wheatstone bridge circuit shown in Fig. 70. For a bridge input voltage of 50.0 volts, the sensitivity was 10.0 mv/Kg load.

The output from the bridge was connected to one of the vertical deflection inputs of a double beam oscilloscope (Tektronix type 585 oscilloscope with type CA preamplifier). A beam deflectinn sensitivity of 5.0 Kg/cm was obtained.

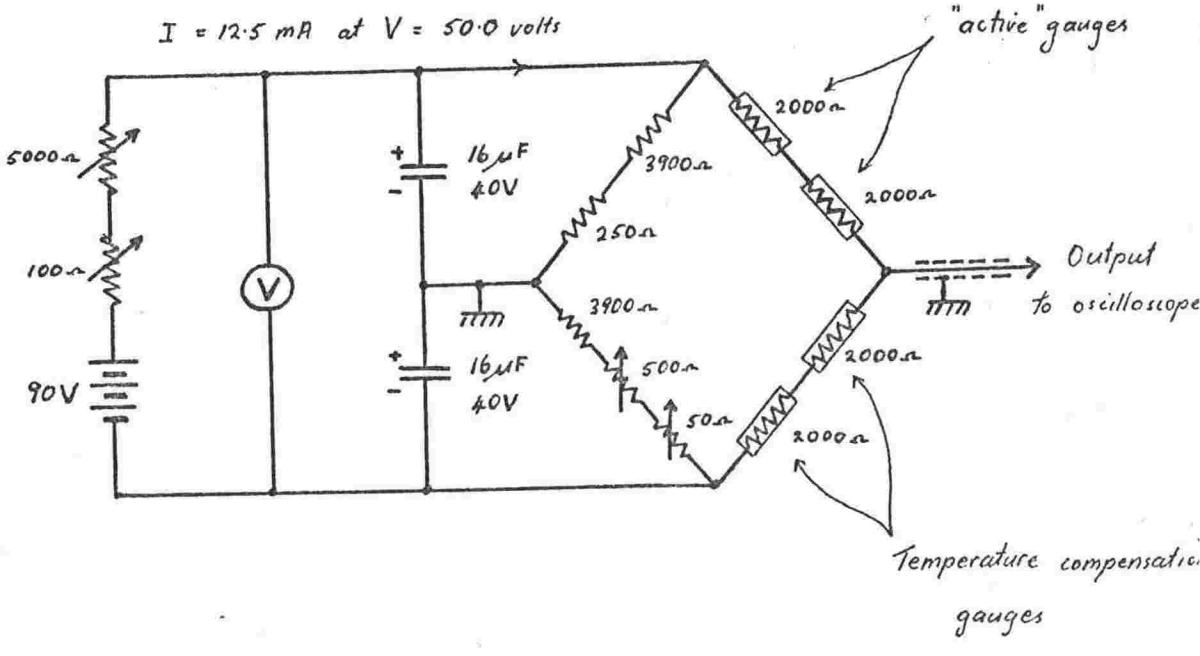

Fig. 70 : Load cell
Bridge and Power supply circuits.

Callibration

The callibration of the system was checked periodically by suspending a range of known weights from the load cell. The deflection sensitivity (5.0 Kg/cm) was found to remain constant within the reading accuracy of the oscilloscope trace, for the range of loads used (up to 10Kg), and for the duration of the experimental tests.

A1: 5 Measurement of Extension at the Higher Strain Rates

At low strain rates (10^{-2} and 10^{-1} sec^{-1}), the displacement of the moving end of the specimen was measured with a Phillips displacement transducer (GM5537) and direct reading bridge (GM5536). The output from the bridge was taken to the horizontal deflection input of the oscilloscope, giving a sensitivity of 37 ± 1 μm/cm beam deflection. (Callibration was checked with a micrometer before and after each series of tests.)

Because the displacement transducer has a frequency response of 1000 H_Z, fracture times must be much greater than one millesecond. Therefore, it is suitable for strain rates of up to 10^{-1} sec^{-1} (fracture times = 100 millisec).

At higher strain rates (10^{0} to 10^{2} sec^{-1}) displacement was not measured directly, but was computed from velocity vs time curves. The velocity of the moving end of the specimen was measured with a Sanborn "Linear velocity transducer" (6LVI-N). This consists of a cylindrical magnet which moves along the axis of a cylindriaal coil. The D.C. output voltage from the coil is directly proportional

to the linear velocity of the magnet. Sensitivity is 10V/m/sec. The coil output was connected to the second vertical deflection input of the oscilloscope. Both traces were swept across the oscilloscope screen at constant rate so that the load vs time and velocity vs time curves were displayed together.

All oscilloscope traces were photographed, with a polaroid camera, so that analysis could be carried out a leisure. Examples of traces are shown in Figs. 71 to 74.

A1:6 Limitations at High Strain Rates

Load Cell

One of the basic requirements of this type of load measuring device is that stress and strain are constant throughout the load cell. This condition will be met if the loading time is very much greater than the time taken for a stress wave to travel the length of the load cell. For low stress levels, the stress wave velocity is equal to the velocity of the sound waves, which in the steel used is about 0.5 ~~mm/sec~~ μsec/cm. Therefore, it takes a stress wave 7 μsec to travel from one end of the load cell to the other. At the highest strain rate used (10^2 sec^{-1}) the time taken to reach failure load was 100 μsec, and this is 14 times greater than the stress wave traverse time. Load readings obtained at this rate are, therefore, likely to be reliable; but with a further tenfold increase in strain rate the condition that stress and strain are constant throughout the load cell could no longer be assumed. This sets the upper ~~load~~ limit of strain rate used in this investigation (10^2 sec^{-1}).

Fig. 71 : Typical load-extension curve for strain rates of 10^{-2} and 10^{-1} sec^{-1}.

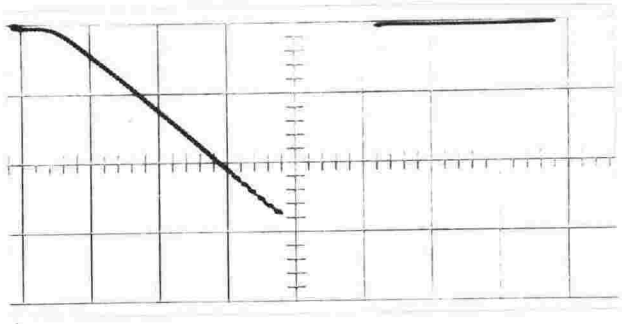

Fig. 72 : Load-time (upper) and velocity-time (lower) curves for a strain rate of 10^{0} sec^{-1}.

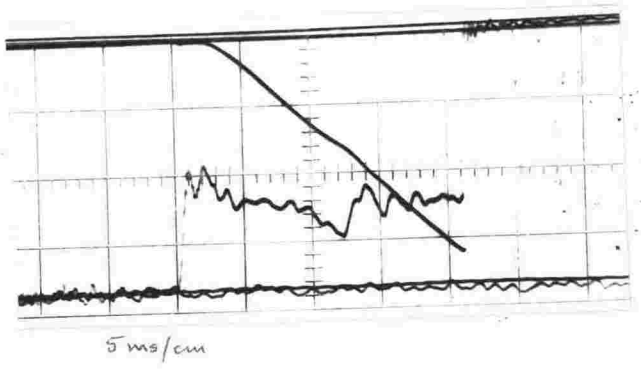

Fig. 73 : Load-time and velocity-time curves for a strain rate of 10 sec^{-1}.

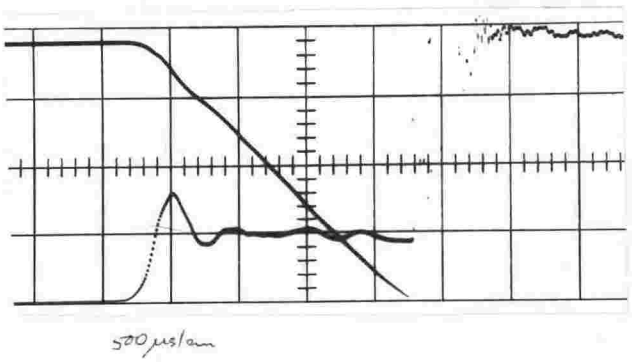

Fig. 74 : Load-time and velocity-time curves for a strain rate of 10^{2} sec^{-1}.

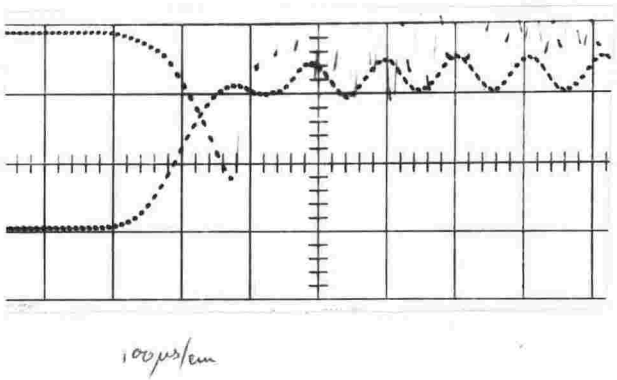

Velocity Transducer

The transducer consits of a two inch long cylindrical magnet, which moves along the axis of a pickup coil. The magnet has to be coupled to the object whose velocity is being measured by a pushrod, as is shown in Figs. 68 and 75.

To obtain a strain rate of 10^2 sec^{-1}, it is necessary to displace the moveable end of the specimen at a velocity of 1.00 m/sec. As it is initially at rest, and complete fracture takes only 100μsec a very high acceleration is needed, about 10^4 m/sec^2. The magnet too must undergo this acceleration, so large forces must be applied to the end of the pushrod. As a result, the pushrod, and the magnet itself, are slightly compressed.

Let

L_{11} = compression of the pushrod due to its own inertia

L_{12} = compression of the pushrod due to the inertia of the magnet

L_{22} = compression of the magnet due to its own inertia.

It can be shown that -

$$L_{11} = \frac{\rho_1 \alpha l_1^2}{2 Y_1} \quad , \quad L_{22} = \frac{\rho_2 \alpha l_2^2}{2 Y_2} \quad , \quad L_{12} = \frac{r_2^2 l_1 l_2}{r_1^2 Y_1} \rho_2 \alpha \qquad \ldots\ldots(13)$$

Where

ρ_1 = pushrod density = 7.87×10^3 Kg/m^3

l_1 = pushrod length = 4.25×10^{-2} m

Y_1 = pushrod Young's modulus = 2×10^{11} N/m^2

r_1	=	pushrod radius	=	2.5×10^{-3} m
ρ_2	=	magnet density	=	7.87×10^{3} Kg/m^3
l_2	=	magnet length	=	7.0×10^{-2} m
Y_2	=	magnet Young's Modulus	=	2×10^{11} N/m^2
r_2	=	magnet radius	=	2.5×10^{-3} m
Let α	=	acceleration	=	10^4 m/sec^2

To reduce compression as much as possible it is necessary to maximise the Young's modulus and radius of the pushrod, and to minimise its length and density. The material which best satisfies these conditions, and is readily available, is non-magnetic stainless steel.

The figures given are for the pushrod (and magnet) actually used and substituting these into equation (13) gives

$L_{11} = 0.35\,\mu m$, $L_{22} = 0.75\,\mu m$, $L_{12} = 1.16\,\mu m$.

When the magnet reaches its final velocity and its acceleration ceases, energy stored as a result of the compression will be released as linear vibrations of the magnet and pushrod. The average linear vibration of the magnet will give rise to an oscillating voltage output, which will be superimposed on top of the desired signal.

Because the magnet has uniform cross section and composition, its average linear oscillating motion is the same as the motion of its centre of gravity, which is easily determined since the magnet and pushrod approximate to a continuous steel rod.

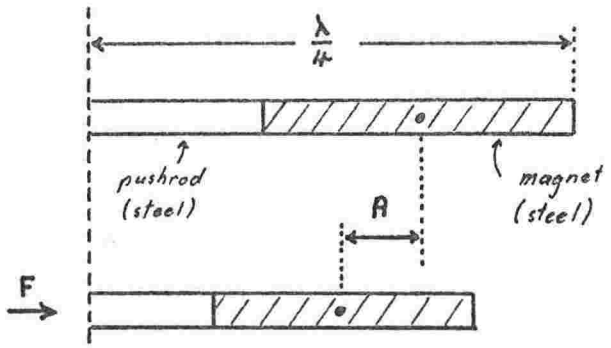

Fig. 75 Compression of Pushrod and Magnet.

Frequency of vibration (in fixed-free mode) is $f = 1.1 \times 10^{4}$ Hz, and maximum displacement of the centre of gravity is $A = L_{11} + L_{12} + \frac{L_{22}}{2} \doteq 2\,\mu m$.

Hence the amplitude of the velocity vibration dv is given by

$$dv = 2\,fA = 0.14 \text{ m/sec.}$$

This is 14% of the steady velocity of 1.00 m/sec.

If there is metal to metal contact between striking pins and the cross piece, accelerations are very high, in the range 10^5 to 10^6 m/sec^2. The resulting oscillations make the transducer unusable. To prevent this from happening a layer of cloth tape is placed on each impacted surface of the crosspiece. Then oscillations observed prior to failure are small enough to be ignored for strain rates of up to 10^2 sec^{-1} (see Fig. 74). After fracture has occurred, large oscillations appear, but they are of no consequence. Therefore, this transducer can be used at strain rates of up to, but not beyond, 10^2 sec^{-1}.

Appendix 2 ELASTIC CONSTANTS OF THE TRACHEID WALL

Much of the work in chapters 4, 5, and 6 requires a knowledge of the elastic constants of the tracheid wall. These are calculated in this appendix.

A2:1 Tracheid Wall Model

For simplicity, assume that the tracheid wall consists of S_1 and S_2 layers only. Since the S_3 layer is very thin (see Table 2), and has the same microfibrillar orientation as the S_1 layer, it may be included as part of the S_1 layer. Also, since the P layer comprises only 10% crystalline cellulose, it is a reasonable assumption to consider it to be a part of the middle lamella. This is a commonly used combination, and it is called the "compound middle lamella". (For brevity it has been called "middle lamella" in chapters 4,5, and 6.)

The resulting model wall compositions are -

	Springwood	Summerwood
S_1	15%	5%
S_2	85%	95%

,

where S_1 and S_2 have the compositions and structures given in Table 1. The angle between the S_2 microfibrillar direction and the cell longitudinal axis is 15°, corresponding to that of the samples of wood actually broken. The S_1 angles are $+80^\circ$ and -80°, and it is, therefore, necessary to consider the S_1 to be composed of two separate layers.

The cellulose microfibrils within each layer are parallel, and uniformly distributed. Each layer is isotropic in a plane perpendicular to the microfibril direction, i.e. is transversely isotropic.

A2:2 Elastic Constants of Single Cell Wall Layers

Hill (47) derived expressions relating the elastic stiffness constants of a tranversely isotropic fibre reinforced material to those of its constituents, fibre and amorphous matrix. In the case of the tracheid wall, cellulose microfibrils are the reinforcing fibres, and hemicellulose and lignin comprise the amorphous matrix.

The elastic stiffness constants of crystalline cellulose may be derived from the technical moduli given by Mark (48). They are, in matrix form -

$$\begin{bmatrix} 1.57 & .0035 & .158 & 0 & 0 & 0 \\ & 1.57 & .158 & 0 & 0 & 0 \\ & & 13.7 & 0 & 0 & 0 \\ & & & .38 & 0 & 0 \\ & & & & .38 & 0 \\ & & & & & .78 \end{bmatrix} \times 10^3 \text{ Kg/mm}^2$$

(47) Hill, R. (1965) J. Mech. Phys. Solids. 13 p.189 "Theory of Mechanical Properties of Fibre Strengthened Materials, Part 3 - Self Consistent Model".

(48) Mark, R.E. (1965) in W.A. Côté, Jr. (Ed.) Cellular Ultrastructure of Woody Plants" (Syracuse Univ. Press, Syracuse).

(The "3" axis is the microfibril direction and the "1" and "2" axes are transverse directions.)

Since water does not enter into the structure of crystalline cellulose, the above figures will be applicable in wood of all moisture contents.

Unfortunately, the stiffness constants of hemicellulose and lignin are not well known. So far it has proved impossible to make insitu measurements, and hemicellulose, and lignin cannot be removed from wood without drastic structural changes.

The only reported measurements were made by Mark (48) on wet, regenerated lignin. His technical moduli lead to the following figures -

C_{11} = 275 Kg/mm^2

C_{12} = 118 Kg/mm^2

C_{44} = 78.5 Kg/mm^2.

These constants are probably close to those of wet insitu lignin. No figures are available for hemicellulose, but since intermolecular bonding is of the same type in both hemicellulose and lignin, the best possible assumption is that both have the same elastic properties. (When one considers the fact that they are intimately mixed in wood, it would be difficult to assume otherwise.)

Because wood matrix material (hemicellulose and lignin) absorbs moisture its elastic constants will depend on its moisture content.

To obtain the elastic constants at other moisture contents, one can do little more than guess. Barkas (49) and Cave (private communication) have stated that the bulk modulus of the matrix does not vary with moisture content. Cave has also suggested that the shear moduli, of wet and dry matrix, lie in the following ranges -

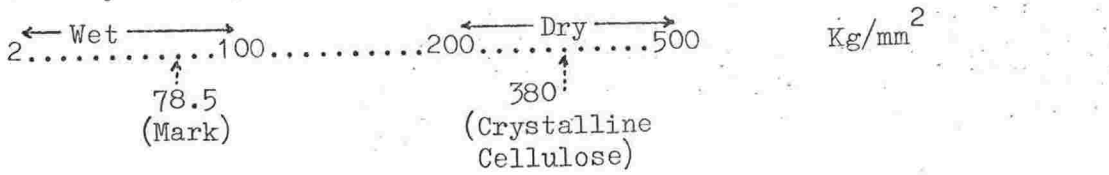

If a value is assumed for G, the shear modulus, it is possible to calculate the stiffness constants from the following relations -

$C_{11} + 2C_{12}$ = 3x bulk modulus (= 511 from Mark's figures),

$C_{11} - C_{12} = 2G$, and

$C_{44} = G$.

C_{11}, C_{12} and Y_m (matrix Young's modulus) are tabulated in Table 14 for various values of G.

---

(49) Barkas, W.W. (1945) D.S.I.R. Forest Products Research, Special Report No. 6. H.M.S.O. "Swelling Stresses in Gels".

G (Kg/mm^2)	2	10	50	100	200	500
Y_m (Kg/mm^2)	6.0	36	137	250	430	758
C_{11} (Kg/mm^2)	173	183	237	303	437	837
C_{12} (Kg/mm^2)	167	163	137	103	37	-163

Table 14 : Possible Elastic Constants of the Matrix

On applying Hill's relations to each column of Table 14 in turn, possible elastic stiffness constants for S_1 and S_2 types of composite material are obtained. The constants of S_2 material (50% cellulose, 50% matrix) are tabulated in Table 15, and those of S_1 material (25% cellulose, 75% matrix) in Table 16. At the top of each column is the value assumed for G. The reference axes are orthogonal, with the "3" axis being the fibre direction, and the "1" and "2" axes being transverse to the fibre. These axes are the axes of symmetry of the composite, and in this system for a transversely isotropic material,

$C_{11} = C_{22}$, $C_{13} = C_{23}$, $C_{44} = C_{55}$, $C_{14} = C_{24} = C_{34} = C_{56} = 0$,

$C_{66} = \frac{1}{2}(C_{11} - C_{12})$.

Also, $C_{i5} = C_{i6} = 0$ $(i = 1...4)$ always, even for non-symmetry orthogonal axes.

It is often convenient to view the composite from axes that are obtained from the symmetry axes by a rotation about the "1" axis. The stiffness constants referred to the new axes can be calculated from those referred to the old by the standard rotation relations listed below -

$$
\begin{aligned}
C_{11} &= C'_{11} \\
C_{22} &= C'_{11}\, c^4 + C'_{33}\, s^4 + 2(C'_{13} + 2C'_{44})\, c^2 s^2 \\
C_{33} &= C'_{11}\, s^4 + C'_{33} c^4 + 2(C'_{13} + 2C'_{44})\, c^2 s^2 \\
C_{12} &= C'_{12}\, c^2 + C'_{13}\, s^2 \\
C_{13} &= C'_{12}\, s^2 + C'_{13}\, c^2 \\
C_{23} &= (C'_{11} + C'_{33} - 2(C'_{13} + 2C'_{44}))\, c^2 s^2 + C'_{13} \\
C_{44} &= (C'_{11} + C'_{33} - 2(C'_{13} + 2C'_{44}))\, c^2 s^2 + C'_{44} \\
C_{55} &= C'_{44}\, c^2 + C'_{66}\, s^2 \\
C_{66} &= C'_{44}\, s^2 + C'_{66}\, c^2 \\
C_{14} &= (C'_{13} - C'_{12})\, cs \\
C_{56} &= (C'_{44} - C'_{66})\, cs \\
C_{24} &= (C'_{33}\, s^2 - C'_{11}\, c^2 + (C'_{13} + 2C'_{44})\, (c^2 - s^2))\, cs \\
C_{34} &= (C'_{33}\, c^2 - C'_{11}\, s^2 - (C'_{13} + 2C'_{44})\, (c^2 - s^2))\, cs,
\end{aligned}
$$

where $c = \cos\theta$, $s = \sin\theta$, and positive θ is the angle of rotation measured from the "new" axes to the "old".

In the tracheid wall, the S_2 microfibrils are at an angle of 15° to the longitudinal axis, and the S_1 microfibrils are at angles of $+ 80^\circ$ and $- 80^\circ$ (see Fig. 76). The most convenient set of reference axes is as follows. The "3" and "2" axes lie in the plane of the tracheid wall, with the 3 axis being parallel to the tracheid longitudinal axis. The "1" axis is perpendicular to the wall.

When viewed from these axes, the stiffness constants of the S_2 layer have the values tabulated in Table 17, and those of the S_1 layer have the values in Table 18.

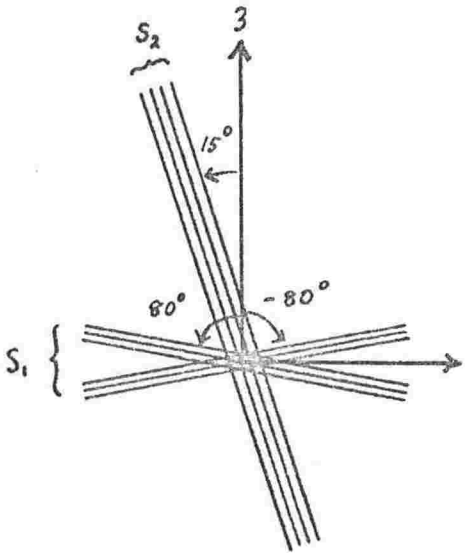

Fig. 76 Orientation of Microfibrils in the wood tracheid wall.

The S_1 values are calculated for a single layer of parallel fibres, at an angle of $+80^{\circ}$ to the "3" axis. In real wood, however, there are two S_1 layers, one at $+80^{\circ}$ and the other at -80°. They are firmly bonded together to give a balanced structure in which tensile forces cannot give rise to shear strains, and vice versa. The stiffness constants of such an array are exactly the same as for a single unbalanced layer, except that $C_{14} = C_{24} = C_{34} = C_{56} = 0$.

A2:3 Elastic Constants of a Complete Tracheid Wall

To obtain the elastic stiffness constants of a complete tracheid wall, it is necessary to combine S_1 and S_2 material in the correct proportions, in the manner shown in Fig. 77. In springwood, a : b = 17 : 3, and in summerwood a : b = 19 : 1.

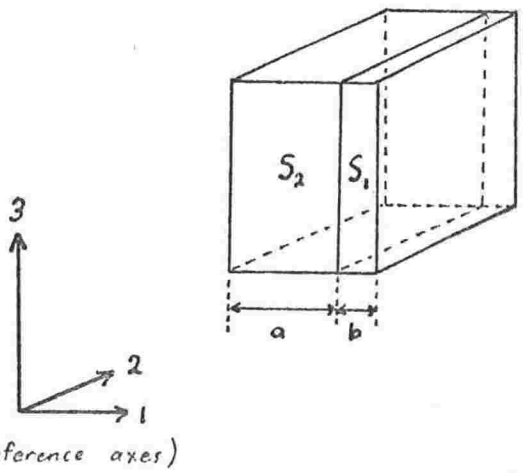

Fig. 77 Model of Complete Cell Wall.

The overall stiffness constants may be determined by applying a series of suitable strains, calculating the stresses over each surface, summing forces, and dividing total force by surface area to give overall stress.

Written in full, the stress - strain relations are :

$$\begin{bmatrix} \sigma_1 \\ \sigma_2 \\ \sigma_3 \\ \sigma_4 \\ \sigma_5 \\ \sigma_6 \end{bmatrix} = \begin{bmatrix} C_{11} & C_{12} & C_{13} & C_{14} & 0 & 0 \\ C_{12} & C_{22} & C_{23} & C_{24} & 0 & 0 \\ C_{13} & C_{23} & C_{33} & C_{34} & 0 & 0 \\ C_{14} & C_{24} & C_{34} & C_{44} & 0 & 0 \\ 0 & 0 & 0 & 0 & C_{55} & C_{56} \\ 0 & 0 & 0 & 0 & C_{56} & C_{66} \end{bmatrix} \begin{bmatrix} \varepsilon_1 \\ \varepsilon_2 \\ \varepsilon_3 \\ \varepsilon_4 \\ \varepsilon_5 \\ \varepsilon_6 \end{bmatrix}$$

This matrix of stiffness constant may be partitioned into independent submatrices, one of which is $\begin{bmatrix} C_{55} & C_{56} \\ C_{56} & C_{66} \end{bmatrix}$

This (and the zero submatrices), will be omitted from all following equations, since strains ε_5, ε_6, and stresses σ_5, σ_6, are not required in future calculations.

As an example, apply the strains $\varepsilon_1 = \varepsilon_3 = \varepsilon_4 = 0$, $\varepsilon_2 = 1$. Since the $S_1 : S_2$ boundary is free to move, ε_{1A} and ε_{1B} are non zero. Therefore,

$$a\,\varepsilon_{1A} + b\,\varepsilon_{1B} = 0 \text{ , and} \qquad \ldots\ldots(14)$$

$$C_{11A}\,\varepsilon_{1A} + C_{12A}\,\varepsilon_2 = C_{11B}\,\varepsilon_{1B} + C_{12}\,\varepsilon_2 . \qquad \ldots\ldots(15)$$

Equations (14) and (15) determine ε_{1A} and ε_{1B}. The appropriate

strains can then be applied to each layer. The resulting layer stresses are -

$$\begin{bmatrix} \sigma_{1A} \\ \sigma_{2A} \\ \sigma_{3A} \\ \sigma_{4A} \end{bmatrix} = \begin{bmatrix} C_{11A} & C_{12A} \\ C_{12A} & C_{22A} \\ C_{13A} & C_{23A} \\ C_{14A} & C_{24A} \end{bmatrix} \begin{bmatrix} \varepsilon_1 \\ \varepsilon_2 \end{bmatrix}, \quad \begin{bmatrix} \sigma_{1B} \\ \sigma_{2B} \\ \sigma_{3B} \\ \sigma_{4B} \end{bmatrix} = \begin{bmatrix} C_{11B} & C_{12B} \\ C_{12B} & C_{22B} \\ C_{13B} & C_{23B} \\ C_{14B} & C_{24B} \end{bmatrix} \begin{bmatrix} \varepsilon_1 \\ \varepsilon_2 \end{bmatrix}.$$

Hence, $\sigma_i\,(\text{overall}) = \dfrac{a\sigma_{iA} + b\sigma_{iB}}{a+b}$

and $C_{i2}(\text{overall}) = \dfrac{\sigma_i\,(\text{overall})}{\varepsilon_2} \qquad (i = 1, \ldots 4)$

Similar procedures give the remaining overall stiffness constants. Overall summerwood C_{ij} are tabulated in Table 19, and springwood C_{ij} in Table 20.

G	2	10	50	100	200	500
C_{11}	311	358	490	605	780	1137
C_{12}	267	250	200	150	69	- 99
C_{13}	165	161	144	121	71	-123
C_{33}	6950	6957	6983	7016	7078	7200
C_{44}	28	62	138	195	276	436

Table 15 : Stiffness Constants for S_2 Material

(Referred to symmetry axes.) (Units : Kg/mm^2)

G	2	10	50	100	200	500
C_{11}	217	237	320	410	571	972
C_{12}	209	200	164	125	53	-135
C_{13}	168	163	139	109	53	-105
C_{33}	3560	3570	3610	3659	3757	4044
C_{44}	4	19	78	137	234	467

Table 16 : Stiffness Constants for S_1 Material.

(Referred to symmetry axes.) (Units : Kg/mm^2)

G	2	10	50	100	200	500
C_{11}	311	358	490	605	780	1137
C_{12}	260	244	196	149	69	-101
C_{13}	172	167	148	123	71	-121
C_{14}	- 25	- 22	- 14	- 7	0.5	- 6
C_{22}	330	378	510	622	789	1116
C_{23}	591	583	559	533	484	304
C_{24}	92	95	94	87	71	17
C_{33}	6079	6093	6133	6174	6243	6365
C_{34}	1568	1555	1530	1516	1503	1498
C_{44}	454	484	553	607	689	863
C_{55}	28	61	138	197	281	448
C_{56}	1	2	- 2	- 8	- 20	- 45
C_{66}	22	55	145	225	350	606

Table 17 : Stiffness constants of S_2 material referred to cell axes (as in Fig. 76).

(Units : Kg/mm^2)

G	2	10	50	100	200	500
C_{11}	217	237	320	410	571	972
C_{12}	169	164	140	109	53	-106
C_{13}	208	199	164	125	53	-134
C_{14}	- 7	- 6	- 4	- 3	0	5
C_{22}	3361	3370	3413	3464	3565	3853
C_{23}	268	263	237	206	149	- 7
C_{24}	561	559	550	543	536	532
C_{33}	218	238	322	411	571	966
C_{34}	11	11	13	12	8	- 7
C_{44}	104	119	176	234	330	565
C_{55}	4	19	78	142	258	551
C_{56}	0	0	0	- 1	- 4	- 15
C_{66}	4	19	78	137	235	470

Table 18 : Stiffness constants of S_1 material referred to cell axes.

(Units : Kg/mm^2)

Summerwood

G	2	10	50	100	200	500
C_{11}	304	349	477	591	766	1127
C_{12}	254	238	192	145	68	-101
C_{13}	175	169	149	123	70	-122
C_{14}	- 23	- 20	- 13	- 6	0	- 6
C_{22}	480	526	655	764	928	1253
C_{23}	576	568	543	517	467	288
C_{24}	88	91	89	83	67	16
C_{33}	5786	5800	5842	5886	5959	6095
C_{34}	1489	1477	1453	1440	1428	1423
C_{44}	436	466	534	588	671	848

Table 19 : Stiffness constants of summerwood cell wall $(S_1 + S_2)$ referred to cell axes.

Springwood

G	2	10	50	100	200	500
C_{11}	292	333	454	565	739	1109
C_{12}	242	227	184	140	66	-102
C_{13}	179	174	151	123	68	-123
C_{14}	- 20	- 17	- 11	- 6	0	- 5
C_{22}	780	824	948	1048	1205	1527
C_{23}	544	536	511	484	434	257
C_{24}	79	82	80	74	60	14
C_{33}	5199	5214	5261	5310	5392	5555
C_{34}	1332	1321	1300	1289	1278	1273
C_{44}	401	429	496	551	635	818

Table 20 : Stiffness constants of springwood cell wall $(S_1 + S_2)$ referred to cell axes.

A2 : 4 Stiffness Constants after S_1 Layer Splitting

During transverse loading of the tracheid wall, the S_1 layer is always the first to fail. Splits form in the matrix, in a direction parallel to the reinforcing microfibrils. After this has occurred, some of the stiffness constants of the S_1 layer become zero. The only non-zero ones (referred to the symmetry axes) are C_{11}, C_{13} and C_{33}, which are all unchanged from their original values. After setting the appropriate constants of Table 7 equal to zero it is possible to calculate the stiffness constants of -

(a) balanced S_1 layers,

(b) summerwood tracheid walls, and

(c) springwood tracheid walls,

all containing split S_1 layers.

The resulting constants are tabulated below (Table 21).

	Balanced S_1 Layer		Summerwood		Springwood	
G	10	200	10	200	10	200
C_{11}	237	571	349	766	333	739
C_{12}	158	51	238	68	226	66
C_{13}	5	2	155	66	133	58
C_{14}	0	0	- 20	0	- 17	0
C_{22}	3368	3537	526	926	833	1201
C_{23}	265	176	564	468	528	438
C_{24}	0	0	91	67	82	60
C_{33}	236	544	5795	5985	5021	5387
C_{34}	0	0	1478	1428	1324	1278
C_{44}	102	123	465	661	426	604

Table 21 : Stiffness constants for a balanced S_1 layer, and single cell walls after initial splitting of the S_1 layer.

Appendix 3 MEASUREMENT OF MEAN MICROFIBRIL ANGLES OF SPLIT TRACHEIDS

When wood is split, the fracture surface will contain some tracheids which have been split in half by transwall failure. Such half tracheids, which can be removed by the following process, are suitable for microfibril angle measurements.

Procedure

The specimen is delignified by boiling in a suitable solution (for example a 2 : 1 mixture of 100 volumes hydrogen peroxide and glacial acetic acide). After lignin removal, the wood block retains its original shape, although it is very fragile. It is then washed, dried and glued to a glass microscope slide, with the surface containing the split tracheids against the slide. The glue should be quite stiff when applied, as it must penetrate the specimen no further than the first layer of tracheids. ("Araldite" epoxy resin is a suitable glue.)

As soon as the glue has hardened, the block is rewetted and all tracheids except those bonded by the glue can be brushed off. All that remains attached to the slide is the single layer of split tracheids.

It is now possible to determine the mean microfibril angle of each half tracheid by viewing the slide in a polarising microscope. The mean microfibril angle is given by the angle between the cell

longitudinal axis at maximum extinction and the plane of polarisation. (Preston (50))

The method works equally well with a surface that has been cut by a knife. In this case the average microfibril angle for the specimen can be obtained.

Note : The tracheids are glued when dry and must be viewed when dry. "Araldite" shows strain birefringence and may be strained if the cells are wetted and allowed to swell.

---

(50) Preston, R.D. (1952) "The Molecular Architecture of Plant Cell Walls" (Chapman and Hall, London) p.59.

Appendix 4 STRESSES IN OVERLAPPING TRACHEID WALLS : FINITE ELEMENT METHOD

In this appendix the distributions of stresses in overlapping tracheid walls and linking middle lamellae are determined by means of a finite element technique. The most important stresses are -

(a) the maximum tensile stress in the radial tracheid wall,

(b) the maximum shear stress in the radial middle lamella, and

(c) the maximum tensile stress in the tangential middle lamella.

To check its validity the finite element technique is first applied to a lap joint, and the stresses it gives are compared with those obtained via an existing lap joint formula.

A4:1 Lap Joints

A glued lap joint consists of two overlapping plates, with a thin layer of glue joining them throughout the region of overlap. In almost all situations, the loading on such a joint is as indicated in Fig. 78, and the glue has to withstand shearing stresses.

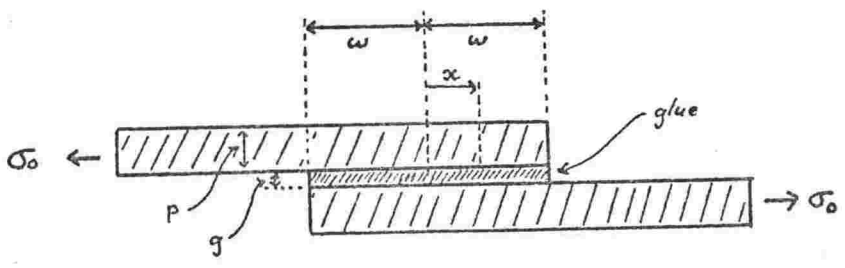

Fig. 78 : Lap Joint

If the plates are very much stiffer than the glue, shear stresses are uniform throughout the glue layer. Otherwise, shear stresses are highest at the ends of the joint.

In the latter case, several workers have derived expressions for the variations of glue shear stress along the joint, (e.g. see review by Benson (51)). One of the earliest, and simplest, is due to Volkersen.

τ , the glue shear stress, is given by -

$$\frac{\tau}{\sigma_o} = \frac{p}{2w} \frac{\cosh\left(\delta \frac{x}{w}\right)}{\sinh \delta} \quad \text{where} \quad \delta = w\sqrt{\frac{2G}{Ypg}} \qquad \ldots\ldots(16)$$

Y = Young's modulus of plate

G = shear modulus of glue

g = glue thickness

p = plate thickness

2w = joint length

x = is shown in Fig. 78.

The derivation of this formula assumes that there is no joint bending so it is applicable either to a double lap joint, or to a lap joint in which bending is prevented from occurring.

---

(51) Benson, N.K. (1969) in "Adhesion, Fundamentals and Practice". (McLaren & Sons, London)

A suitable lap joint to which this formula can be applied is one composed of two plates of tracheid wall glued together by a middle lamella of matrix.

Plate thickness (p) = 1.8×10^{-3} mm

Glue thickness (g) = 4.8×10^{-4} mm

Other constants are -

	Wet Wood	Dry Wood	(Units)
Glue Shear Modulus (G)	10	200	Kg/mm^2
Plate Young's Modulus (Y)	633	1160	Kg/mm^2

The ratio $\frac{\text{glue shear stress}}{\text{applied tensile stress}}$ $\left(\frac{\tau}{\sigma_0}\right)$ is tabulated for various values of $\frac{x}{w}$ in Table 22. Two values of w were chosen, 5×10^{-3} mm and 15×10^{-3} mm.

w (mm) / x/w	Wet		Dry	
	5×10^{-3}	15×10^{-3}	5×10^{-3}	15×10^{-3}
0	.152	.019	.047	.000
.1	.153	.020	.049	.000
.2	.155	.022	.057	.000
.3	.159	.027	.070	.001
.4	.164	.033	.090	.002
.5	.170	.043	.120	.005
.6	.178	.056	.162	.012
.7	.188	.073	.220	.032
.8	.200	.097	.300	.084
.9	.213	.129	.411	.217
1.0	.228	.171	.564	.562

Table 22 : Variations of stress along a glued lap joint.

A4:2 Finite Element Technique

Consider the system of 2n identical shearable blocks of material shown in Fig. 79. Adjacent blocks are connected at the centres of their upper and lower faces by identical springs. Assume that the upper and lower faces of the blocks cannot rotate during deformation.

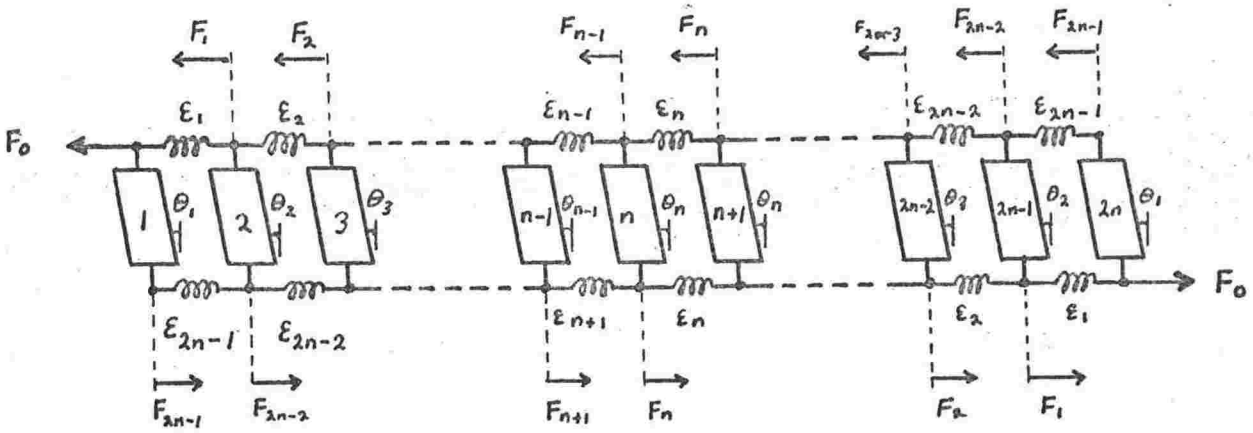

Fig. 79 Sheared Blocks.

Let forces F_o be applied to the upperleft and lower right edges of the array as shown. Block shear strain is denoted by θ_i, spring tensile strain by ε_i, and spring tensile load by F_i. There is an inherent symmetry in the strains and forces as is indicated by the labelling.

Analysis : Each tensile force can be expressed as a sum of shear forces i.e.

$$F_o = 2K_1(\theta_1 + \theta_2 + \ldots\ldots + \theta_n)$$

$$F_1 = K_1(\theta_1 + 2\theta_2 + 2\theta_3 + \ldots + 2\theta_n)$$

$$F_2 = K_1(\theta_1 + \theta_2 + 2\theta_3 + \ldots + 2\theta_n)$$

$$\vdots$$

$$F_{2n-2} = K_1(\theta_1 + \theta_2)$$

$$F_{2n-1} = K_1\theta_1 \quad , \qquad \ldots\ldots(17)$$

where $K_1 = a\ b\ G$.

- a = depth (into page) of shear block
- b = width of shear block
- G = shear modulus

Considering the deformations in each group of two blocks and two springs gives the following set of equations –

$$\begin{aligned} l_2(\varepsilon_1 - \varepsilon_{2n-1}) &= l_1(\theta_1 - \theta_2) \\ l_2(\varepsilon_2 - \varepsilon_{2n-2}) &= l_1(\theta_2 - \theta_3) \\ &\vdots \\ l_2(\varepsilon_{n-1} - \varepsilon_{n+1}) &= l_1(\theta_{n-1} - \theta_n), \end{aligned} \qquad \ldots\ldots(18)$$

where l_2 = spring length,

l_1 = sheared block height.

If K_2 is the spring constant of each spring, then $F_i = K_2 l_2 \varepsilon_i$, ……(19)

and equations 17, 18 and 19 lead to –

$$\begin{aligned} F_1 - F_{2n-1} &= K_2 l_1(\theta_1 - \theta_2) = 2K_1(\theta_2 + \ldots\ldots + \theta_n) \\ F_2 - F_{2n-2} &= K_2 l_1(\theta_2 - \theta_3) = 2K_1(\theta_3 + \ldots\ldots + \theta_n) \\ &\vdots \\ F_{n-2} - F_{n+2} &= K_2 l_1(\theta_{n-2} - \theta_{n-1}) = 2K_1(\theta_{n-1} + \theta_n) \\ F_{n-1} - F_{n+1} &= K_2 l_1(\theta_{n-1} - \theta_n) = 2K_1\theta_n. \end{aligned} \qquad \ldots\ldots(20)$$

Finally, rearranging equations 20 gives –

$$\begin{aligned} \theta_1 &= K\theta_2 - \theta_3 \\ \theta_2 &= K\theta_3 - \theta_4 \\ &\vdots \\ \theta_{n-2} &= K\theta_{n-1} - \theta_n \\ \theta_{n-1} &= \left(1 + \frac{2K_1}{K_2 l_1}\right)\theta_n, \text{ where } K = 2 + \frac{2K_1}{K_2 l_1}. \end{aligned} \qquad \ldots\ldots(21)$$

The remaining independent equation necessary for solution is

$$F_o = 2K_1(\theta_1 + \ldots\ldots + \theta_n).$$

Solution of this set of equations leads to all shear strains (and hence shear stresses).

A4 : 3 Application to a Lap Joint

Imagine that there are very many sheared blocks, and that the connecting springs are so short that the blocks almost touch.

The blocks then approximate to a continuous strip of material which is in non-uniform shear. Such a strip could be the glue layer in a lap joint. The springs would then represent the two plates. The hypothetical pattern of division necessary in a lap joint to give the finite element model is illustrated in Fig. 80.

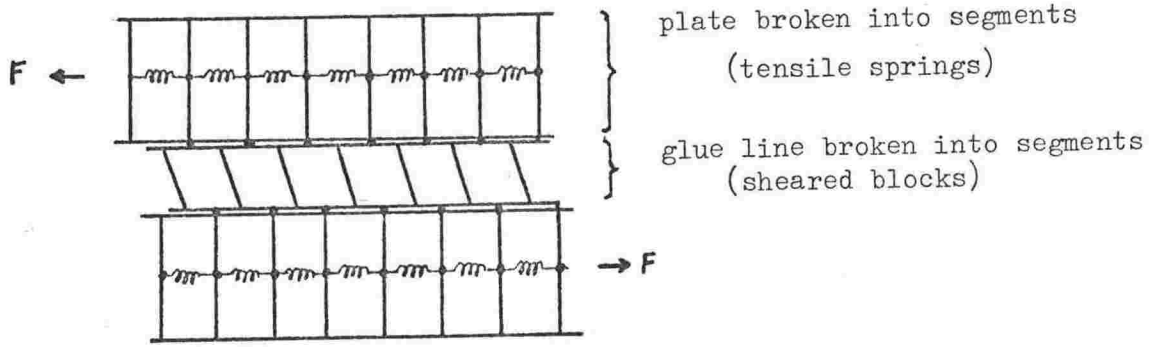

Fig. 80 Division of Lap Joint into Finite Elements.

Let each of the lap joints previously examined by means of Volkersen's formula be divided into 2000 elements in the above manner. Then the

stress variations in each joint can be determined by application of equations 21. The resulting values of τ/σ_o are listed in Table 23. It can be seen that almost all of the figures are identical to those resulting from the use of Volkersen's formula. Obviously the two methods are giving the same answers.

Finite Element Model Results

	Wet Wood		Dry Wood	
w(mm) / x/w	5×10^{-3}	15×10^{-3}	5×10^{-3}	15×10^{-3}
0	.152	.019	.047	.000
.1	.153	.020	.049	.000
.2	.155	.022	.057	.000
.3	.159	.027	.070	.001
.4	.164	.033	.090	.002
.5	.170	.043	.120	.005
.6	.178	.055	.161	.012
.7	.188	.073	.219	.072
.8	.200	.097	.300	.083
.9	.213	.129	.411	.216
1.0	.229	.171	.564	.560

Table 23 : Variation of stress along a glued lap joint.

In the overlap situation encountered in wood, bending of the "lap joint" will be prevented by wood's cellular structure. In any lap joint, bending moments arise (shown by M in Fig. 81), but in

a tracheid "lap joint" these will be countered by forces F' exerted by suitably oriented walls. Therefore, Volkersen's formula is likely to be the most suitable one to apply.

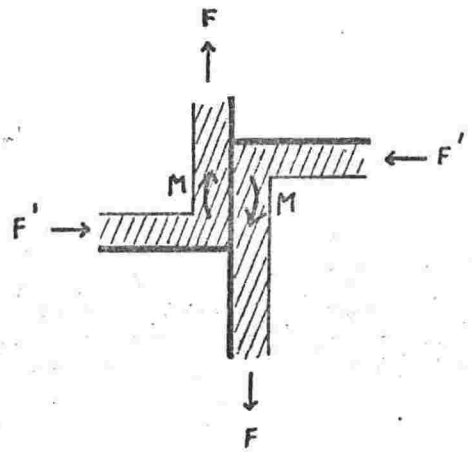

Fig. 81 Lap Joint Stresses

This in turn inspires confidence in the results of the finite element model, despite its obvious faults of -

(a) allowing relative motions between block-block, and block-plate edges, and

(b) ignoring any plate shear strains.

These will be most serious in situations in which middle lamella shear stresses are large. Therefore, they will be of least importance in -

(a) long lap joints, and

(b) the tracheid overlap model considered in the next section.

A4 : 4 Application to Overlapping Tracheid Walls

Before the tracheid wall overlap region of Fig. 60 can be reduced to a finite element model one simplification is necessary. The projecting tangential walls and middle lamellae are difficult to include in the analysis, but may be ignored if that portion of the tangential middle lamella which lies directly between each pair of radial walls is replaced by slightly stiffer material. For example, in wet springwood, $\sigma_{ML(max)} = 0.68\,\sigma_0$ (section 4:1).

Therefore, $\varepsilon_{ML(max)} = 0.68\,\sigma_0 / Y_m$

$= \sigma_0 / Y_m'$, where $Y_m' = Y_m / 0.68$.

(Y_m = matrix Young's modulus.)

(In dry springwood, $Y_m' = Y_m / 0.84$.)

The replacement process is illustrated in Fig. 82. The tangential middle lamella of Fig. 82(a) consists of "normal" matrix, whilst that of Fig. 82(b) consists of material having a Young's modulus Y_m'. Middle lamella strains, relative displacements of the two radial walls, and radial wall stresses and strains will be identical in both (a) and (b).

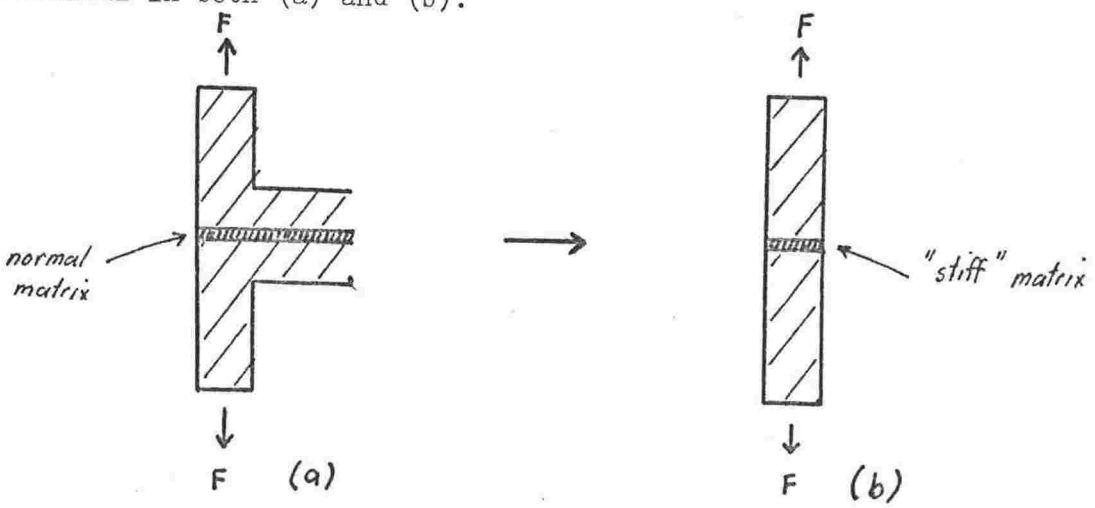

Fig. 82 : Elimination of projecting tangential walls.

A series of overlapping tracheids before the replacement of tangential walls is illustrated in Fig. 83(a), and after the replacement process in Fig. 83(b). Such a structure has one very important property under radial loading. Whenever a "stiff" tangential middle lamella is acting in parallel with an even stiffer tracheid wall, the wall will carry more than half of the total load. This results from the coupling between the upper and lower walls via the radial (sheared) middle lamella. Tensile strains in the "stiff" middle lamella and in the portion of radial wall acting in parallel with it are constrained to be more nearly the same than would have been the case in the absence of such coupling.

A second important property is that the coupling efficiency is dependent on the degree of tracheid overlap. The stress carried by the "stiff" middle lamella will be least in the case of 50% overlap (Fig. 83(a)), and it will increase as overlap decreases, until it reaches a maximum in the situation of zero overlap shown in Fig. 83(c).

It should also be noted that as a result of the symmetry of the situation, stresses in opposing tracheid walls are equal at positions midway between neighbouring regions of "stiff" middle lamella. (See Fig. 83(b).) A repetitive stress distribution results, so it is necessary to consider only a small portion of the model; that between two planes of uniform stress. Such a section is drawn in Fig. 84 in order to show the applied loads.

Breaking Fig. 84 up into segments as was done for the lap joint gives the finite element model of Fig. 85. All segments are identical, except that which encompasses the "stiff" middle lamella region, and which contains only two springs, one representing the "stiff" middle lamella, and the other representing the segment of wall acting in parallel with it. (A small amount of coupling middle lamella between the two is neglected, but this will have no significant effect on the results obtained.)

Fig. 83 : Overlapping Springwood Tracheids

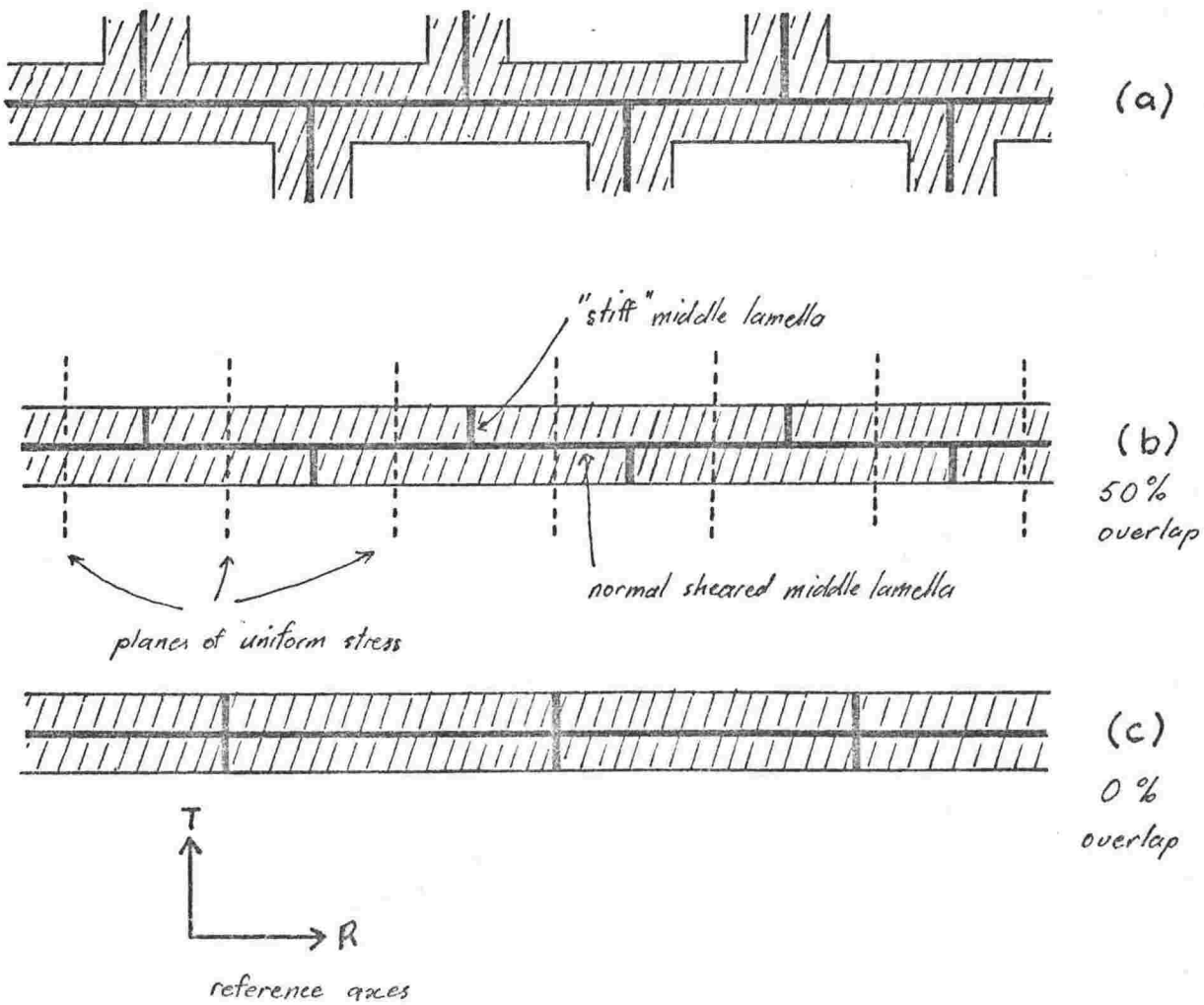

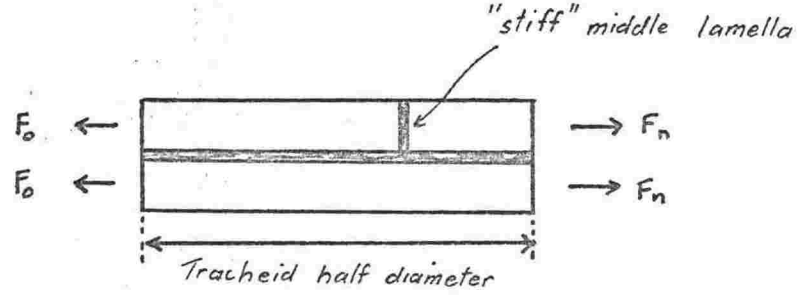

Fig. 84 : Block of cell wall between two planes of uniform stress.

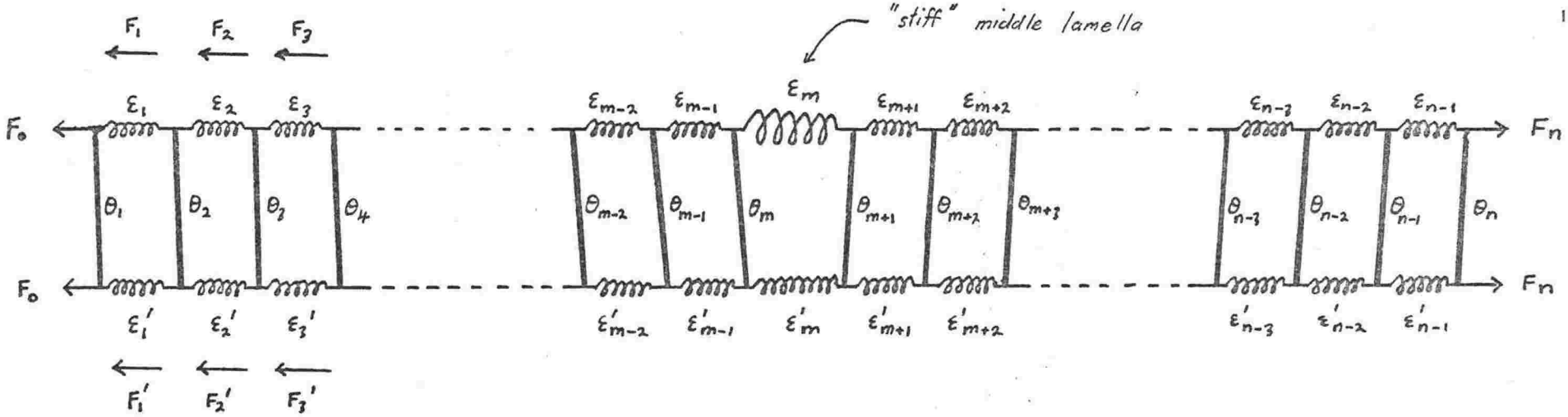

Fig. 85 : Discrete element model of the block of cell wall shown in Fig. 84.

(For clarity, sheared blocks are shown by lines.)

A system of equations governing the shear distribution in Fig. 85 can be derived in the same way as was done for the lap joint. The final set of equations is -

$$\theta_1 = K\theta_2 - \theta_3$$

$$\theta_2 = K\theta_3 - \theta_4$$

$$\vdots$$

$$\theta_{m-2} = K\theta_{m-1} - \theta_m$$

$$\theta_{m-1} = \theta_m\left(1 + \frac{2K_1}{K_2 l_1} + \frac{K_m'}{K_2}\right) - \theta_{m+1}\frac{K_m'}{K_2} + \frac{(K_m - K_m')}{K_m K_2 l_1} F_m$$

$$\theta_m = \theta_{m+1}\left(1 + \frac{2K_1}{K_m' l_1} + \frac{K_2}{K_m'}\right) - \theta_{m+2}\frac{K_2}{K_m'} - \frac{(K_m - K_m')}{K_m K_m' l_1} F_m$$

$$\theta_{m+1} = K\theta_{m+2} - \theta_{m+3}$$

$$\vdots$$

$$\theta_{n-2} = K\theta_{n-1} - \theta_n$$

$$\theta_{n-1} = \left(1 + \frac{2K_1}{K_2 l_1}\right)\theta_n$$

$$(\theta_1 + \ldots\ldots\ldots + \theta_n) = 0$$

$$F_m' = \left[1 - \frac{(K_m - K_m')}{K_m}\right] F_m - K_m' l_1 (\theta_m - \theta_{m+1})$$

$$2F_o = -2F_n = F_m + F_m'$$

.....(22)

K, K_1, K_2, l_1, l_2 have the same definitions as previously,

K_m = spring constant of "stiff" middle lamella, and

K_m' = spring constant of wall segment opposite "stiff" middle lamella.

Changes in the degree of overlap can be simulated by varying the integer "m". 50% overlap occurs when $m = {}^{n}/_{2}$, and

0% overlap when m = 1 or n.

Fm is equivalent to the load applied to the "bent plate" of section 4:1. Therefore, the peak stresses in the tangential middle lamella (which are labelled "σ_m" in Fig. 48) will be equal to "plate" stress x 0.68 in wet wood, and "plate" stress x 0.84 in dry. F_m' is the load present in the tracheid wall opposing the "stiff" middle lamella, and $2F_o$ is the total load carried by the radial double tracheid wall. These respectively give rise to σ_ω and σ_o of Fig. 48.

Appendix 5 YIELD STRENGTHS OF THE S_1 AND S_2 LAYERS OF THE TRACHEID WALL

A5 : 1 Longitudinal Strength

Mark (44) lists the longitudinal tensile strengths for tracheids of many species of wood. They show a wide variation (9 Kg/mm^2 → 150 Kg/mm^2) even within a given species. Unfortunately, the S_2 layer microfibril angles are not given. Since Tsai (33,34) shows theoretically and experimentally that the strength of a fibre reinforced composite decreases greatly as the angle between the applied load and fibre direction increases from zero, variations in S_2 microfibril angles may be partly responsible for the wide range of figures quoted by Mark. If this is so, the higher strengths will belong to tracheids with low microfibril angles, and will be nearer to the required Γ_3 . The highest strength given for Pinus Radiata is 83 Kg/mm^2.

Cave (39) measured longitudinal strength and microfibril angle for many samples of Pinus Radiata. His results cover the range 10^o to 40^o, and when extrapolated approach a value near 80 Kg/mm^2 at 0^o microfibril angle.

The S_1 layer, because of its microfibril orientation and size, will make very little contribution to the tracheid longitudinal strength. Hence the longitudinal strength of S_2 type material is likely to be 83/.85 = 100 Kg/mm^2. This in turn suggests a strength for cellulose microfibrils of 200 Kg/mm^2, since they make up 50% of the volume of

S_2 material. Hence Γ_3 for S_1 material (comprising only 25% crystalline cellulose) will be 50 Kg/mm^2.

Since the longitudinal strength of the composite is almost entirely due to the crystalline cellulose microfibrils, which are insensitive to moisture changes, the longitudinal strength is likely to be independent of wood moisture content. The only possible effect of moisture would be to enhance microfibril slippage, but since microfibrils are thought to anastomose, this process is unlikely to occur.

A5 : 2 Transverse Strength

In composites with poor fibre-matrix bonding, transverse strength generally decreases as the fibre content increases (Gerberich (52)). Conversely, in solids where fibre-matrix bonding is as strong as matrix-matrix bonding, transverse strength will always be near the matrix strength.

The latter situation is true in wood. In fact, there is probably no distinct fibre-matrix interface, but instead a gradual change from crystalline cellulose through amorphous cellulose to hemicellulose. Chemically, they are all very similar and exhibit the same type of intermolecular bonding. Hence, bonds between hemicellulose and cellulose molecules are likely to be at least as strong as those

---

(52) Gerberich, W.W. (1971) J. Mech. Phys. Solids 19 p.71
"Fracture Mechanics of a Composite with Ductile Fibres"

between two hemicellulose molecules.

Unfortunately, it is not possible to measure directly the transverse strengths of any of the layers of the wood cell wall. However, a good approximation is to set the transverse strength of all layers equal to the strength of matrix material, as measured during summerwood intra wall failure. In this type of failure splits form in a direction parallel to the reinforcing fibres, thus giving the transverse strength of the layers concerned (P or S_1).

A5 : 3 Shear Strength

This too is difficult to determine. To gain an estimate, samples of wood were broken in double shear by forces applied along the grain. The results obtained are as follows -

Airdry wood : Shear strength = 1.4 ± 2 Kg/mm^2 (4 specimens)

Saturated Wood : Shear strength = $.56 \pm .02$ kg/mm^2 (3 specimens)

(Failure time = 600 secs. The corresponding matrix transverse strengths are $2.0 \pm .3$ and $0.6 \pm .1$ Kg/mm^2 respectively.)

There is some evidence that "shear strengths" given by double shear tests may be lower than actual shear strengths. (Iosipescu (53).) Photo-elastic studies have shown that stress concentrations do occur at the edges of the shear planes. Also, Tsai's measurements showed that $\Gamma_4 = 1.5 \times \Gamma_2$

---

(53) Iosipescu, N. (1967) J. of Materials 2(3) p.537

"New Accurate Procedure for Single Shear Testing of Materials"

The above measurements on wood gave shear strengths that were somewhat lower than transverse strengths. Since these are likely to be lower than true shear strengths, it seems that the best possible approximation is to set $\Gamma_4 = \Gamma_2$ in each case.

Appendix 6 ACTIVATION ENERGIES AND HEATS OF REACTION FOR PROCESSES INVOLVING THE DEFORMATION AND RUPTURE OF HYDROGEN BONDS.

(T = room temperature)

Gibbs Free Energy of Activation for Rupture Reaction (G_2)

(Units : Kcal/mole)

Value	Author	Origin of Figure
5.7 4.8	Nissan (18)	Stress relaxation in cellophane.
6.0	Kingston & Clarke (16)	Creep of wood.
4.6 3.1	Kauman (9)	Collapse of wood tracheids.
7.8	Stamm (6)	Cyclic fatigue testing of cotton tyre cord.
4.5	Corte & Schascheck (54)	Paper strength.
5.2 mean		

(54) Corte, H., and H. Schascheck (1955) Das Papier 9 p.519 "H-bonds and Paper Strength".

Gibbs Free Energy of Reaction (ΔF)

(Units : Kcal/mole)

Value	Author	Origin of Figure
1.6	Kelsey & Clarke (55)	Sorption of water by wood
3.0	Brown, Panshin & Forsaith (56)	
2.3	Browning (57)	
1.6	Pimentel (58)	Formation of H-bonds in carboxylic acids (mean of 40 values).
2.0	Pimentel (58)	Formation of H-bonds in alcohols (mean of 8 values).
2.1 mean		

(55) Kelsey, K.E., and L.N. Clarke (1956) Aust. J. Appl. Sci. 7(2) p.160 "The Heat of Sorption of Water by Wood".

(56) Brown, H.P., A.J. Panshin, C.C. Forsaith, (1952) "Textbook of Wood Technology Vol. 2" (McGraw-Hill, N.Y.)

(57) Browning, B.L. (1963) "The Chemistry of Wood" (Interscience, N.Y.)

(58) Pimentel, G.C. and A.L. McLellan (1960) "The Hydrogen Bond" (W.H. Freeman & Co., San Francisco & London.) Ch. 7.